Title
Actin assembly by the Formin Homology Domain-containing Protein (Fhod) family of formins

Author
Patel, Aanand Anup

Publication Date
2019

Peer reviewed|Thesis/dissertation

UNIVERSITY OF CALIFORNIA

Los Angeles

Actin assembly by the Formin Homology Domain-containing Protein (Fhod) family of formins

A dissertation submitted in partial satisfaction of the requirements

for the degree Doctor of Philosophy in Molecular Biology

by

Aanand Anup Patel

2019

ABSTRACT OF THE DISSERTATION

Actin assembly by the Formin Homology Domain-containing Protein (Fhod) family of formins

by

Aanand Anup Patel

Doctor of Philosophy in Molecular Biology

University of California, Los Angeles, 2019

Professor Margot Elizabeth Quinlan, Chair

Actin and myosin form contractile structures that drive muscle contraction, cell motility, cytokinesis, and many other cellular functions. These functions depend crucially on the correct assembly, organization, and maintenance of actin filaments. Formins are a major class of actin nucleators that assemble many actin-based structures through their formin homology (FH) 1 and 2 domains, which together both nucleate and processively elongate actin filaments. The formin homology domain-containing protein (Fhod) family of formins is responsible for the assembly of several contractile actin structures, including sarcomeres in muscle cells and stress fibers in many non-muscle cells. Although Fhod family members are required for actin assembly *in vivo*, mammalian Fhods were reported to instead inhibit actin assembly *in vitro*. Here, we establish that *Drosophila* Fhod, human Fhod1, and human Fhod3 all nucleate and elongate actin filaments *in vitro*. We show that the nucleation activity of Fhod1 depends on the actin isoform, with a significantly weaker ability to nucleate skeletal muscle actin compared to other isoforms. *Drosophila* and human Fhod proteins are weak elongators, with slow elongation rates and short run lengths compared to other formins. Elongation by *Drosophila* Fhod is impaired by a coiled coil in the N-terminus, which constrains the ability of the FH1 domain to capture profilin-

actin, and a disordered C-terminal tail, which promotes dissociation of Fhod from growing actin filaments. Finally, we establish human stem cell-derived cardiomyocytes as a model system to investigate how Fhod proteins assemble and organize actin in the sarcomere. Taken together, this work establishes a framework to understand the mechanisms by which the Fhod family of formins assembles contractile actin structures.

The dissertation of Aanand Anup Patel is approved.

Alison Renee Frand

Dana Leanne Jones

Emil Reisler

Stephen Lawrence Zipursky

Margot Elizabeth Quinlan, Committee Chair

University of California, Los Angeles

2019

TABLE OF CONTENTS

List of figures

Acknowledgements

I thank my advisor, Dr. Margot Quinlan, for her incredible mentorship. From my first weeks in the lab, I have been blown away by Margot's dedication to mentorship and investment in her students. I am so privileged to have worked in such a supportive learning environment with great people. I thank the members of the Quinlan and Reisler labs, whose advice, encouragement, and friendship were invaluable to my scientific and personal growth. I am also grateful to my committee members, Dr. Frand, Dr. Jones, Dr. Reisler, and Dr. Zipursky, for their support and advice during my PhD.

I thank my parents for their unwavering love, constant encouragement, commitment to education, and the many life lessons that allowed me to succeed in graduate school. Mommy taught me how to work and learn efficiently, anticipate what will be needed and find ways to help, to focus and manage my time, to think positively and see each challenge as a learning opportunity, and countless other lessons sprinkled throughout my life. Paaoo taught me to take pride in your work, to persevere in the face of challenges and failures, and to never let the setbacks stop me from smiling and laughing. I thank my brother, my best friend since the day I was born, who has inspired, encouraged, challenged, taught, and played with me my whole life. I thank my gigantic extended family, who have all cheered me on throughout my time here. I am equally grateful for the family I acquired at UCLA, through the medical school, MSTP, and Graduate Programs in Bioscience.

Chapter 2 is a reprint of Patel et al, *J. Biol. Chem.* 2019. I thank my coauthors for their contributions to this manuscript: Zeynep A. Oztug-Durer performed initial cloning and purification of *Drosophila* Fhod, Aaron P. van Loon and Kathryn V. Bremer contributed to cosedimentation experiments, and Margot E. Quinlan was principal investigator. In Chapter 3, Kathryn V. Bremer performed most of the protein purification and kinetic assays with help from Nicole Lynn. Dylan Valencia purified proteins and performed some experiments with the Fhod

coiled coil. Lara Clemens, Lucy Dolmadjian, Katherine McPhie, and Jun Allard performed mathematical modeling related to the Fhod coiled coil. I thank Sanchaita Das for her generous help with electron microscopy experiments not included here and Drs. Will Silkworth and Martin Phillips for their help with circular dichroism. I thank our collaborators Haruko and Atsushi (Austin) Nakano for providing cardiomyocytes, performing transfections, and sharing their expertise for the work in Chapter 4. I thank the Torres lab for the use of their fluorescence microscope to acquire the images in Chapter 4. Appendix A includes data with recombinant β-actin collected by Alex Grunfeld and Andrea Chaney. I am grateful to my funding sources, the UCLA Medical Scientist Training Program (T32 GM008042) and the National Heart, Lung, and Blood Institute (HL137263) for supporting my work and training.

Vita

Education
B.S., Molecular, Cell, and Developmental Biology — June 2013
University of California, Los Angeles

Research Experience
Graduate Student Researcher — June 2015 – June 2019
Laboratory of Dr. Margot E. Quinlan
Department of Chemistry and Biochemistry
University of California, Los Angeles

Undergraduate Researcher — August 2010 – July 2013
Laboratory of Dr. Joan S. Valentine
Department of Chemistry and Biochemistry
University of California, Los Angeles

Siemens Foundation Summer Undergraduate Research Fellow — June 2010 – August 2010
Laboratory of Dr. Scott E. Fraser
Department of Biology
California Institute of Technology

Intern — June 2008 – September 2008
Laboratory of Dr. Nilay Patel
Department of Cellular and Developmental Biology
California State University, Fullerton

Publications
Patel AA, Oztug Durer ZA, van Loon AP, Bremer KV, Quinlan ME. *Drosophila* and human FHOD family formin proteins nucleate actin filaments. *J. Biol. Chem.*, 2018 Jan 12;293(2):532-540.

Abstracts
Patel AA, Grunfeld AM, Nakano H, Chaney A, Nakano A, Quinlan ME. The sarcomeric formin Fhod3 nucleates actin filaments. Poster presentation, American Society for Cell Biology Annual Meeting, San Diego, CA 2018

Patel AA, Oztug Durer ZA, van Loon AP, Bremer KV, Quinlan ME. *Drosophila* and human Fhod family formins nucleate actin filaments. Oral presentation, Molecular Biology Institute Retreat, Ventura, CA, 2018

Patel AA, Oztug Durer ZA, van Loon AP, Bremer KV, Quinlan ME. The *Drosophila* formin Fhod nucleates actin filaments. Poster presentation, Biophysical Society Annual Meeting, San Francisco, CA, 2018

Patel AA, Oztug Durer ZA, van Loon AP, Quinlan ME. The *Drosophila* formin Fhod nucleates actin filaments. Poster presentation, American Society for Cell Biology Annual Meeting, Philadelphia, PA, 2017

Patel AA, Oztug Durer ZA, van Loon AP, Quinlan ME. Biochemical characterization of actin assembly by the *Drosophila* formin FHOD. Oral presentation, Gordon Research Conference on Motile and Contractile Systems, New London, NH, 2017

Patel AA, Oztug Durer ZA, van Loon AP, Quinlan ME. *Drosophila* Formin Homology Domain-Containing Protein (FHOD) nucleates and bundles actin filaments but does not affect elongation. Poster presentation, American Society for Cell Biology Annual Meeting, San Francisco, CA, 2016

Patel AA, Lelie HL, Chattopadhyay M, Gralla EB, Whitelegge JP, Borchelt DR, Valentine JS. Conformational antibodies against Cu/Zn superoxide dismutase mutants linked to amyotrophic lateral sclerosis. Poster presentation, UCLA Molecular, Cell, and Developmental Biology Poster Session, Los Angeles, CA, 2013

Patel AA, Lelie HL, Gralla EB, Whitelegge JP, Borchelt DR, Valentine JS. Non-native post-translational modifications to copper-zinc superoxide dismutase. Poster presentation, UCLA Science Poster Day, Los Angeles, CA, 2012

Patel AA, Fraser SE, Koos DR. Neurogenesis in the Grueneberg ganglion. Oral presentation, California Institute of Technology Summer Seminar Day, Pasadena, CA, 2010

Awards

American Society for Cell Biology travel award (December 2017)
F30 Ruth L. Kirschstein National Research Service Award (April 2017 – October 2019)
Emil Reisler Award for Summer Research (June 2012 – August 2012)

Mentorship

Dylan Valencia — Winter 2019
Rotation student in Biochemistry, Molecular, and Structural Biology

Andrea Chaney — Summer 2018
Undergraduate student in HBCU-Pathways in Chemistry

Kathryn Bremer — Summer 2016 – Spring 2019
SMC-UCLA / Undergraduate / Masters Student

Service

Committee Member — 2017 - 2018
Scientific Excellence through Diversity Seminar Series at UCLA

Chapter 1: Introduction

Actin cytoskeleton

Actin is an abundant, highly conserved protein that self-assembles into filaments. Spontaneous assembly of actin filaments occurs sequentially, one subunit at a time, with a prolonged lag phase due to the instability of actin dimers and trimers. The addition of a fourth actin subunit results in a much more stable structure, called a nucleus (Pollard, 2016). Once an actin filament has been nucleated, it will readily elongate at either end as long as the concentration of free actin monomers exceeds a critical concentration, 0.16 μM for Mg-ATP-actin. Although actin filaments can elongate at either end, these ends are distinct and grow at different rates, with the more dynamic barbed end growing about ten-fold faster than the pointed end (Pollard, 1986).

Actin filaments can generate forces by directly polymerizing to push a surface, acting as a track for myosin motors, or providing structural rigidity to resist forces. To function in these ways requires that actin filaments be assembled and disassembled precisely at the correct place and time. Because spontaneous actin assembly is slow and uncontrolled, cells rely on over a hundred actin-binding proteins to control the assembly, organization, and disassembly of each actin-based structure.

Mammals have six closely related actin isoforms that carry out distinct functions. These isoforms include four muscle-specific isoforms ($\alpha_{skeletal}$, $\alpha_{cardiac}$, α_{smooth}, and γ_{smooth}) and two ubiquitously expressed isoforms ($\beta_{cytoplasmic}$ and $\gamma_{cytoplasmic}$). Any pair of mammalian actin isoforms shares at least 93% sequence identity; most of the differences between isoforms are conservative changes in the acidic residues at the N-terminus that do not affect the overall structure. Despite the strong conservation between actin isoforms, they have non-overlapping functions: knockouts of each actin isoform display a distinct phenotype, and in many cases

overexpression of a different actin isoform fails to rescue the knockout phenotype (Perrin and Ervasti, 2010). There is some evidence to support multiple mechanisms by which each actin isoform carries out a different function. These mechanisms include differences between actin isoforms in their assembly and disassembly dynamics (Bergeron et al., 2010), differences in their interactions with various actin-binding proteins (Chen et al., 2017; De La Cruz, 2005; Silkworth et al., 2018), and non-coding differences in their nucleotide sequences (Patrinostro et al., 2018; Vedula et al., 2017).

Formins

Formins are one of three known classes of actin nucleators. They are defined by their formin homology (FH) 1 and 2 domains, with which they both nucleate and processively elongate actin filaments. Because of these two activities, formins generally assemble long parallel or antiparallel bundles of actin filaments, in stark contrast with the short, branched networks of actin filaments nucleated by the Arp2/3 complex (Goode and Eck, 2007).

The FH2 domain homodimerizes to form a donut shape (Xu et al., 2004) that is necessary and sufficient for actin nucleation. The FH2 domain is thought to nucleate filaments by stabilizing actin dimers (Otomo et al., 2005). Upon nucleating a filament, the FH2 binds tightly to and remains processively associated with the more dynamic barbed end of the actin filament. While associated with the barbed end, the FH2 domain fluctuates between an “open” state that permits addition of actin monomers and a “closed” state that prevents addition of monomers (Otomo et al., 2005; Xu et al., 2004). The fraction of time spent in the closed state, termed the gating factor (Vavylonis et al., 2006), results in slowed barbed end elongation when the FH2 domain alone is bound to the barbed end.

The intrinsically disordered FH1 domain contains polyproline tracks, generally consisting of at least five prolines in six consecutive amino acids, that bind to profilin. Because most actin monomers in the cell are bound to profilin, the FH1 domain rapidly recruits actin monomers to

the FH2-bound barbed end. The effectiveness of a polyproline track in recruiting actin monomers is determined by its “capture” rate (how quickly it binds a profilin-bound actin monomer) and its “delivery” rate (how quickly it transfers the actin subunit to the barbed end) (Courtemanche, 2018).

Several parameters control the capture and delivery rates of a polyproline track. Polyproline tracks with a stronger affinity for profilin (related to the number of prolines in the track) have faster capture rates at the cost of slower delivery rates. The optimal affinity of a polyproline track for profilin depends on its distance from the FH2 domain, with polyproline tracks further from the FH2 domain requiring stronger affinities for profilin to efficiently recruit or deliver profilin-actin (Courtemanche and Pollard, 2012). Although consecutive polyproline tracks increase the elongation rate of a formin, they have diminishing returns (Kovar et al., 2006; Paul and Pollard, 2008). The elongation rate of a formin-bound barbed end thus depends on several factors: the gating factor of the FH2 domain (how permissive it is to the addition of actin monomers), the capture and delivery rates of the FH1 polyproline tracks, and the concentrations of profilin and actin. Formins vary considerably in their elongation rates owing to the diversity in their gating factors and their FH1 domains.

In addition to their FH1 and FH2 domain, most formins contain autoinhibitory domains to regulate their activity. In most formins, these domains are the N-terminal diaphanous inhibitory domain (DID) and the C-terminal diaphanous autoregulatory domain (DAD). Typically, a direct interaction between the DID and the DAD prevents actin assembly by the FH2 domain (Alberts, 2001; Li and Higgs, 2003). Some exceptions include the Fmn family formins, which use the analogous CID and CAD as autoinhibitory domains (Bor et al., 2012), and INF2, which requires cyclase-associated protein and lysine-acetylated actin in addition to the DID and DAD to inhibit its activity (A et al., 2019).

Formins are classified into nine families in animals (Pruyne, 2016). All formin families share the overall domain structure and biochemical activities described above, but differ in their

actin nucleation and elongation rates, their modes of regulation, and capacity to perform additional activities. These additional activities include bundling actin filaments, severing actin filaments, and cross-linking actin filaments to microtubules (Courtemanche, 2018; Goode and Eck, 2007).

Fhod family of formins

The formin homology domain-containing protein (Fhod) family of formins is required for several actin-driven processes, particularly for the assembly of contractile actin structures. Mammals have two Fhod family members, Fhod1 and Fhod3. Fhod1 is broadly expressed and responsible for assembling a variety of actin structures, particularly contractile stress fibers that allow for cell adhesion and motility (Gardberg et al., 2013; Iskratsch et al., 2013; Peippo et al., 2017; Schulze et al., 2014; Takeya et al., 2008). Fhod1 has several other less-studied functions, including nuclear positioning (Kutscheidt et al., 2014), podosome assembly (Panzer et al., 2016), immunological synapse formation (Tabdanov et al., 2015), and vaccinia motility (Alvarez and Agaisse, 2013).

Fhod1 is also expressed in cardiomyocytes but excluded from the sarcomere. Instead, Fhod1 localizes to intercalated discs (Al Haj et al., 2015; Dwyer et al., 2014), the specialized junctions that mechanically and electrically couple adjacent cardiomyocytes (Bennett, 2018). Fhod1 was also proposed to localize to costameres (Al Haj et al., 2015), the specialized focal adhesions connecting sarcomeres to the extracellular matrix. Despite these reports of Fhod1 localization in the heart, loss of Fhod1 does not lead to any major cardiac defects (Sanematsu et al., 2019), and the function of Fhod1 in these cardiac structures remains unknown.

Unlike Fhod1, Fhod3 localizes to the sarcomere and is essential for sarcomere assembly (Fenix et al., 2018; Iskratsch et al., 2010; Kan-o et al., 2012; Taniguchi et al., 2009). Specifically, Fhod3 is required for stress fiber-like premyofibrils to undergo retrograde flow and reorganize into mature sarcomeres (Fenix et al., 2018). Fhod3 remains associated with mature

sarcomeres throughout adulthood, when sarcomeres are no longer actively assembled or turned over (Ushijima et al., 2018). Sarcomeres remain intact in Fhod3 mutants that cannot localize to the sarcomere (Taniguchi et al., 2009) and in conditional adult knockouts of Fhod3 (Ushijima et al., 2018). However, adult Fhod3 knockout mice develop cardiac hypertrophy (Ushijima et al., 2018), and human Fhod3 polymorphisms and mutations are associated with hypertrophic cardiomyopathy (Ochoa et al., 2018; Wooten et al., 2013). In addition to these relatively well established roles in the heart, Fhod3 contributes to actin assembly in some non-muscle contexts, including cancer cell migration (Monzo et al., 2016; Paul et al., 2015) and neurulation (Sulistomo et al., 2019).

The role of Fhod family members in assembling contractile actin structures is well conserved across animals. The *C. elegans* homolog Fhod-1 is required for sarcomere organization (Mi-Mi et al., 2012), and the *Drosophila* homolog Fhod (also known as knittrig) is required for sarcomere assembly in muscle, stress fiber assembly in S2 cells, and migration of hemocytes and tracheal tip cells (Lammel et al., 2014; Shwartz et al., 2016).

Many cellular functions for Fhod family members have now been established. How Fhod proteins contribute to these many functions has remained much less clear. Although formins are known for two major mechanisms, nucleation and processive elongation, neither activity had been observed previously for Fhod family members. In fact, both Fhod1 and Fhod3 were instead reported to inhibit actin assembly *in vitro* (Schonichen et al., 2013; Taniguchi et al., 2009). These *in vitro* observations sharply contrast with *in vivo* observations that Fhod family members are required for the assembly of stress fibers and sarcomeres. In this dissertation, I describe our efforts to understand the biochemical mechanisms by which Fhod family members assemble contractile actin structures. In chapter 2, we show that two Fhod proteins, *Drosophila* Fhod and human Fhod1, in fact nucleate and processively elongate actin filaments *in vitro*. In chapter 3, we perform biophysical experiments to investigate the factors controlling *Drosophila* Fhod's relatively poor elongation activity. In chapter 4, we demonstrate that human Fhod3 also

nucleates actin and show preliminary work to characterize Fhod3 function *in vitro* and in stem cell-derived cardiomyocytes. Taken together, this work establishes that Fhod family members nucleate and elongate actin filaments and identifies multiple factors setting Fhod family members apart from other formins.

References

A, M., Fung, T.S., Kettenbach, A.N., Chakrabarti, R., and Higgs, H.N. 2019. A complex containing lysine-acetylated actin inhibits the formin INF2. *Nat Cell Biol*. 21:592-602.

Al Haj, A., Mazur, A.J., Radaszkiewicz, K., Radaszkiewicz, T., Makowiecka, A., et al. 2015. Distribution of formins in cardiac muscle: FHOD1 is a component of intercalated discs and costameres. *Eur J Cell Biol*. 94:101-113.

Alberts, A.S. 2001. Identification of a carboxyl-terminal diaphanous-related formin homology protein autoregulatory domain. *J Biol Chem*. 276:2824-2830.

Alvarez, D.E., and Agaisse, H. 2013. The formin FHOD1 and the small GTPase Rac1 promote vaccinia virus actin-based motility. *J Cell Biol*. 202:1075-1090.

Bennett, P.M. 2018. Riding the waves of the intercalated disc of the heart. *Biophys Rev*. 10:955-959.

Bergeron, S.E., Zhu, M., Thiem, S.M., Friderici, K.H., and Rubenstein, P.A. 2010. Ion-dependent polymerization differences between mammalian beta- and gamma-nonmuscle actin isoforms. *J Biol Chem*. 285:16087-16095.

Bor, B., Vizcarra, C.L., Phillips, M.L., and Quinlan, M.E. 2012. Autoinhibition of the formin Cappuccino in the absence of canonical autoinhibitory domains. *Mol Biol Cell*. 23:3801-3813.

Chen, A., Arora, P.D., McCulloch, C.A., and Wilde, A. 2017. Cytokinesis requires localized beta-actin filament production by an actin isoform specific nucleator. *Nat Commun*. 8:1530.

Courtemanche, N. 2018. Mechanisms of formin-mediated actin assembly and dynamics. *Biophys Rev*. 10:1553-1569.

Courtemanche, N., and Pollard, T.D. 2012. Determinants of Formin Homology 1 (FH1) domain function in actin filament elongation by formins. *J Biol Chem*. 287:7812-7820.

De La Cruz, E.M. 2005. Cofilin binding to muscle and non-muscle actin filaments: isoform-dependent cooperative interactions. *J Mol Biol*. 346:557-564.

Dwyer, J., Pluess, M., Iskratsch, T., Dos Remedios, C.G., and Ehler, E. 2014. The formin FHOD1 in cardiomyocytes. *Anat Rec (Hoboken)*. 297:1560-1570.

Fenix, A.M., Neininger, A.C., Taneja, N., Hyde, K., Visetsouk, M.R., et al. 2018. Muscle-specific stress fibers give rise to sarcomeres in cardiomyocytes. *Elife*. 7.

Gardberg, M., Kaipio, K., Lehtinen, L., Mikkonen, P., Heuser, V.D., et al. 2013. FHOD1, a formin upregulated in epithelial-mesenchymal transition, participates in cancer cell migration and invasion. *PLoS One*. 8:e74923.

Goode, B.L., and Eck, M.J. 2007. Mechanism and function of formins in the control of actin assembly. *Annu Rev Biochem*. 76:593-627.

Iskratsch, T., Lange, S., Dwyer, J., Kho, A.L., dos Remedios, C., et al. 2010. Formin follows function: a muscle-specific isoform of FHOD3 is regulated by CK2 phosphorylation and promotes myofibril maintenance. *J Cell Biol*. 191:1159-1172.

Iskratsch, T., Yu, C.H., Mathur, A., Liu, S., Stevenin, V., et al. 2013. FHOD1 is needed for directed forces and adhesion maturation during cell spreading and migration. *Dev Cell*. 27:545-559.

Kan-o, M., Takeya, R., Abe, T., Kitajima, N., Nishida, M., et al. 2012. Mammalian formin Fhod3 plays an essential role in cardiogenesis by organizing myofibrillogenesis. *Biol Open*. 1:889-896.

Kovar, D.R., Harris, E.S., Mahaffy, R., Higgs, H.N., and Pollard, T.D. 2006. Control of the assembly of ATP- and ADP-actin by formins and profilin. *Cell*. 124:423-435.

Kutscheidt, S., Zhu, R., Antoku, S., Luxton, G.W., Stagljar, I., et al. 2014. FHOD1 interaction with nesprin-2G mediates TAN line formation and nuclear movement. *Nat Cell Biol*. 16:708-715.

Lammel, U., Bechtold, M., Risse, B., Berh, D., Fleige, A., et al. 2014. The Drosophila FHOD1-like formin Knittrig acts through Rok to promote stress fiber formation and directed macrophage migration during the cellular immune response. *Development*. 141:1366-1380.

Li, F., and Higgs, H.N. 2003. The Mouse Formin mDia1 Is a Potent Actin Nucleation Factor Regulated by Autoinhibition. *Current Biology*. 13:1335-1340.

Mi-Mi, L., Votra, S., Kemphues, K., Bretscher, A., and Pruyne, D. 2012. Z-line formins promote contractile lattice growth and maintenance in striated muscles of C. elegans. *J Cell Biol*. 198:87-102.

Monzo, P., Chong, Y.K., Guetta-Terrier, C., Krishnasamy, A., Sathe, S.R., et al. 2016. Mechanical confinement triggers glioma linear migration dependent on formin FHOD3. *Mol Biol Cell*. 27:1246-1261.

Ochoa, J.P., Sabater-Molina, M., Garcia-Pinilla, J.M., Mogensen, J., Restrepo-Cordoba, A., et al. 2018. Formin Homology 2 Domain Containing 3 (FHOD3) Is a Genetic Basis for Hypertrophic Cardiomyopathy. *J Am Coll Cardiol*. 72:2457-2467.

Otomo, T., Tomchick, D.R., Otomo, C., Panchal, S.C., Machius, M., et al. 2005. Structural basis of actin filament nucleation and processive capping by a formin homology 2 domain. *Nature*. 433:488-494.

Panzer, L., Trube, L., Klose, M., Joosten, B., Slotman, J., et al. 2016. The formins FHOD1 and INF2 regulate inter- and intra-structural contractility of podosomes. *J Cell Sci*. 129:298-313.

Patrinostro, X., Roy, P., Lindsay, A., Chamberlain, C.M., Sundby, L.J., et al. 2018. Essential nucleotide- and protein-dependent functions of Actb/beta-actin. *Proc Natl Acad Sci U S A*. 115:7973-7978.

Paul, A.S., and Pollard, T.D. 2008. The role of the FH1 domain and profilin in formin-mediated actin-filament elongation and nucleation. *Curr Biol*. 18:9-19.

Paul, N.R., Allen, J.L., Chapman, A., Morlan-Mairal, M., Zindy, E., et al. 2015. alpha5beta1 integrin recycling promotes Arp2/3-independent cancer cell invasion via the formin FHOD3. *J Cell Biol*. 210:1013-1031.

Peippo, M., Gardberg, M., Lamminen, T., Kaipio, K., Carpen, O., et al. 2017. FHOD1 formin is upregulated in melanomas and modifies proliferation and tumor growth. *Exp Cell Res*. 350:267-278.

Perrin, B.J., and Ervasti, J.M. 2010. The actin gene family: function follows isoform. *Cytoskeleton (Hoboken)*. 67:630-634.

Pollard, T.D. 1986. Rate constants for the reactions of ATP- and ADP-actin with the ends of actin filaments. *J Cell Biol*. 103:2747-2754.

Pollard, T.D. 2016. Actin and Actin-Binding Proteins. *Cold Spring Harb Perspect Biol*. 8.

Pruyne, D. 2016. Revisiting the Phylogeny of the Animal Formins: Two New Subtypes, Relationships with Multiple Wing Hairs Proteins, and a Lost Human Formin. *PLoS One*. 11:e0164067.

Sanematsu, F., Kanai, A., Ushijima, T., Shiraishi, A., Abe, T., et al. 2019. Fhod1, an actin-organizing formin family protein, is dispensable for cardiac development and function in mice. *Cytoskeleton (Hoboken)*.

Schonichen, A., Mannherz, H.G., Behrmann, E., Mazur, A.J., Kuhn, S., et al. 2013. FHOD1 is a combined actin filament capping and bundling factor that selectively associates with actin arcs and stress fibers. *J Cell Sci*. 126:1891-1901.

Schulze, N., Graessl, M., Blancke Soares, A., Geyer, M., Dehmelt, L., et al. 2014. FHOD1 regulates stress fiber organization by controlling the dynamics of transverse arcs and dorsal fibers. *J Cell Sci*. 127:1379-1393.

Shwartz, A., Dhanyasi, N., Schejter, E.D., and Shilo, B.Z. 2016. The Drosophila formin Fhos is a primary mediator of sarcomeric thin-filament array assembly. *Elife*. 5.

Silkworth, W.T., Kunes, K.L., Nickel, G.C., Phillips, M.L., Quinlan, M.E., et al. 2018. The neuron-specific formin Delphilin nucleates nonmuscle actin but does not enhance elongation. *Mol Biol Cell*. 29:610-621.

Sulistomo, H.W., Nemoto, T., Yanagita, T., and Takeya, R. 2019. Formin homology 2 domain-containing 3 (Fhod3) controls neural plate morphogenesis in mouse cranial neurulation by regulating multidirectional apical constriction. *J Biol Chem*. 294:2924-2934.

Tabdanov, E., Gondarenko, S., Kumari, S., Liapis, A., Dustin, M.L., et al. 2015. Micropatterning of TCR and LFA-1 ligands reveals complementary effects on cytoskeleton mechanics in T cells. *Integr Biol (Camb)*. 7:1272-1284.

Takeya, R., Taniguchi, K., Narumiya, S., and Sumimoto, H. 2008. The mammalian formin FHOD1 is activated through phosphorylation by ROCK and mediates thrombin-induced stress fibre formation in endothelial cells. *EMBO J*. 27:618-628.

Taniguchi, K., Takeya, R., Suetsugu, S., Kan, O.M., Narusawa, M., et al. 2009. Mammalian formin fhod3 regulates actin assembly and sarcomere organization in striated muscles. *J Biol Chem*. 284:29873-29881.

Ushijima, T., Fujimoto, N., Matsuyama, S., Kan, O.M., Kiyonari, H., et al. 2018. The actin-organizing formin protein Fhod3 is required for postnatal development and functional maintenance of the adult heart in mice. *J Biol Chem*. 293:148-162.

Vavylonis, D., Kovar, D.R., O'Shaughnessy, B., and Pollard, T.D. 2006. Model of formin-associated actin filament elongation. *Mol Cell*. 21:455-466.

Vedula, P., Kurosaka, S., Leu, N.A., Wolf, Y.I., Shabalina, S.A., et al. 2017. Diverse functions of homologous actin isoforms are defined by their nucleotide, rather than their amino acid sequence. *Elife*. 6.

Wooten, E.C., Hebl, V.B., Wolf, M.J., Greytak, S.R., Orr, N.M., et al. 2013. Formin homology 2 domain containing 3 variants associated with hypertrophic cardiomyopathy. *Circ Cardiovasc Genet*. 6:10-18.

Xu, Y., Moseley, J.B., Sagot, I., Poy, F., Pellman, D., et al. 2004. Crystal structures of a Formin Homology-2 domain reveal a tethered dimer architecture. *Cell*. 116:711-723.

Chapter 2: *Drosophila* and human Fhod family formin proteins nucleate actin filaments

JBC ARTICLE

Drosophila and human FHOD family formin proteins nucleate actin filaments

Received for publication, June 19, 2017, and in revised form, October 26, 2017 Published, Papers in Press, November 10, 2017, DOI 10.1074/jbc.M117.800888

Aanand A. Patel[†], **Zeynep A. Oztug Durer**[§1], **Aaron P. van Loon**[†], **Kathryn V. Bremer**[§], **and Margot E. Quinlan**[§¶2]

From the [‡]*Molecular Biology Interdepartmental Doctoral Program, the* [§]*Department of Chemistry and Biochemistry, and the* [¶]*Molecular Biology Institute, University of California Los Angeles, Los Angeles, California 90095*

Edited by Velia M. Fowler

Formins are a conserved group of proteins that nucleate and processively elongate actin filaments. Among them, the formin homology domain–containing protein (FHOD) family of formins contributes to contractility of striated muscle and cell motility in several contexts. However, the mechanisms by which they carry out these functions remain poorly understood. Mammalian FHOD proteins were reported not to accelerate actin assembly *in vitro*; instead, they were proposed to act as barbed end cappers or filament bundlers. Here, we show that purified *Drosophila* Fhod and human FHOD1 both accelerate actin assembly by nucleation. The nucleation activity of FHOD1 is restricted to cytoplasmic actin, whereas *Drosophila* Fhod potently nucleates both cytoplasmic and sarcomeric actin isoforms. *Drosophila* Fhod binds tightly to barbed ends, where it slows elongation in the absence of profilin and allows, but does not accelerate, elongation in the presence of profilin. Fhod antagonizes capping protein but dissociates from barbed ends relatively quickly. Finally, we determined that Fhod binds the sides of and bundles actin filaments. This work establishes that Fhod shares the capacity of other formins to nucleate and bundle actin filaments but is notably less effective at processively elongating barbed ends than most well studied formins.

Formins are a major, conserved group of proteins known for their ability to both nucleate new actin filaments and remain processively associated with fast-growing barbed ends via their formin homology 2 (FH2)[3] domains. While bound to the barbed end, many formins accelerate elongation, using their proline-rich FH1 domains to recruit profilin-bound actin monomers to the barbed end. In addition to these classic activities, many formins have additional effects on actin filaments, such as severing, bundling, or cross-linking to microtubules (1). Animals have seven formin families, which share the same domain structure, including the highly conserved FH2 domains. Importantly, formins differ in their actin assembly activities and modes of regulation, allowing them to fulfill distinct cellular roles.

The formin homology domain–containing protein (FHOD) family of formins has two mammalian isoforms, FHOD1 and FHOD3, which assemble contractile actin structures in several contexts. FHOD1 is widely expressed and assembles stress fibers that contribute to the adhesion, spreading, and motility of numerous cell types (2–8). FHOD3 has also been implicated in the motility of some cancers (9, 10), but its expression is predominantly restricted to striated muscle (11, 12). In cardiomyocytes, FHOD3 localizes to the sarcomere and is required for its assembly and maintenance (12–15), whereas FHOD1 distinctly localizes to costameres and intercalated discs (16, 17). Changes in expression level and polymorphisms of both FHOD1 and FHOD3 are associated with cardiomyopathies (12, 17–20).

The mechanisms by which FHOD family members function remain poorly understood. Unlike other formins, purified FHOD1 and FHOD3 were shown to slow, rather than accelerate, actin assembly *in vitro* and have therefore been proposed to act as actin cappers or bundlers (13, 21). In contrast, the cell biology data suggest that FHOD1 and FHOD3 function as actin nucleators *in vivo*. Across a wide range of cell types, expression of constitutively active FHOD1 or FHOD3 is sufficient to induce the formation of stress fibers (2–5, 13). Furthermore, FHOD3 is required for sarcomere assembly following latrunculin washout (12). These data are most suggestive of actin nucleation, although FHOD1 and FHOD3 might instead function by stabilizing or reorganizing existing actin filaments.

Drosophila melanogaster has a single FHOD family member, referred to here as Fhod (it is also known as Fhos or knittrig). The Fhod gene is alternatively spliced to produce eight different isoforms, which maintain constant FH1 and FH2 domains but alter their regulatory N termini and C-terminal tails. The role of FHOD proteins in cell motility and contractility is well conserved in *Drosophila*, because Fhod contributes to motility in macrophages and tracheal tip cells (22), sarcomere organization in striated muscle (23, 24), and cardiac contractility (18).

Here, we show that purified *Drosophila* Fhod and human FHOD1 accelerate actin assembly by nucleation. The nucleation activity of FHOD1 is restricted to cytoplasmic actin, whereas *Drosophila* Fhod potently nucleates both cytoplasmic

This work was supported by National Institutes of Health Grant NRSA F30 HL137263 (to A. A. P.), UCLA Medical Scientist Training Program T32 GM008042 (to A. A. P.), and R01 GM096133 (to M. E. Q.). The authors declare that they have no conflicts of interest with the contents of this article. The content is solely the responsibility of the authors and does not necessarily represent the official views of the National Institutes of Health.

[1] Present address: Dept. of Biophysics, Acibadem Mehmet Ali Aydinlar University School of Medicine, Istanbul 34752, Turkey.

[2] To whom correspondence should be addressed: Dept. of Chemistry and Biochemistry, 611 Charles E. Young Dr. E., University of California, Los Angeles, CA 90095. Tel.: 310-206-8064; Fax: 310-206-5213; E-mail: Margot@chem.ucla.edu.

[3] The abbreviations used are: FH2, formin homology 2 domain; FHOD, formin homology domain–containing protein; TIRF, total internal reflection fluorescence.

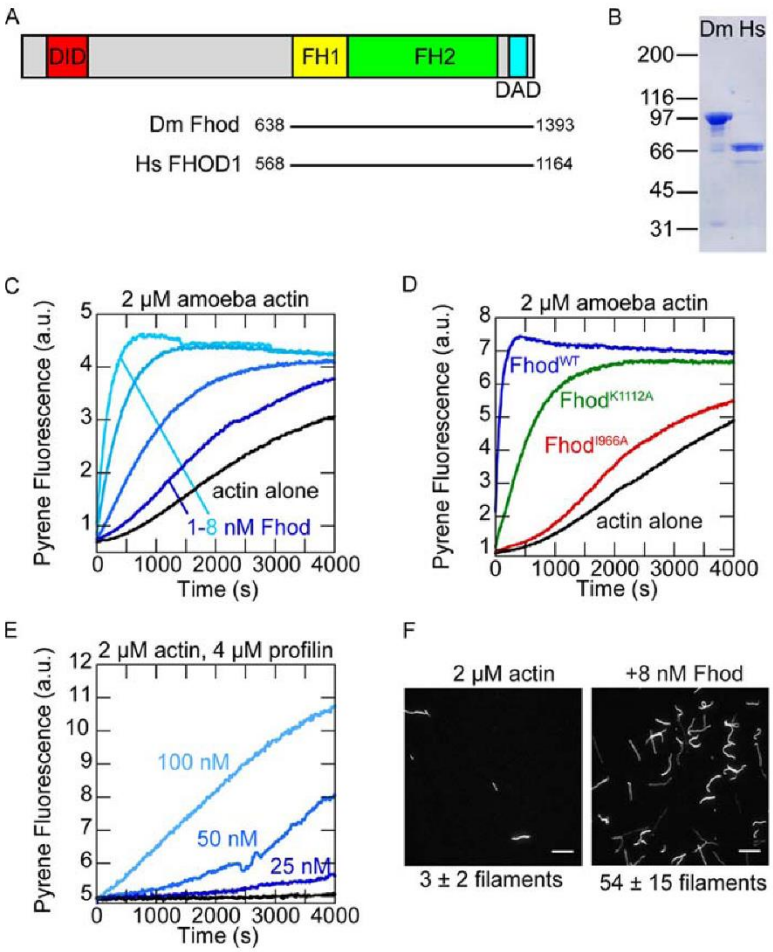

Figure 1. The *Drosophila* formin Fhod accelerates actin assembly. *A*, domain structure of *Drosophila* Fhod isoform A. Fhod includes formin homology domains for actin assembly and the Diaphanous inhibitory domain (*DID*) and Diaphanous autoregulatory domain (*DAD*) for autoinhibition and regulation. The Fhod construct used in this work spans residues 638–1393 and includes the FH1 domain, FH2 domain, and tail. Human FHOD1 has a nearly identical domain structure. *B*, Coomassie-stained polyacrylamide gel showing purified *Drosophila* Fhod and human FHOD1 constructs. *C*, assembly of 2 μM *A. castellanii* actin (10% pyrene-labeled) with 1–8 nM Fhod. Fhod accelerates actin assembly in a dose-dependent manner. *D*, assembly of 2 μM amoeba actin (10% pyrene-labeled) in the presence of 16 nM wild-type (*blue*) or mutant (I966A, *red*; K1112A, *green*) Fhod. Actin assembly by Fhod is reduced moderately by the K1112A mutation and severely by the I966A mutation. *E*, assembly of 2 μM amoeba actin (5% pyrene-labeled) in the presence of 4 μM *S. pombe* profilin and the indicated concentrations of Fhod. Fhod accelerates actin assembly in the presence of profilin. *F*, 2 μM actin was polymerized in the presence or absence of 8 nM Fhod for 5 min, stabilized with Alexa Fluor 488-phalloidin, and imaged by TIRF microscopy. *Scale bars*, 10 μm. Numbers of filaments per field of view from three independent experiments are indicated below (means ± standard deviation).

and sarcomeric actin isoforms. *Drosophila* Fhod remains processively associated with the barbed end, where it slows elongation in the absence of profilin and allows elongation, at rates similar to actin alone, in the presence of profilin. Although Fhod does not accelerate barbed-end elongation, we find that Fhod protects barbed ends from capping protein with a characteristic run length of ~2 μm. Fhod additionally binds tightly to the sides of filaments and bundles filaments together.

Results

Fhod accelerates actin assembly

We purified the C-terminal half of *Drosophila* Fhod isoform A, encompassing the FH1 domain, FH2 domain, and C-terminal tail (Fig. 1, *A* and *B*). This isoform is sufficient to rescue viability in Fhod null flies (22), and its C terminus is identical to that of isoform H, which rescues sarcomere organization in indirect flight muscle (23). We first tested the effect of Fhod on the assembly of *Acanthamoeba* actin in bulk pyrene assays; Fhod potently accelerated actin assembly in a dose-dependent manner (Fig. 1*C*).

To further compare Fhod to characterized formins, we introduced two classical mutations, I966A and K1112A, in conserved residues of the FH2 domain (25). The I966A mutation almost completely abolished activity, whereas the K1112A mutation markedly reduced, but did not eliminate, activity (Fig. 1*D*). We also tested the ability of Fhod to promote actin assembly in the presence of profilin, which binds most actin mono-

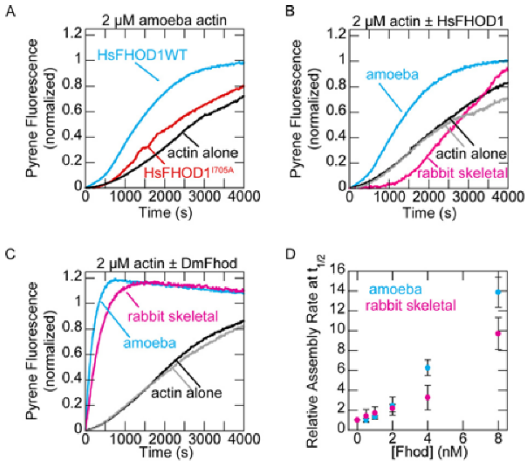

Figure 2. Human FHOD1 accelerates assembly of *Acanthamoeba* actin, but not rabbit skeletal actin. *A*, assembly of 2 μM *A. castellanii* actin (10% pyrene-labeled) alone or in the presence of 40 nM human FHOD1. *B*, assembly of 2 μM actin from *Acanthamoeba* or rabbit skeletal muscle (10% pyrene-labeled) alone or in the presence of 40 nM human FHOD1. *C*, assembly of 2 μM actin from *Acanthamoeba* or rabbit skeletal muscle (10% pyrene-labeled) alone or in the presence of 8 nM *Drosophila* Fhod. *D*, quantification of actin assembly rates from *C*. The data are means ± standard deviation from three independent experiments.

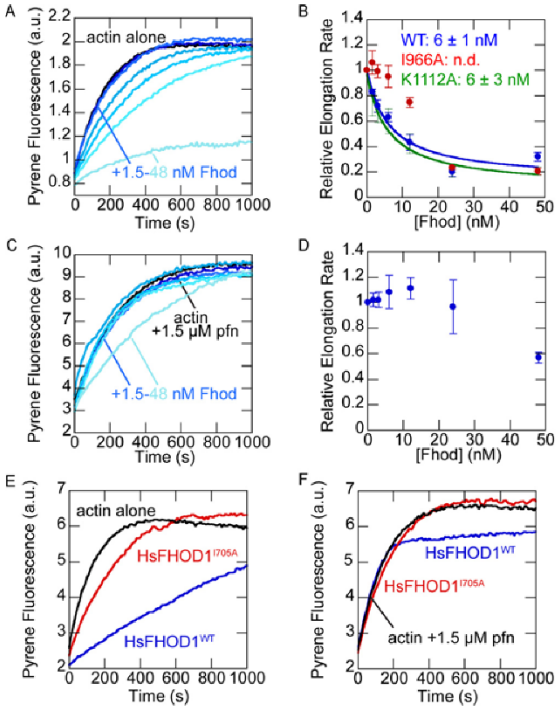

Figure 3. Fhod does not accelerate barbed-end elongation. *A*, actin elongation from preformed seeds. Final conditions were 0.25 μM F-actin seeds (~0.4 nM barbed ends), 0.5 μM G-actin (10% pyrene-labeled), and 1.5–48 nM Fhod. Fhod slows barbed-end elongation in a dose-dependent manner. *B*, quantification of elongation rates from *A*. Elongation rates were measured as the initial slope over the first 90 s, relative to the slope of actin alone. The data are the means ± standard deviation from three independent experiments. The *binding curves* show the best fit to the average values. *C*, actin elongation from preformed seeds, as in *A*, with 1.5 μM *S. pombe* profilin. Fhod does not slow elongation in the presence of profilin. *D*, quantification of elongation rates from *C*. The data are the means ± standard deviation from three independent experiments. *E*, actin elongation from preformed seeds. Final conditions were 0.25 μM F-actin seeds (~0.4 nM barbed ends), 0.5 μM G-actin (10% pyrene-labeled), and 40 nM human FHOD1. FHOD1 slows barbed-end elongation. *F*, actin elongation from preformed seeds, as in *E*, with 1.5 μM *S. pombe* profilin. FHOD1 allows barbed-end elongation at rates similar to actin alone.

mers in the cell and inhibits spontaneous nucleation. Profilin strongly impaired actin assembly by Fhod, but Fhod still accelerated actin assembly in a dose-dependent manner under these conditions (Fig. 1*E*).

Formins can promote both nucleation and elongation. To more directly assess nucleation activity, we imaged actin filaments polymerized in the absence or presence of Fhod. Fhod greatly increased the number of filaments per field of view, indicating that Fhod promotes actin assembly by nucleation (Fig. 1*F*). Fhod is thus similar to other studied formins in its ability to nucleate.

Human FHOD1 nucleates Acanthamoeba actin, but not rabbit skeletal actin

We compared *Drosophila* Fhod with human FHOD1, which was reported to inhibit actin assembly (21). Surprisingly, FHOD1 accelerated actin assembly in our hands, albeit weakly (Fig. 2*A*). Previous work with both FHOD1 and FHOD3 used actin from rabbit skeletal muscle (13, 21). Because formin activity can depend on the actin isoform,[4] we asked whether our use of *Acanthamoeba* actin could account for these conflicting results. Indeed, human FHOD1 did not nucleate rabbit skeletal actin (Fig. 2*B*). As previously observed, actin assembly was inhibited over the first 1000 s (21). The pyrene trace suggests that FHOD1 does interact with rabbit skeletal actin, despite its inability to nucleate this isoform. In contrast, *Drosophila* Fhod nucleated both actin isoforms, with only slightly lower activity in the presence rabbit skeletal actin (Fig. 2, *C* and *D*). These results are consistent with the more restricted localization of human FHOD1 to cytoplasmic actin structures, *versus* the role of *Drosophila* Fhod in both sarcomeric and cytoplasmic structures (22, 23). *Drosophila* Fhod actin assembly activity is thus representative of FHOD family members, at least in non-sarcomere contexts. Although *Drosophila* Fhod appeared substantially more potent than human FHOD1, we note that human FHOD1 was highly prone to C-terminal truncation (Fig. 1*B*), which might reduce its nucleation activity (26–28). Unless otherwise indicated, all subsequent experiments were performed with *Drosophila* Fhod and *Acanthamoeba* actin.

Fhod does not promote barbed-end elongation

Formins typically slow elongation in the absence of profilin and accelerate elongation in the presence of profilin. Using bulk seeded elongation assays, we found that Fhod slows barbed-end elongation in the absence of profilin with an affinity of 6 nM (Fig. 3, *A* and *B*). This effect was unchanged by the K1112A mutation but strongly reduced by the I966A mutation. Although high concentrations of I966A mutant appeared to slow elongation, we attribute this decrease to filament bundling (see "Fhod bun-

[4] W.T. Silkworth, K.C. Kunes, G.C. Nickel, M.L. Phillips, M.E. Quinlan, C.L. Vizcarra, *Mol. Biol. Cell*, in press.

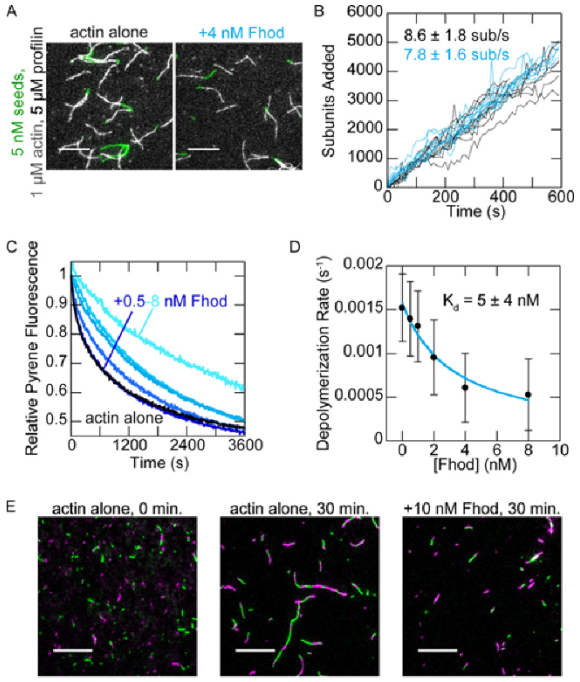

Figure 4. *Drosophila* Fhod binds barbed ends. *A*, direct observation of barbed-end elongation by TIRF microscopy with 5 nM F-actin seeds (1% biotinylated, labeled with Alexa Fluor 647-phalloidin), 1 μM G-actin (10% Alexa Fluor 594-labeled), and 5 μM *S. pombe* profilin, ± 4 nM Fhod. Images were taken 8 min after the start of polymerization. *Scale bars*, 10 μm. *B*, quantification of elongation from *A*. Ten representative traces from each condition are plotted. Elongation rates are average ± standard deviation from three flow chambers for each condition (n = 60, actin alone; n = 36, +4 nM Fhod). *C*, actin filaments depolymerized by dilution to 0.1 μM (70% pyrene-labeled) with varying concentrations of Fhod. The data were normalized against the initial pyrene fluorescence. *D*, quantification of depolymerization rates from *C*, represented by the initial slope over the first 90 s. Fhod binds barbed ends and slows depolymerization. The data and reported K_d are the means ± standard deviation from six independent experiments. The *binding curve* shows the best fit to the average values. *E*, reannealing of sheared actin filaments. Actin filaments were stabilized with Alexa Fluor 488- (*green*) or rhodamine- (*magenta*) phalloidin, sheared, and allowed to reanneal for 30 min at a concentration of 0.25 μM F-actin ± 10 nM Fhod. Fhod inhibits reannealing of the sheared filaments. *Scale bars*, 10 μm.

dles actin filaments") rather than a true effect on barbed-end elongation because the trend does not follow the expected dose-response curve, and substantial fluorescence artifacts were observed in other assays with high concentrations of Fhod.

In the presence of profilin, Fhod had a minimal effect on elongation at most concentrations we tested (Fig. 3, *C* and *D*). At high concentrations of Fhod, the elongation rate appeared to decrease, which we again attribute to bundling. To confirm that Fhod does not alter barbed-end elongation in the presence of profilin, we directly measured elongation rates using total internal reflection fluorescence (TIRF) microscopy. In agreement with our bulk assays, we detected no difference in elongation rates (Fig. 4, *A* and *B*). Human FHOD1 had a nearly identical effect on barbed-end elongation, slowing elongation in the absence of profilin and permitting elongation in the presence of profilin (Fig. 3, *E* and *F*).

Because we did not observe clear evidence of processive elongation by Fhod, we used several additional assays to verify and characterize the interaction between Fhod and barbed ends. We first verified barbed end binding in bulk barbed end depolymerization assays. The dose dependence gives us an additional measure of the affinity between Fhod and barbed ends. Fhod inhibited actin depolymerization with a K_d of 5 nM (Fig. 4, *C* and *D*), similar to our measurement from the seeded elongation assays. We then used actin reannealing assays, in which two colors of sheared actin filaments were mixed and allowed to reanneal. Fhod inhibited actin reannealing, indicating that it binds barbed ends and can remain bound on the timescale of minutes (Fig. 4*C*). Thus Fhod binds barbed ends tightly, like other formins, but does not accelerate elongation, unlike most formins.

Fhod antagonizes capping protein

We measured the ability of Fhod to antagonize capping protein, which binds tightly to barbed ends and prevents elongation. In bulk seeded elongation assays, 6 nM capping protein was sufficient to completely abolish actin elongation. Fhod abrogated this effect when added to F-actin seeds prior to capping protein (Fig. 5*A*). We fit these data to a competition binding equation to determine that Fhod has an apparent K_d of 7 nM for growing barbed ends (Fig. 5*B*), consistent with our previous measurements. Recent evidence suggests that formins can antagonize capping protein not only by passive competition for the barbed end but also by binding capped barbed ends and actively displacing capping protein (29, 30). However, filaments did not grow when capping protein was added before Fhod (data not shown), indicating that the actin elongation we observed was due to Fhod processively protecting the barbed end and not due to Fhod actively displacing capping protein from barbed ends.

We used TIRF microscopy to observe competition between Fhod and capping protein on individual filaments. We incubated seeds with Fhod prior to adding capping protein and actin monomers and then measured how long Fhod could protect the growing barbed ends. Consistent with our bulk assays, we found that barbed ends were completely capped by capping protein in the absence of Fhod but were able to grow in the presence of Fhod. Because the vast majority of filaments were capped by the time we could start imaging (2–3 min after the start of polymerization), we measured filament lengths in static images taken 5 min after addition of actin monomers (Fig. 5, *C* and *D*). By fitting the filament lengths to a single exponential curve, we determined that Fhod has a characteristic run length of 2 μm (Fig. 5*E*). This provides us with an approximate measure of Fhod processivity, with two assumptions: 1) capping protein binds to barbed ends as soon as Fhod dissociates, and 2) capping protein does not cap barbed ends that are already bound by Fhod. The first assumption is consistent with the strong affinity (~0.4 nM) of capping protein for barbed ends. However, the ability of capping protein to bind mDia1-bound barbed ends and displace mDia1 (29, 30) suggests that capping protein might also bind Fhod-bound barbed ends, which would make our measurement of Fhod processivity an underestimate.

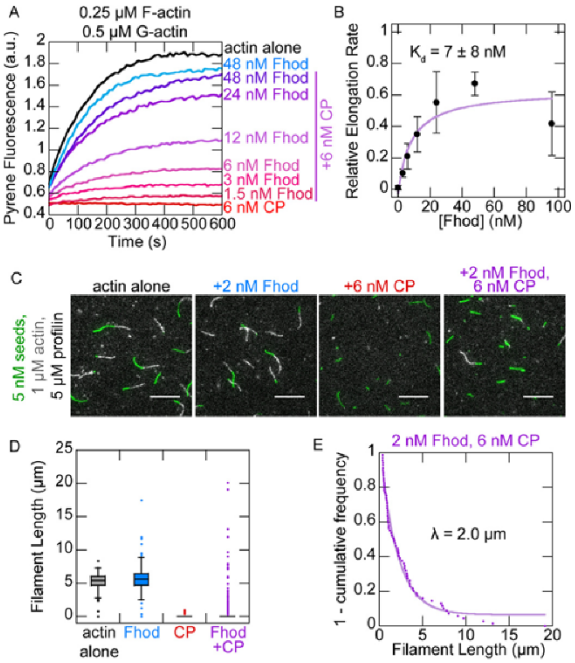

Figure 5. Fhod antagonizes capping protein. *A*, actin elongation from preformed seeds with a range of Fhod concentrations added before capping protein. Final conditions were 0.25 μM F-actin seeds (~0.4 nM barbed ends), 0.5 μM G-actin (10% pyrene-labeled), 1.5 μM *S. pombe* profilin, ± 6 nM mouse capping protein and 1.5–48 nM Fhod. *B*, quantification of elongation rates from *A*, measured as the initial slope over the first 90 s relative to the slope of actin alone. Fhod antagonizes capping protein, allowing elongation. Data with Fhod and capping protein were fit to a competition binding model to determine the affinity of Fhod to barbed ends. The data and reported K_d are means ± standard deviation from four independent experiments. The *binding curve* shows the best fit to the average values. *C*, observation of actin elongation (*white*) from preformed seeds (*green*) with Fhod added before capping protein. Final conditions were 5 nM F-actin seeds (1% biotinylated, labeled with Alexa Fluor 647-phalloidin), 1 μM G-actin (10% Alexa Fluor 594-labeled), 5 μM *S. pombe* profilin, ± 2 nM Fhod, and 6 nM capping protein. Images were taken 5 min after initiation of polymerization. *Scale bars*, 10 μm. *D*, quantification of filament lengths from *C*. The data represent the amount of elongation from preformed seeds ($n > 150$ for each condition). At least five fields of view from one (actin alone) or two (all other conditions) flow chambers were analyzed for each condition. In conditions with capping protein, no box is visible because over 75% of seeds did not elongate. *E*, exponential fit of filament lengths in the presence of both Fhod and capping protein from *D*, excluding seeds that did not elongate ($n = 69$ filaments from two flow chambers). Fhod has a characteristic run length of 2.0 μm.

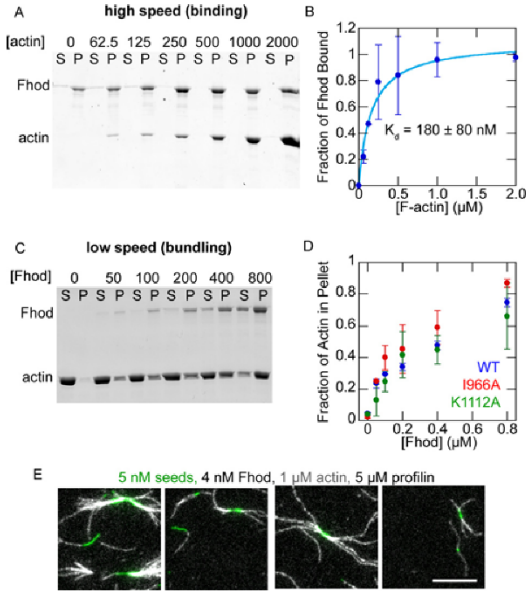

Figure 6. Fhod binds the sides of actin filaments and forms actin bundles. *A*, high-speed cosedimentation assay with 250 nM Fhod and the indicated concentrations of phalloidin-actin (in nM). *B*, quantification of *A*. The fraction of Fhod bound to F-actin was quantified by measuring the amount of Fhod in the pellet and correcting for the amount of Fhod that pellets in the absence of F-actin. The data and reported K_d are means ± standard deviation from three independent experiments. The *binding curve* shows the best fit to the average values. *C*, low-speed cosedimentation assay with 5 μM phalloidin-actin and the indicated concentrations of Fhod (in nM). *D*, quantification of *C*. The data are means ± standard deviation from two independent experiments. *E*, representative images of Fhod-induced actin bundles visualized by TIRF microscopy. Final conditions were 5 nM F-actin seeds (1% biotinylated, labeled with Alexa Fluor 647-phalloidin), 1 μM G-actin (10% Alexa Fluor 594-labeled), 5 μM *S. pombe* profilin, and 4 nM Fhod. Bundles elongate at both ends, indicating mixed or antiparallel polarity. *Scale bar*, 10 μm.

Fhod bundles actin filaments

Finally, we asked whether Fhod shares the capacity of other formins to bind the sides of actin filaments and bundle them. In high-speed cosedimentation experiments, Fhod pelleted with F-actin, demonstrating that Fhod binds the sides of actin filaments, with a K_d of 180 nM (Fig. 6, *A* and *B*). In low-speed cosedimentation, Fhod increased the amount of F-actin in the pellet, indicating that it forms actin bundles (Fig. 6, *C* and *D*). The I966A and K1112A mutations had no detectable effect on bundling activity (Fig. 6*D*). We used TIRF microscopy to determine the polarity of actin bundles formed by Fhod. Actin bundles typically elongated from both ends, indicating that the filaments in these bundles were not arranged exclusively in parallel (Fig. 6*E*).

Discussion

Here, we show that *Drosophila* Fhod shares the classic activities of formins, actin nucleation and processive elongation, with the additional capacity to bundle actin filaments. Our observation of actin assembly with both *Drosophila* Fhod and human FHOD1 contrasts substantially with the previous reports that mammalian FHOD proteins slow actin assembly *in vitro* (13, 21). We resolved these conflicting results for FHOD1 by showing that FHOD1 nucleates actin from *Acanthamoeba* effectively but does not nucleate actin from rabbit skeletal muscle. Our group previously reported a similar preference for the formin Delphilin, which nucleates cytoplasmic actin isoforms much more effectively than actin from rabbit skeletal muscle.[4] Although Delphilin is expressed exclusively in neurons and therefore unlikely to encounter sarcomeric actin isoforms, FHOD1 is expressed in both muscle and non-muscle cells. In cardiomyocytes, FHOD1 is largely excluded from the sarcomere, instead localizing primarily to the costamere and intercalated disc (16, 17). Therefore, the inability of FHOD1 to nucleate sarcomeric actin might be important to its function in this context.

The use of rabbit skeletal actin in previous work is unlikely to explain why FHOD3 did not nucleate *in vitro*, because FHOD3

is expressed predominantly in striated muscle and required for sarcomere assembly. Given the conserved role of FHOD family members in striated muscle, *Drosophila* Fhod and mammalian FHOD3 likely share a common mechanism in assembling sarcomeric actin. Although we find the cellular data with FHOD3 most suggestive of nucleation (12, 13), it remains possible that FHOD proteins instead stabilize or bundle filaments that are polymerized by a different actin nucleator. Flies carrying the I966A mutation, which abolishes nucleation and barbed end binding while retaining bundling activity, have relatively mild defects in sarcomere organization (23), supporting the possibility that the side binding and bundling activities of Fhod are more critical than nucleation or barbed end binding.

We did not observe evidence of accelerated barbed-end elongation with either Fhod or human FHOD1. This is not unprecedented, because some formins such as *Drosophila* Daam (31) and mouse FMNL1 (32) either slow barbed-end elongation or leave the elongation rate unchanged in the presence of profilin. We expect that both the FH1 and FH2 domains contribute to the inability of Fhod to accelerate barbed-end elongation. The slow barbed-end elongation in the absence of profilin is suggestive of an FH2 domain that spends most of the time in a closed conformation, similar to Cdc12 (33). The addition of profilin restores the elongation rate to that of actin alone, indicating that the FH1 domain has some ability to recruit profilin-actin but perhaps not as effectively as the FH1 domains of other formins. The effectiveness of polyproline tracks in the FH1 domain depends on the number of prolines and their distance from the FH2 domain (34, 35). The polyproline tracks of the Fhod FH1 domain are located relatively far from the FH2 domain, with the closest track (PPPMMPP) located 31 residues from the FH2 domain. For comparison, the weak elongator Cdc12 has its closest polyproline track 26 residues away from the FH2 domain, whereas the closest polyproline tracks of the strong elongators Bni1 and mDia1 are only 22 and 16 residues away, respectively.

We approximate that Fhod has a characteristic run length of 2 μm, which is equivalent to a dissociation rate of ~0.01 s^{-1} based on the elongation rate of 8 subunits/s. This dissociation rate is an order of magnitude faster than mDia1 and several orders of magnitude faster than mDia2, Bni1, Cdc12, and Capu (26, 36), which does not fit the general trend of faster elongation rates, resulting in faster dissociation rates (34). We observed evidence of Fhod protecting barbed ends only when experiments were performed in a tube, *i.e.* reannealing assays and when Fhod was incubated with seeds and actin monomers in a tube prior to introducing the mixture onto the surface. This suggests that the surface hinders Fhod processivity, making our measurement of Fhod processive elongation activity an underestimate. However, that Fhod is sensitive to conditions that do not perturb the processivity of other formins may indicate that processive elongation is not a critical activity of Fhod. FHOD family members generally localize to the relatively short actin filaments found in stress fibers and the sarcomere, which likely do not require accelerated barbed end growth. Therefore, Fhod nucleation and bundling activities might be more important in these contexts. We found that Fhod is indeed a potent actin bundler; its affinity of 0.18 μM for sides of actin filaments is comparable with the formins Fus1 (37) and AFH1 (38) and an order of magnitude stronger than mDia1 (39), Daam (31), and Capu (26). Alternatively, it is possible that Fhod accelerates actin elongation *in vivo* through collaborations with other proteins; for example, CLIP-170 was recently shown to augment the processive elongation of mDia1 (40).

Experimental procedures

Protein expression, purification, and labeling

cDNA for *Drosophila* Fhod isoform A (SD08909, obtained from the Drosophila Genomics Resource Center) and human FHOD1 (generous gift from T. Iskratsch) were used as templates to clone C-terminal constructs into a modified version of the pET-15b plasmid with an N-terminal His_6 tag. Point mutations were generated by site-directed mutagenesis as described (41). *Drosophila* Fhod constructs were transformed in Rosetta (DE3) cells (Novagen), which were grown in 1 liter of Terrific Broth supplemented with 100 mg/liter ampicillin and 32 mg/liter chloramphenicol. Expression was induced at an OD of 0.6–0.8 by adding 0.25 mM isopropyl β-D-thiogalactoside and shaking overnight at 18 °C. The cells were harvested by centrifugation, washed in PBS, and flash frozen in liquid nitrogen. Human FHOD1 was expressed in Rosetta 2 (DE3) cells induced with 0.5 mM isopropyl β-D-thiogalactoside as above.

Cell pellets expressing *Drosophila* Fhod were thawed in extraction buffer (10 mM MOPS, pH 7, 0.5% Triton X-100, 1 mM DTT, 1 mM PMSF, 2 μg/ml DNaseI). All subsequent steps were performed on ice or at 4 °C. The cells were lysed by microfluidizing, cleared by centrifugation at 20,000 × *g* for 20 min, and then purified using a HitrapSP-FF cation exchange column (GE Life Sciences) with a gradient of 0.3–1 M NaCl over 16 column volumes. Pooled fractions were diluted at least 6-fold into 10 mM Tris, pH 8, 1 mM DTT and further purified on a MonoQ anion exchange column (GE Life Sciences) with a gradient of 40–500 mM NaCl over 50 column volumes. Peak fractions were exchanged into storage buffer (10 mM Tris, pH 8, 150 mM NaCl, 1 mM DTT, 0–20% glycerol), centrifuged at 20,000 × *g* for 20 min, flash frozen in liquid nitrogen, and stored at −80 °C.

Cell pellets expressing human FHOD1 were resuspended in extraction buffer (50 mM sodium phosphate, pH 8, 300 mM NaCl, 1 mM βME) supplemented with PMSF and DNaseI and lysed as above. Clarified lysates were nutated with 1 ml of Talon resin (Clontech) per liter of culture for 1 h. Resin was washed with 20 column volumes of extraction buffer, followed by 20 column volumes of wash buffer (50 mM sodium phosphate, pH 7, 300 mM NaCl, 1 mM βME). Resin was washed twice for 30 min each with 20 column volumes of wash buffer supplemented with 10 mM $MgCl_2$ and 5 mM ATP. FHOD1 was eluted with 200 mM imidazole in wash buffer. Eluted protein was dialyzed into 10 mM MOPS, pH 7, 200 mM NaCl, 1 mm DTT, and then run on a Mono S cation exchange column (GE Life Sciences) with a gradient of 0.2–1 M NaCl over 32 column volumes. Peak fractions were dialyzed overnight into storage buffer (10 mM Tris, pH 8, 150 mM NaCl, 1 mM DTT), centrifuged at 20,000 × *g* for 20 min, flash frozen in liquid nitrogen, and stored at −80 °C. Actin assembly activity remained stable after freeze-thaw or up to 4 days on ice.

Drosophila Fhod protein concentrations were determined using the absorbance at 280 nm with an extinction coefficient of 122,840 M^{-1} cm^{-1} (ProtParam), which was verified by comparing the absorbances of native and denatured protein. The concentration of human FHOD1 was determined by quantitative Sypro Red staining. All *Drosophila* Fhod and human FHOD1 concentrations are reported in terms of dimer concentrations.

Acanthamoeba castellani actin was purified (42) and labeled with pyrene iodoacetamide (42), Alexa Fluor 594 succinimidyl ester (43), or EZ-link maleimide-PEG2-biotin (Thermo Scientific) (44) according to published protocols. Unlabeled and pyrene-labeled rabbit skeletal actin were kindly provided by the Reisler laboratory (University of California, Los Angeles). *Schizosaccharomyces pombe* profilin was purified as described (32) on a polyproline column provided by the Reisler laboratory. The concentration was determined using the absorbance at 280 nm with an extinction coefficient of 1.63 OD/mg/ml (45). Mouse capping protein was purified as described (46).

Pyrene assays

Pyrene assays were performed essentially as described (47) on an Infinite 200 Pro plate reader (Tecan). In all assays, Fhod was diluted in storage buffer before addition to polymerization buffer to improve stability. The concentration of barbed ends was calculated from the slope (obtained by linear regression over 90 s) using the equation [be] = elongation rate/(k_+[G-actin] − k_-), where $k_+ = 11.6\ \mu M^{-1}\ s^{-1}$, and $k_- = 1.4\ s^{-1}$ (48). For seeded elongation assays, actin filaments were sheared by passing three times through a 24-gauge needle and then aliquoted into each well of a microplate. Proteins were added to the seeds and incubated for 2–4 min at room temperature; in experiments with both Fhod and capping protein, capping protein was added 2–4 min after addition of Fhod. Seeds and additional proteins in KMEH (10 mM HEPES, pH 7, 1 mM EGTA, 50 mM KCl, 1 mM $MgCl_2$) were added to magnesium-actin to initiate actin elongation. Elongation rates were determined by linear regression over the first 90 s and normalized against the rate of actin alone in each experiment. For experiments without capping protein, the affinity of Fhod for barbed ends was determined by fitting the data to the simplified binding equation, r = [Fhod]/([Fhod] + K_d) * a + b, where r is the normalized elongation rate. The data for capping protein experiments were analyzed using a competition binding model (49). The following equation was used to determine the K_d of Fhod for growing barbed ends,

$$r = \left(1 - \frac{1}{K_{d1}\dfrac{[\text{Fhod}] + K_{d2}}{K_{d2}\,R_0} + 1}\,\frac{[\text{CP}]}{[\text{be}]}\right) \times a + b \qquad \text{(Eq. 1)}$$

where r is the normalized elongation rate, K_{d1} is the affinity of capping protein for barbed ends (0.4 nM, measured in a seeded elongation assay in the absence of Fhod), K_{d2} is the affinity of Fhod for barbed ends, and R_0 is the concentration of free barbed ends when [Fhod] = 0. The total concentration of barbed ends was calculated from the initial slope of the polymerization trace for actin alone as described above.

For depolymerization assays, 1 μM F-actin (70% pyrene-labeled) was incubated for at least 15 min at room temperature and then depolymerized by diluting 10-fold in 1× KMEH with additional proteins. The depolymerization rate was determined by linear regression over the first 90 s. The affinity of Fhod for barbed ends was determined by fitting the data to the simplified binding equation as above.

TIRF microscopy

In nucleation assays, assembly of 2 μM actin was initiated by the addition of KMEH with or without Fhod. After 5 min, actin was removed from the reaction and stabilized by diluting 10-fold in 1× KMEH containing Alexa Fluor 488-phalloidin. Actin was incubated with phalloidin for 10 min, diluted 20-fold in 1× KMEH supplemented with 100 mM DTT, spotted on a poly-L-lysine-coated coverslip, and imaged. All steps were performed as delicately as possible with cut pipette tips to minimize shearing.

For elongation experiments, biotinylated coverslips were prepared as follows. Coverslips were rinsed three times in MilliQ water, placed in 2% Hellmanex (Hellma Analytics) at 60–65 °C for 2 h, and then rinsed another five times in MilliQ water. Once dry, the coverslips were silanized with (3-glycidyloxypropyl)trimethoxysilane for 1 h in a hybridization oven. Unreacted (3-glycidyloxypropyl)trimethoxysilane was removed by rinsing three times with acetone. Coverslips were then PEGylated with a mixture of methoxy-PEG-NHS and biotin-PEG-NHS as described (47).

Flow chambers of ~15 μl were assembled on the slide using strips of double-sided tape. Flow chambers were prepared with the following steps: 1) block with 25 μl of 1% Pluronic F-127 (Sigma), 50 μg/ml casein, in PBS, for 2 min; 2) 25 μl of 1× KMEH; 3) 25 μl of 40 nM streptavidin in 1× KMEH; 4) 25 μl of 1× TIRF buffer (1× KMEH, 0.5% methylcellulose (400 cP, Sigma), 50 mM DTT, 0.2 mM ATP, 20 mM glucose); 5) 50 μl of magnesium-actin and additional proteins to be assayed, in 1× TIRF buffer supplemented with 5 nM F-actin seeds (1% biotinylated, stabilized with Alexa Fluor 647-phalloidin), 250 μg/ml glucose oxidase, 50 μg/ml catalase, and 50 μg/ml casein. Fhod was incubated with seeds for at least 30 s prior to addition of magnesium-actin; in experiments with both Fhod and capping protein, Fhod was incubated with seeds for 15 s prior to addition of capping protein, and magnesium-actin was added after an additional 30 s.

To determine the characteristic run length of Fhod on barbed ends in the presence of capping protein, 1 − cumulative frequency was treated as the fraction of filaments that were still elongating at a particular length. The data were fit to the exponential equation, $1 - cf = e^{\,l/\lambda} * a + b$, where cf is the cumulative frequency, l is the filament length, and λ is the characteristic run length.

Reannealing assays were conducted essentially as described (50) using Alexa Fluor 488- or rhodamine-labeled phalloidin-actin, sheared by passing three times through a 27-gauge needle. The final concentrations were 250 nM F-actin and 10 nM Fhod. The samples were diluted 50-fold, spotted on poly-L-lysine-coated coverslips, and imaged.

In all experiments, actin filaments were visualized on a DMI6000 TIRF microscope (Leica) with an HCX PL APO

objective (100× magnification, N.A. = 1.47), and an Andor DU-897 camera, using the Leica application suite advanced fluorescence software. The experiments were conducted at room temperature. The images were obtained at 10-s intervals for 10 min. The images were processed by applying rolling ball background subtraction and a Gaussian filter. Filament lengths were quantified using the JFilament plugin for Fiji (51).

Cosedimentation

For high-speed cosedimentation, 250 nM Fhod was incubated with varying concentrations of phalloidin-stabilized F-actin for 30 min at room temperature. Samples were centrifuged at 90,000 rpm for 25 min in a TLA-100 rotor. Pellets were concentrated by resuspending in one-fourth the original volume. The supernatants and pellets were analyzed with SDS-PAGE, and the gels were stained with SyproRed. The amount of Fhod in each fraction was quantified using QuantityOne software, dividing the intensities of pellet bands by four to correct for the 4-fold concentration of pellets with resuspension. The fraction of Fhod bound to F-actin was calculated by adjusting for the amount of Fhod that pellets in the absence of F-actin with the following equation: $\theta = (p - p_0)/(1 - p_0)$, where θ is the fraction of Fhod bound to F-actin, p is the fraction of Fhod in the pellet, and p_0 is the fraction of Fhod in the pellet in the absence of F-actin. The affinity of Fhod for F-actin was determined by fitting the data to the binding equation, $\theta = [\text{F-actin}]/([\text{F-actin}] + K_d) * a + b$.

For low-speed cosedimentation, Fhod was incubated with phalloidin-stabilized actin filaments (final concentration, 5 μM) for 1 h at room temperature and then centrifuged at 12,000 × g for 15 min. The amount of actin in the supernatants and pellets was quantified by Coomassie-staining SDS-PAGE gels.

Author contributions—A. A. P., Z. A. O. D., A. P. v. L., and M. E. Q. designed the experiments. A. A. P., Z. A. O. D., A. P. v. L., and K. V. B. performed the experiments. A. A. P. and M. E. Q. wrote the manuscript with input from all authors.

Acknowledgments—We thank members of the Quinlan lab for feedback, the Reisler labs for valuable discussions and reagents, and Thomas Iskratsch for human FHOD1 cDNA.

References

1. Goode, B. L., and Eck, M. J. (2007) Mechanism and function of formins in the control of actin assembly. *Annu. Rev. Biochem.* **76,** 593–627 CrossRef Medline
2. Gasteier, J. E., Madrid, R., Krautkrämer, E., Schröder, S., Muranyi, W., Benichou, S., and Fackler, O. T. (2003) Activation of the Rac-binding partner FHOD1 induces actin stress fibers via a ROCK-dependent mechanism. *J. Biol. Chem.* **278,** 38902–38912 CrossRef Medline
3. Schulze, N., Graessl, M., Blancke Soares, A., Geyer, M., Dehmelt, L., and Nalbant, P. (2014) FHOD1 regulates stress fiber organization by controlling the dynamics of transverse arcs and dorsal fibers. *J. Cell Sci.* **127,** 1379–1393 CrossRef Medline
4. Takeya, R., Taniguchi, K., Narumiya, S., and Sumimoto, H. (2008) The mammalian formin FHOD1 is activated through phosphorylation by ROCK and mediates thrombin-induced stress fibre formation in endothelial cells. *EMBO J.* **27,** 618–628 CrossRef Medline
5. Jurmeister, S., Baumann, M., Balwierz, A., Keklikoglou, I., Ward, A., Uhlmann, S., Zhang, J. D., Wiemann, S., and Sahin Ö. (2012) MicroRNA-200c represses migration and invasion of breast cancer cells by targeting actin-regulatory proteins FHOD1 and PPM1F. *Mol. Cell. Biol.* **32,** 633–651 CrossRef Medline
6. Iskratsch, T., Yu, C. H., Mathur, A., Liu, S., Stévenin, V., Dwyer, J., Hone, J., Ehler, E., and Sheetz, M. (2013) FHOD1 is needed for directed forces and adhesion maturation during cell spreading and migration. *Dev. Cell* **27,** 545–559 CrossRef Medline
7. Koka, S., Neudauer, C. L., Li, X., Lewis, R. E., McCarthy, J. B., and Westendorf, J. J. (2003) The formin-homology-domain-containing protein FHOD1 enhances cell migration. *J. Cell Sci.* **116,** 1745–1755 CrossRef Medline
8. Gardberg, M., Kaipio, K., Lehtinen, L., Mikkonen, P., Heuser, V. D., Talvinen, K., Iljin, K., Kampf, C., Uhlen, M., Grénman, R., Koivisto, M., and Carpén, O. (2013) FHOD1, a formin upregulated in epithelial-mesenchymal transition, participates in cancer cell migration and invasion. *PLoS One* **8,** e74923 CrossRef Medline
9. Paul, N. R., Allen, J. L., Chapman, A., Morlan-Mairal, M., Zindy, E., Jacquemet, G., Fernandez del Ama, L., Ferizovic, N., Green, D. M., Howe, J. D., Ehler, E., Hurlstone, A., and Caswell, P. T. (2015) $\alpha5\beta1$ integrin recycling promotes Arp2/3-independent cancer cell invasion via the formin FHOD3. *J. Cell Biol.* **210,** 1013–1031 CrossRef Medline
10. Monzo, P., Chong, Y. K., Guetta-Terrier, C., Krishnasamy, A., Sathe, S. R., Yim, E. K., Ng, W. H., Ang, B. T., Tang, C., Ladoux, B., Gauthier, N. C., and Sheetz, M. P. (2016) Mechanical confinement triggers glioma linear migration dependent on formin FHOD3. *Mol. Biol. Cell.* **27,** 1246–1261 CrossRef Medline
11. Krainer, E. C., Ouderkirk, J. L., Miller, E. W., Miller, M. R., Mersich, A. T., and Blystone, S. D. (2013) The multiplicity of human formins: Expression patterns in cells and tissues. *Cytoskeleton* **70,** 424–438 CrossRef Medline
12. Iskratsch, T., Lange, S., Dwyer, J., Kho, A. L., dos Remedios, C., and Ehler, E. (2010) Formin follows function: a muscle-specific isoform of FHOD3 is regulated by CK2 phosphorylation and promotes myofibril maintenance. *J. Cell Biol.* **191,** 1159–1172 CrossRef Medline
13. Taniguchi, K., Takeya, R., Suetsugu, S., Kan-O, M., Narusawa, M., Shiose, A., Tominaga, R., and Sumimoto, H. (2009) Mammalian formin Fhod3 regulates actin assembly and sarcomere organization in striated muscles. *J. Biol. Chem.* **284,** 29873–29881 CrossRef Medline
14. Fujimoto, N., Kan-O, M., Ushijima, T., Kage, Y., Tominaga, R., Sumimoto, H., and Takeya, R. (2016) Transgenic expression of the formin protein Fhod3 selectively in the embryonic heart: role of actin-binding activity of Fhod3 and its sarcomeric localization during myofibrillogenesis. *PLoS One* **11,** e0148472 CrossRef Medline
15. Kan-o, M., Takeya, R., Taniguchi, K., Tanoue, Y., Tominaga, R., and Sumimoto, H. (2012) Expression and subcellular localization of mammalian formin Fhod3 in the embryonic and adult heart. *PLoS One* CrossRef
16. Al Haj, A., Mazur, A. J., Radaszkiewicz, K., Radaszkiewicz, T., Makowiecka, A., Stopschinski, B. E., Schönichen, A., Geyer, M., and Mannherz, H. G. (2015) Distribution of formins in cardiac muscle: FHOD1 is a component of intercalated discs and costameres. *Eur. J. Cell Biol.* **94,** 101–113 CrossRef Medline
17. Dwyer, J., Pluess, M., Iskratsch, T., dos Remedios, C. G., and Ehler, E. (2014) The formin FHOD1 in cardiomyocytes. *Anat. Rec. (Hoboken)* **297,** 1560–1570 CrossRefMedline
18. Wooten, E. C., Hebl, V. B., Wolf, M. J., Greytak, S. R., Orr, N. M., Draper, I., Calvino, J. E., Kapur, N. K., Maron, M. S., Kullo, I. J., Ommen, S. R., Bos, J. M., Ackerman, M. J., and Huggins, G. S. (2013) Formin homology 2 domain containing 3 variants associated with hypertrophic cardiomyopathy. *Circ. Cardiovasc. Genet.* **6,** 10–18 CrossRef Medline
19. Arimura, T., Takeya, R., Ishikawa, T., Yamano, T., Matsuo, A., Tatsumi, T., Nomura, T., Sumimoto, H., and Kimura, A. (2013) Dilated cardiomyopathy-associated FHOD3 variant impairs the ability to induce activation of transcription factor serum response factor. *Circ. J.* **77,** 2990–2996 CrossRef Medline
20. Esslinger, U., Garnier, S., Korniat, A., Proust, C., Kararigas, G., Müller-Nurasyid, M., Empana, J.-P., Morley, M. P., Perret, C., Stark, K., Bick, A. G., Prasad, S. K., Kriebel, J., Li, J., Tiret, L., *et al.* (2017) Exome-wide association study reveals novel susceptibility genes to sporadic dilated cardiomyopathy. *PLoS One* **12,** e0172995 CrossRef Medline

21. Schönichen, A., Mannherz, H. G., Behrmann, E., Mazur, A. J., Kühn, S., Silván, U., Schoenenberger, C.-A., Fackler, O. T., Raunser, S., Dehmelt, L., and Geyer, M. (2013) FHOD1 is a combined actin filament capping and bundling factor that selectively associates with actin arcs and stress fibers. *J. Cell Sci.* **126,** 1891–1901 CrossRef Medline
22. Lammel, U., Bechtold, M., Risse, B., Berh, D., Fleige, A., Bunse, L., Jiang, X., Klämbt, C., and Bogdan, S. (2014) The *Drosophila* FHOD1-like formin Knittrig acts through Rok to promote stress fiber formation and directed macrophage migration during the cellular immune response. *Development* **141,** 1366–1380 CrossRef Medline
23. Shwartz, A., Dhanyasi, N., Schejter, E. D., and Shilo, B.-Z. (2016) The *Drosophila* formin Fhos is a primary mediator of sarcomeric thin-filament array assembly. *Elife* **5,** e16540 Medline
24. Kucherenko, M. M., Marrone, A. K., Rishko, V. M., Magliarelli, H. F., and Shcherbata, H. R. (2011) Stress and muscular dystrophy: A genetic screen for Dystroglycan and Dystrophin interactors in *Drosophila* identifies cellular stress response components. *Dev. Biol.* **352,** 228–242 CrossRef Medline
25. Xu, Y., Moseley, J. B., Sagot, I., Poy, F., Pellman, D., Goode, B. L., and Eck, M. J. (2004) Crystal structures of a formin homology-2 domain reveal a tethered dimer architecture. *Cell* **116,** 711–723 CrossRef Medline
26. Vizcarra, C. L., Bor, B., and Quinlan, M. E. (2014) The role of formin tails in actin nucleation, processive elongation, and filament bundling. *J. Biol. Chem.* **289,** 30602–30613 CrossRef Medline
27. Gould, C. J., Maiti, S., Michelot, A., Graziano, B. R., Blanchoin, L., and Goode, B. L. (2011) The formin DAD domain plays dual roles in autoinhibition and actin nucleation. *Curr. Biol.* **21,** 384–390 CrossRef Medline
28. Ramabhadran, V., Gurel, P. S., and Higgs, H. N. (2012) Mutations to the formin homology 2 domain of INF2 protein have unexpected effects on actin polymerization and severing. *J. Biol. Chem.* **287,** 34234–34245 CrossRef Medline
29. Bombardier, J. P., Eskin, J. A., Jaiswal, R., Corrêa, I. R., Jr., Xu, M.-Q., Goode, B. L., and Gelles, J. (2015) Single-molecule visualization of a formin-capping protein "decision complex" at the actin filament barbed end. *Nat. Commun.* **6,** 8707 CrossRef Medline
30. Shekhar, S., Kerleau, M., Kühn, S., Pernier, J., Romet-Lemonne, G., Jégou, A., and Carlier, M.-F. (2015) Formin and capping protein together embrace the actin filament in a ménage à trois. *Nat. Commun.* **6,** 8730 CrossRef Medline
31. Barkó, S., Bugyi, B., Carlier, M. F., Gombos, R., Matusek, T., Mihály, J., and Nyitrai, M. (2010) Characterization of the biochemical properties and biological function of the formin homology domains of *Drosophila* DAAM. *J. Biol. Chem.* **285,** 13154–13169 CrossRef Medline
32. Harris, E. S., Li, F., and Higgs, H. N. (2004) The mouse formin, FRLα, slows actin filament barbed end elongation, competes with capping protein, accelerates polymerization from monomers, and severs filaments. *J. Biol. Chem.* **279,** 20076–20087 CrossRef Medline
33. Kovar, D. R., Kuhn, J. R., Tichy, A. L., and Pollard, T. D. (2003) The fission yeast cytokinesis formin Cdc12p is a barbed end actin filament capping protein gated by profilin. *J. Cell Biol.* **161,** 875–887 CrossRef Medline
34. Paul, A. S., and Pollard, T. D. (2008) The role of the FH1 domain and profilin in formin-mediated actin-filament elongation and nucleation. *Curr. Biol.* **18,** 9–19 CrossRef Medline
35. Courtemanche, N., and Pollard, T. D. (2012) Determinants of formin homology 1 (FH1) domain function in actin filament elongation by formins. *J. Biol. Chem.* **287,** 7812–7820 CrossRef Medline
36. Kovar, D. R., Harris, E. S., Mahaffy, R., Higgs, H. N., and Pollard, T. D. (2006) Control of the assembly of ATP- and ADP-actin by formins and profilin. *Cell.* **124,** 423–435 CrossRef Medline
37. Scott, B. J., Neidt, E. M., and Kovar, D. R. (2011) The functionally distinct fission yeast formins have specific actin-assembly properties. *Mol. Biol. Cell.* **22,** 3826–3839 CrossRef Medline
38. Michelot, A., Guérin, C., Huang, S., Ingouff, M., Richard, S., Rodiuc, N., Staiger, C. J., and Blanchoin, L. (2005) The formin homology 1 domain modulates the actin nucleation and bundling activity of *Arabidopsis* FORMIN1. *Plant Cell* **17,** 2296–2313 CrossRef Medline
39. Li, F., and Higgs, H. N. (2003) The mouse formin mDia1 is a potent actin nucleation factor regulated by autoinhibition. *Curr. Biol.* **13,** 1335–1340 CrossRef Medline
40. Henty-Ridilla, J. L., Rankova, A., Eskin, J. A., Kenny, K., and Goode, B. L. (2016) Accelerated actin filament polymerization from microtubule plus ends. *Science* **352,** 1004–1009 CrossRef Medline
41. Liu, H., and Naismith, J. H. (2008) An efficient one-step site-directed deletion, insertion, single and multiple-site plasmid mutagenesis protocol. *BMC Biotechnol.* **8,** 91 CrossRef Medline
42. Zuchero, J. B. (2007) *In vitro* actin assembly assays and purification from *Acanthamoeba*. *Methods Mol. Biol.* **370,** 213–226 CrossRef Medline
43. Grintsevich, E. E., Yesilyurt, H. G., Rich, S. K., Hung, R. J., Terman, J. R., and Reisler, E. (2016) F-actin dismantling through a redox-driven synergy between Mical and cofilin. *Nat. Cell Biol.* **18,** 876–885 CrossRef Medline
44. Roth-Johnson, E. A., Vizcarra, C. L., Bois, J. S., and Quinlan, M. E. (2014) Interaction between microtubules and the *Drosophila* formin cappuccino and its effect on actin assembly. *J. Biol. Chem.* **289,** 4395–4404 CrossRef Medline
45. Lu, J., and Pollard, T. D. (2001) Profilin binding to poly-L-proline and actin monomers along with ability to catalyze actin nucleotide exchange is required for viability of fission yeast. *Mol. Biol. Cell.* **12,** 1161–1175 CrossRef Medline
46. Palmgren, S., Ojala, P. J., Wear, M. A., Cooper, J. A., and Lappalainen, P. (2001) Interactions with PIP2, ADP-actin monomers, and capping protein regulate the activity and localization of yeast twinfilin. *J. Cell Biol.* **155,** 251–260 CrossRef Medline
47. Bor, B., Vizcarra, C. L., Phillips, M. L., and Quinlan, M. E. (2012) Autoinhibition of the formin Cappuccino in the absence of canonical autoinhibitory domains. *Mol. Biol. Cell.* **23,** 3801–3813 CrossRef Medline
48. Pollard, T. D. (1986) Rate constants for the reactions of ATP-and ADP-actin with the ends of actin filaments. *J. Cell Biol.* **103,** 2747–2754 CrossRef Medline
49. Vinson, V. K., De La Cruz, E. M., Higgs, H. N., and Pollard, T. D. (1998) Interactions of *Acanthamoeba* profilin with actin and nucleotides bound to actin. *Biochemistry* **37,** 10871–10880 CrossRef Medline
50. Vizcarra, C. L., Kreutz, B., Rodal, A. A., Toms, A. V., Lu, J., Zheng, W., Quinlan, M. E., and Eck, M. J. (2011) Structure and function of the interacting domains of Spire and Fmn-family formins. *Proc. Natl. Acad. Sci. U.S.A.* **108,** 11884–11889 CrossRef Medline
51. Smith, M. B., Li, H., Shen, T., Huang, X., Yusuf, E., and Vavylonis, D. (2010) Segmentation and tracking of cytoskeletal filaments using open active contours. *Cytoskeleton* **67,** 693–705 CrossRef Medline

Chapter 3: Multiple domains impair processive elongation by *Drosophila* Fhod

Introduction

Formins processively elongate actin filaments through the combined action of their FH1 and FH2 domains. The FH2 domain homodimerizes to form a donut shape, which binds the dynamic barbed end of the actin filament. The FH2 domain fluctuates between an “open” state that permits addition of an actin monomer and a “closed” state that prevents addition of a monomer in a process known as gating (Otomo et al., 2005; Vavylonis et al., 2006). With each addition of an actin monomer, the FH2 domain must take a step, with one hemidimer sliding past the other, to remain on the barbed end. The FH2 domain processively tracks the barbed end but cannot accelerate the elongation rate on its own; the FH2 domains of most formins slow elongation due to their gating. The FH1 domain enables barbed end elongation through its polyproline tracks, which bind the actin-binding protein profilin to deliver actin monomers to the barbed end. Through this mechanism, formins can accelerate barbed end elongation by over five-fold (Courtemanche, 2018).

In most formins, the FH2 domain is flanked by a disordered tail on the C-terminal side. The C-terminal tail enhances actin assembly in several formins, including *Drosophila* Capu and mammalian mDia1 and INF2 (Gould et al., 2011; Ramabhadran et al., 2012; Vizcarra et al., 2014). The tail of Capu enhances both nucleation and processivity; these effects of the tail are retained after scrambling the sequence of the tail, and gradually lost as the tail is truncated. These findings suggest that the effect of the tail arises from charge interactions between the positively charged tail and negatively charged actin (Vizcarra et al., 2014). Capu, like most well studied formins, is a potent actin elongator, increasing the barbed end elongation rate by at least five-fold over run lengths of hundreds of microns (Vizcarra et al., 2014). In stark contrast,

we identified another *Drosophila* formin, Fhod, that elongates much less effectively, with no detectable effect on elongation rate and a characteristic run length of 2 μm (Chapter 2). In this chapter, we asked whether the effects we observed for Capu's C-terminal tail would also apply to Fhod.

Drosophila Fhod undergoes extensive alternative splicing, which alter the N-terminus and C-terminal tail while maintaining constant FH1 and FH2 domains between all isoforms. In previous work, we used the canonical Fhod isoform A, which is sufficient to rescue viability and hemocyte motility in flies (Lammel et al., 2014). This isoform has an identical C-terminus to isoforms H and I, which are sufficient for sarcomere assembly in indirect flight muscle (Shwartz et al., 2016). Three Fhod splice isoforms (B, D, and E) differ from Fhod-A only by their C-terminal tails.

Here, we took advantage of Fhod splice variants to test how the C-terminal tail of Fhod modulates processive elongation. Unexpectedly, we found that Fhod-B, with a 30 amino acid tail, processively elongates filaments over much longer run lengths than Fhod-A, with a 129 amino acid tail, and Fhod-E, with a 123 amino acid tail. We mapped the region of the Fhod-A tail impairing processivity to the last 24 amino acids and found that the Fhod-A tail binds tightly to filament sides. Finally, we show preliminary data suggesting that the Fhod N-terminus impairs processive elongation through a distinct mechanism, dimerizing the FH1 domains to limit their rate of profilin-actin capture. Taken together, this work establishes multiple mechanisms by which domains beyond the FH1 and FH2 domains determine formin elongation rate and processivity.

Results

The Fhod tail impairs processivity.

We purified the C-terminal halves of three Fhod isoforms (A, B, and E), including their shared FH1 and FH2 domains and their varying C-terminal tails (Figure 3.1). All three isoforms

nucleated actin with similar activity (Figure 3.2). We then asked how the differences in their C-terminal tails would influence processivity. Typically, processive elongation by formins can be directly observed by total internal reflection fluorescence (TIRF) microscopy. Formin-bound filaments elongate several fold faster and appear dimmer than unbound filaments (Kovar et al., 2006) due to the reduced affinity of profilin for Cys 374-labeled actin (Vinson et al., 1998). We previously found that Fhod-A has a relatively low characteristic run length of ~2 μm (Chapter 2); consistent with our previous results, we could not detect any difference in elongation rate or fluorescence intensity when filaments were grown in the presence of Fhod-A. We similarly observed no evidence of processive elongation by Fhod-E. In stark contrast, we observed robust processive elongation by Fhod-B, based on the dim appearance of growing actin filaments (Figure 3.3). Dim-appearing filaments associated with Fhod-B elongated at a rate of ~17 subunits per second, 3-4 fold faster than unbound filaments, with a characteristic run length of 23 μm (Figure 3.4). Our measurement of the characteristic run length is likely an underestimate, since most processive runs extended beyond 50 μm and were too long to be measured accurately. Because Fhod-B is simply a truncated form of isoforms A and E, we concluded that the C-terminal tails of isoforms A and E impair their processivity.

To map which region of the tail impairs processivity, we gradually truncated the C-terminal tail of Fhod-A, resulting in tails that are intermediate between Fhod-A and Fhod-B. We found that truncating the last 24 residues of Fhod-A (equivalent to truncating the last 18 residues of Fhod-E) restored processivity to that of Fhod-B, with further truncation having no major additional effect on processivity (Figure 3.5). If the C-terminal tail adopted a secondary structure, any truncation might impair the function of the tail simply by disrupting the structure. To rule out this possibility, we analyzed the circular dichroism (CD) spectra of each isoform's tail. We found that all three tails lacked secondary structure on their own (Figure 3.6), suggesting that truncation of the tail would not disrupt any secondary structure.

The tails of poorly processive Fhod isoforms bind tightly to filament sides

We considered several models to explain how the C-terminal tails of Fhod-A and -E impair processivity. We previously proposed for Capu that the interaction between the tail and the side of the filament keeps the FH2 domain in close proximity to the barbed end, allowing it to return to the barbed end after dissociating (Vizcarra et al., 2014). This logic leads to the first two models: (1) The Fhod-A and -E tails might reduce the affinity for filament sides relative to Fhod-B. (2) The tails might associate too tightly to filament sides, causing the FH2 domain to slip off the barbed end and remain on the side of the filament. We considered two alternative models: (3) The larger tails might sterically clash with the actin filament, resulting in a force that promotes dissociation from the barbed end. (4) The tails might interact with the FH2 domain, disrupting its ability to interact with the barbed end or step after an actin subunit is incorporated into the filament.

To test the validity of models 1 and 2, we measured the affinity of the tails for F-actin in high speed cosedimentation assays. Because the Fhod-A tail was prone to degradation, we focused our comparison on isoforms B and E. We found that the Fhod-E tail binds tightly to F-actin with a K_d of 80 nM, whereas the Fhod-B tail had no detectable interaction with F-actin (Figure 3.7A-B). Our preliminary data indicate that the Fhod-A tail also binds F-actin with sub-micromolar affinity (data not shown). In contrast, the Capu tail binds F-actin with a K_d of 6 µM (Vizcarra et al., 2014), at least an order of magnitude weaker than the tails of Fhod-A and Fhod-E. Taken together, these data are consistent with model 2 but rule out model 1, since isoforms A and E lack processivity despite binding filament sides more tightly than the processive formins Fhod-B and Capu.

To test model 4, we monitored processive elongation by Fhod-B in the presence of the Fhod-E tail. If model 4 were correct, we predicted that the purified Fhod-E tail would interact with the Fhod-B FH2 domain, impairing processivity. We were still able to observe dim actin

filaments suggestive of processive elongation in the presence of the Fhod-E tail (Figure 3.7C). Therefore, our preliminary data do not support model 4.

A putative coiled-coil in the N-terminus slows processive elongation

Having established that the C-terminal tail can impair processive elongation by Fhod, we asked whether the region N-terminal to the FH1 domain also modulates elongation. This region includes a predicted coiled coil based on the secondary structure prediction software JPred (Drozdetskiy et al., 2015). We hypothesized that a dimerization domain N-terminal to the FH1 domains would restrict their diffusive movement, altering the rates of profilin-actin capture and delivery. To test whether this region in fact dimerizes, we mutated a conserved tryptophan (W898A), which is essential for dimerization of the FH2 domain (Xu et al., 2004), and asked whether the N-terminus could hold the two hemidimers in place in the absence of a dimerized FH2 domain. We used pyrene actin assembly assays to validate that the W898A mutation disrupted FH2 dimerization in the absence of the putative coiled coil, resulting in an inability to nucleate actin (Figure 3.8A). Unexpectedly, we found that the W898A mutation had no effect on actin nucleation in the presence of the putative coiled coil (Figure 3.8B). This result suggests that although the W898A mutation weakens the interaction between two hemidimers, it can be overcome by an additional dimerization domain bringing the two hemidimers in closer proximity. To confirm that this effect was not simply due to the coiled coil nucleating actin, we purified this domain alone. The coiled coil did not affect actin assembly (Figure 3.8C), suggesting that it overcomes the W898A mutation by dimerizing the FH2 domain rather than by nucleating actin itself.

We compared barbed end elongation rates of Fhod-B CT to those of cc Fhod-B CT, which includes the coiled coil in addition to the FH1 domain, FH2 domain, and short C-terminal tail. We found that cc Fhod-B CT also processively elongates barbed ends, but at a ~35% slower rate than Fhod-B CT without the putative coiled coil (Figure 3.8D). To ask whether this

decrease in elongation rate was caused by dimerization of the N-terminus, we compared mathematical simulations of FH1-mediated elongation (Bryant et al., 2017) with or without an N-terminal dimerization domain. In our model, FH1-mediated elongation consists of two steps, capture (profilin-actin binding a polyproline track in the FH1 domain) and delivery (profilin-actin binding the barbed end). Compared to the original model, the model including an N-terminal dimerization domain had slower capture rates (Figure 3.9A) but faster delivery rates (Figure 3.9B). Because capture rates are much slower than delivery rates, the effect of N-terminal dimerization on capture rate dominates. Therefore, the overall polymerization rate was slowed by the N-terminal dimerization (Figure 3.9C). The mathematical predictions follow our experimental observation, suggesting that dimerization is sufficient to explain why the Fhod N-terminus slows elongation.

Discussion

Formins are generally known for their ability to both nucleate and processively elongate actin filaments, resulting in long, unbranched bundles of actin filaments (Goode and Eck, 2007). In contrast, Fhod family members associate with the sides rather than the ends of actin filaments across a range of biological contexts (Fenix et al., 2018; Kan-o et al., 2012; Mi-Mi et al., 2012; Schonichen et al., 2013; Schulze et al., 2014; Shwartz et al., 2016). Although processive barbed end binding is primarily a function of the FH2 domain, we show here that the rapid dissociation of *Drosophila* Fhod from the barbed end is a result of the C-terminal tail rather than a defect in the FH2 domain. In other formins, the formin C-terminal tail enhances actin assembly through interactions with actin monomers and filaments (Gould et al., 2011; Vizcarra et al., 2014). In contrast, the tails of Fhod isoforms A and E inhibit processive elongation, despite (or because of) their strong affinity for actin filaments, suggesting that the Fhod tails play a different role from other formin tails.

We observed a negative correlation between side binding and processivity for Fhod tails, leading us to propose that the strong affinities of the Fhod-A and -E tails for filament sides promote dissociation of the FH2 domain from the barbed end to remain on the side of the filament. Previous work has shown single mDia1 molecules dissociating from the barbed end and sliding along the side of the filament (Bombardier et al., 2015). Whereas mDia1 was able to return to the barbed end and resume processive elongation, Fhod-A and Fhod-E have much stronger affinities for filament sides than mDia1 (Li and Higgs, 2003) and would therefore be expected to remain on the side of the filament. This model can also explain why Fhod family members localize near the pointed end of filaments, rather than simply dissociating from filaments: after nucleating an actin filament, Fhod would bind the side of the nascent filament. Subsequent growth at the faster barbed end would increase the distance between Fhod and the barbed end. Slow growth at the pointed end would make the distance of this end from Fhod difficult to detect.

Our preliminary data disfavor the other mechanisms for impaired processivity that we proposed. If impaired processivity of Fhod-A were simply due to its length, we would have expected a gradual increase in processive run length as we truncated the tail, instead of the all-or-nothing effect we observed after truncating the last 24 amino acids. In our initial experiments, addition of the Fhod-E tail did not disrupt processivity of Fhod-B, arguing against a direct interaction between the tail and the FH2 domain.

We mapped the region impairing Fhod processivity to the last 24 residues of Fhod-A. This region includes a basic motif conserved across Fhod family members from *C. elegans* to human. The conservation of this sequence suggests that poor processivity is an important feature of Fhod family members. The actin filaments in Fhod-associated structures tend to be short, ~0.8-1.5 μm in sarcomeres (Littlefield and Fowler, 1998). Therefore, the short run lengths of Fhod family members might help to limit the lengths of these actin filaments.

Finally, we showed that the Fhod N-terminus slows processive elongation, with preliminary data suggesting that this results from dimerization of the FH1 domains restricting their diffusion. A dimeric N-terminus is not unique to Fhod family members; the N-terminal DID of other diaphanous-related formins and the CID in Capu/Fmn family members are also dimeric. These dimerization domains are typically excluded from preparations of formins used to measure processive elongation. We predict that many other formins might have slower elongation rates than previously measured if their dimerization domains were included, although the extent of inhibition would depend on the geometry of the dimerization domain, the distance between the dimerization domain and the polyproline track, and any tension exerted on the FH1 domain.

Materials and methods

Protein expression and purification

Unless otherwise specified, all Fhod C-terminal constructs (spanning the FH1 domain, FH2 domain, and tail) were cloned into a modified pET-15b vector containing an N-terminal 6xhis tag. All constructs were transformed in Rosetta 1 cells (Novagen), grown in Terrific broth to an OD of 0.6-0.8, and induced with 0.25 mM IPTG overnight at 18 °C. Fhod-A, truncations, and Fhod-E were purified by ion exchange chromatography as described in Chapter 2, with slight modification to improve solubility. Cell pellets were resuspended in 10 mM MOPS pH 7, 150 mM NaCl, 1 mM DTT, 1 mM PMSF, 2 µg/mL DNase, lysed in a microfluidizer, and centrifuged at 20,000 x g for 20 minutes. Clarified lysates were applied to a HitrapSP cation exchange column (GE Life Sciences) with a gradient of 0.3 – 1 M NaCl over 16 column volumes. Peak fractions were dialyzed into 10 mM Tris pH 8, 50 mM NaCl, 1 mM DTT, centrifuged, and run on a MonoQ anion exchange column (GE Life Sciences) with a gradient of 50 – 600 mM NaCl over 55 column volumes. Peak fractions were dialyzed into Fhod storage

buffer (10 mM Tris pH 8, 150 mM NaCl, 1 mM DTT), then flash frozen in liquid nitrogen and stored at -80 °C.

Pellets expressing cc Fhod-B CT (including wild-type and W898A mutant) were resuspended in extraction buffer (50 mM sodium phosphate pH 8, 300 mM NaCl, 1 mM βME) supplemented with 1 mM PMSF, 2 µg/mL DNase, then lysed and centrifuged as above. Clarified lysate was then bound to 1 mL Talon resin (Clontech) for 1 hour, then transferred to a gravity column. Resin was washed with 25 mL extraction buffer, followed by 25 mL of wash buffer (same as extraction buffer except pH 7). Protein was eluted with wash buffer containing 200 mM imidazole. Elution fractions containing cc Fhod-B CT were dialyzed overnight into 10 mM Tris pH 8, 50 mM NaCl, 1 mM DTT, then centrifuged and run on a MonoQ column with a gradient of 50 – 600 mM NaCl over 55 column volumes. Peak fractions were dialyzed into Fhod storage buffer, flash frozen in liquid nitrogen, and stored at -80 °C.

Fhod-B was cloned into pGEX-6P-2 and expressed in Rosetta 1 cells as above. Cell pellets were resuspended in PBS, lysed, and centrifuged. Clarified lysates were bound to 2.5 mL Glutathione Sepharose (GE Life Sciences) for 1 hour. Resin was washed with 25 mL PBS, then protein was eluted with 50 mM Tris pH 8, 20 mM glutathione, 50 mM NaCl, 150 mM KCl, 1 mM DTT. Eluted protein was dialyzed into PBS with 1 mM DTT and cleaved with Prescission Protease overnight. The cleaved protein was filtered through glutathione sepharose, dialyzed into 10 mM Tris pH 8, 50 mM NaCl, 1 mM DTT, then run on MonoQ (50 – 600 mM NaCl over 55 column volumes). Peak fractions were dialyzed into Fhod storage buffer, flash frozen in liquid nitrogen, and stored at -80 °C.

Fhod tails were cloned into pGEX-6P-2 and expressed as above. Cell pellets were resuspended in PBS supplemented with 1 mM DTT, 1 mM PMSF, and 2 µg/mL DNase, then lysed and centrifuged as above. Clarified lysates were bound to 1 mL Glutathione Sepharose for one hour. Resin was washed with 25 mL PBS with 1 mM DTT, then eluted with 15 mL of 50 mM HEPES pH 7.3, 20 mM glutathione, 100 mM NaCl, 1 mM DTT. For preparations of Fhod tails

without the GST tag, the eluted protein was cleaved with Prescission Protease overnight. Cleaved tails were centrifuged at 20,000 x g for 20 minutes, then bound to a MonoS cation exchange column (GE Life Sciences). The column was washed with two column volumes of 50 mM HEPES pH 7.3, 100 mM NaCl, 1 mM DTT, then eluted with a step to 50 mM HEPES pH 7.3, 600 mM NaCl, 1 mM DTT. Eluted protein was dialyzed into 10 mM Tris pH 8, 50 mM NaCl, 0.5 mM TCEP and stored on ice for up to one week.

Concentrations of C-terminal Fhod constructs and the Fhod coiled coil were determined by measuring the absorbance at 280 nm, using predicted extinction coefficients (Expasy), and indicated in terms of dimer concentrations. Concentrations of tail constructs were determined by quantitative SDS-PAGE with SyproRed staining. Concentrations of GST-tails are indicated in terms of monomer concentrations.

Acanthamoeba actin and *Drosophila* profilin (Chic) were purified as described (Bor et al., 2012; Zuchero, 2007).

Kinetic assays

Pyrene assays and TIRF microscopy were conducted as described in Chapter 2. Final conditions for TIRF experiments were 0.5 µM F-actin seeds (1% biotinylated, decorated with equimolar AlexaFluor 647-phalloidin), 1 µM G-actin (20% Oregon Green-labeled, shown in grayscale), 5 µM Chic, 0.5 nM Fhod. Bright and dim filaments were distinguished manually. For processivity measurements, the run length of each Fhod-barbed end binding event was determined by measuring the length of dim-appearing actin in the JFilament plugin (Smith et al., 2010). To be included in analysis, each stretch of dim actin had to be flanked by a patch of bright actin on the barbed end and either a phalloidin-decorated seed or a patch of bright actin on the pointed end. The majority of processive runs were too long to be measured, because they either extended outside the field of view or overlapped extensively with other filaments. The cumulative frequency of run lengths was used to plot the fraction of Fhod-bound barbed ends

versus length, which was fit to the exponential decay curve, $y=e^{-x/\lambda} * a$, where λ is the characteristic run length and a is a constant.

High speed cosedimentation

High speed cosedimentation assays were performed as described in Chapter 2.

Circular dichroism

Secondary structure of Fhod tails was analyzed on a JASCO J-715 circular dichroism spectrophotometer. Each spectrum is the average of two scans with a response time of 4 seconds and a bandwidth of 1 nm.

Model of FH1-mediated elongation

The mathematical model for FH1-mediated elongation was described previously (Bryant et al., 2017). This model was modified by including two FH1 domains, which were dimerized with spacing of 5 nm on the C-terminus (representing the FH2 domain, in both models) and 1 nm on the N-terminus (only in the dimerized N-terminus model).

Figures

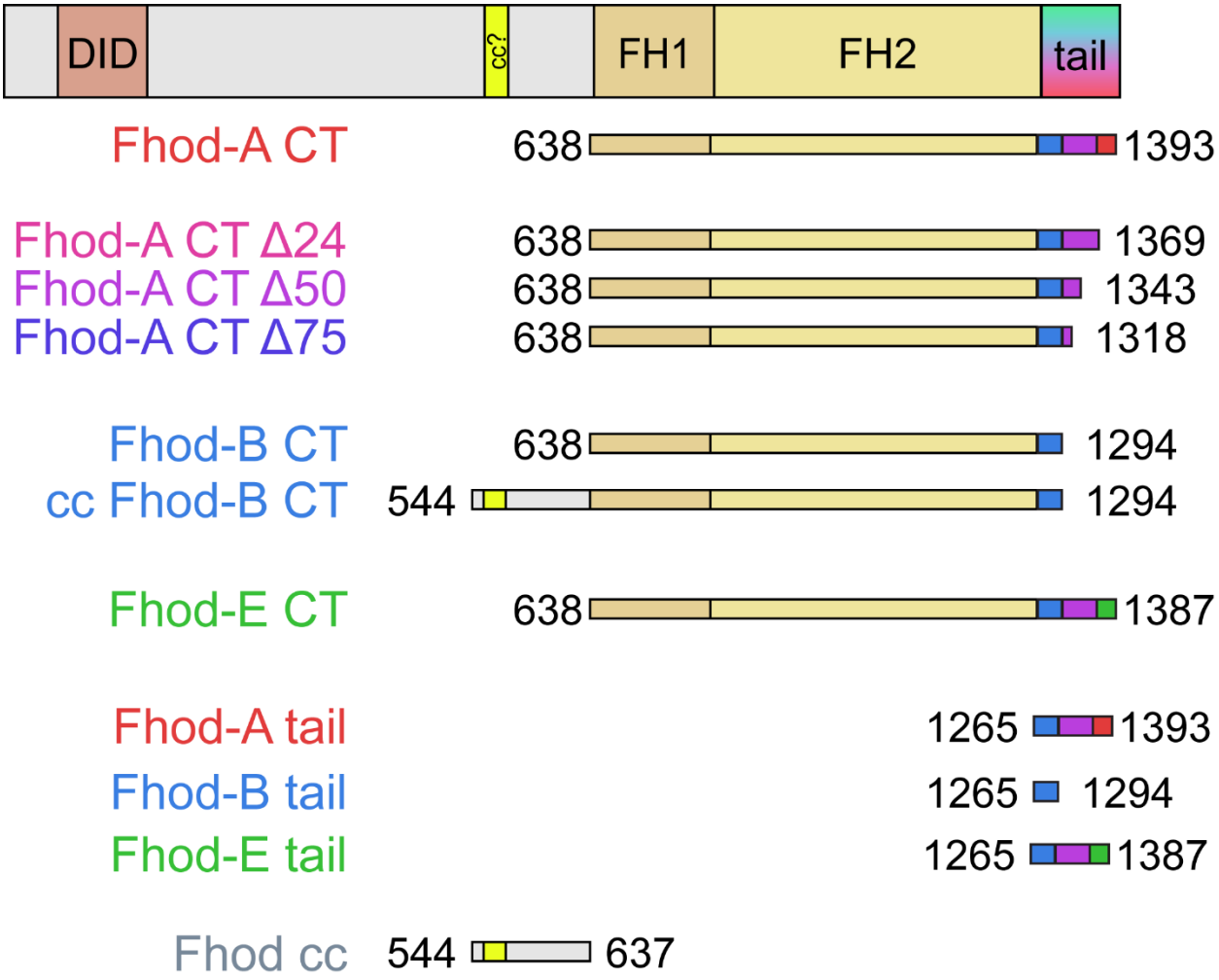

Figure 3.1: Summary of constructs used in this chapter
The upper schematic depicts the domain structure of *Drosophila* Fhod, which includes the regulatory DID-like domain in its N-terminus, a predicted coiled coil N-terminal to the FH1 domain, the FH1 and FH2 domains that polymerize actin, and the C-terminal tail. Below are listed the names of constructs used in this chapter and the domains and amino acid residues they include. Isoforms A, B, and E differ only in their C-terminal tails. The C-terminal tail includes a 30 amino acid segment shared across all three isoforms (blue), a 75 amino acid segment shared between isoforms A and E (purple), a 24 amino acid segment unique to the Fhod-A tail (red), and an 18 amino acid segment unique to the Fhod-E tail (green).

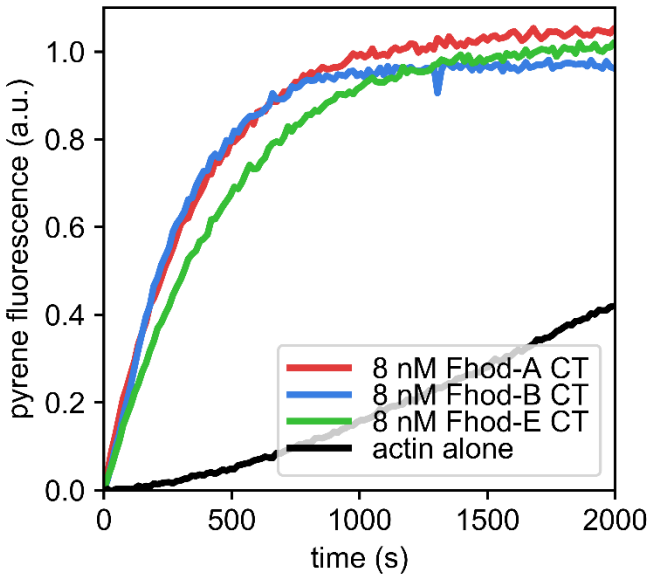

Figure 3.2: Fhod isoforms A, B, and E assemble actin at similar rates.
Pyrene actin assembly assay with 2 µM *Acanthamoeba* actin (10% pyrene-labeled). C-terminal constructs of Fhod-A, -B, and -E all accelerate actin assembly to similar degrees.

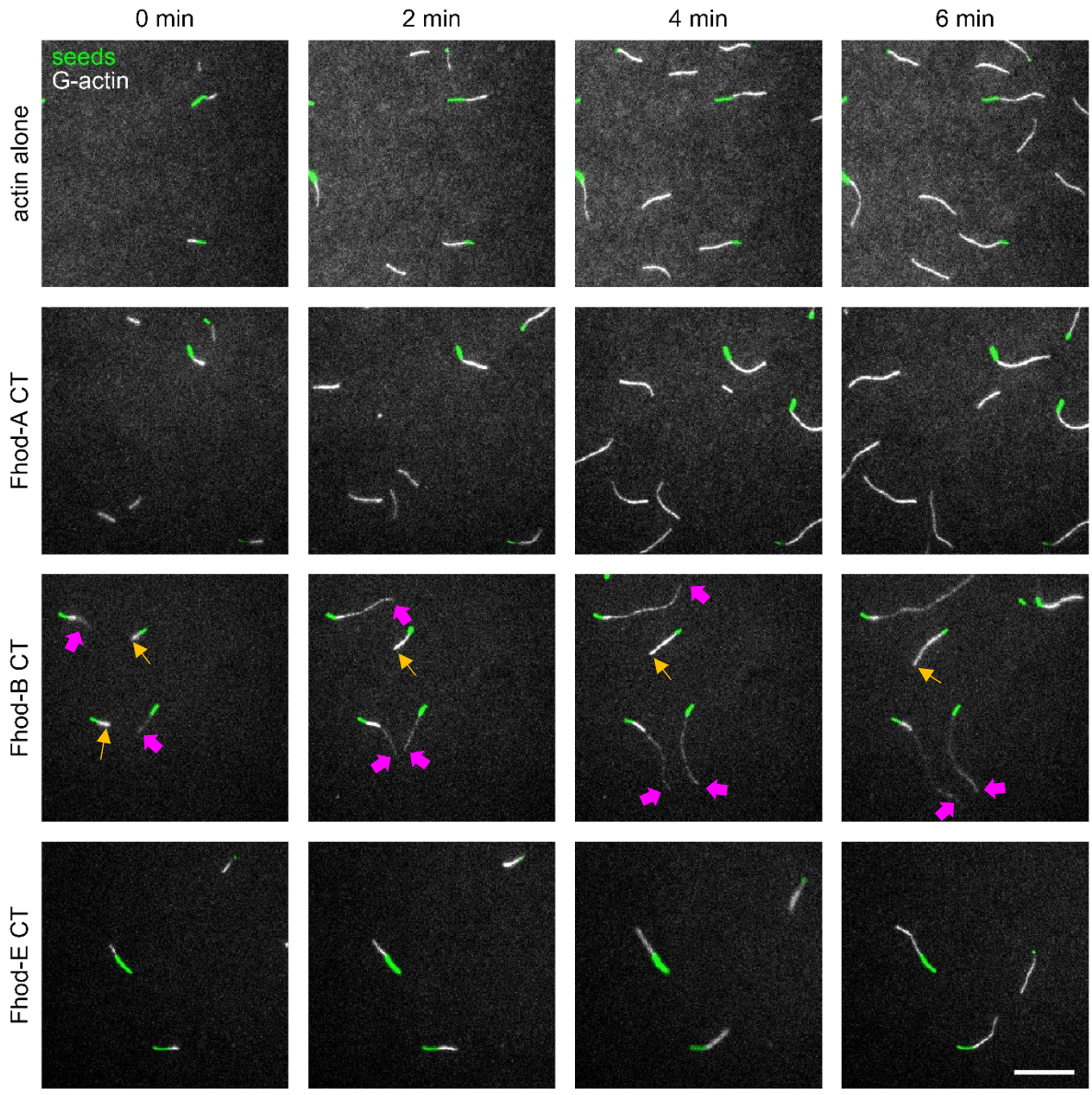

Figure 3.3: Fhod-B processively elongates actin filaments.
TIRF microscopy images of actin filaments elongating alone or in the presence of the indicated Fhod construct. Final conditions were 0.5 µM F-actin seeds (1% biotinylated, decorated with equimolar AlexaFluor 647-phalloidin, shown in green), 1 µM G-actin (20% Oregon Green-labeled, shown in grayscale), 5 µM Chic, 0.5 nM Fhod. Each image was taken at the indicated time after the start of acquisition. In the presence of Fhod-B, two populations of actin filaments can be distinguished: formin-bound filaments appear dim and elongate quickly (magenta arrows), while unbound filaments appear bright and elongate slowly (orange arrows). Scale bar is 10 µm.

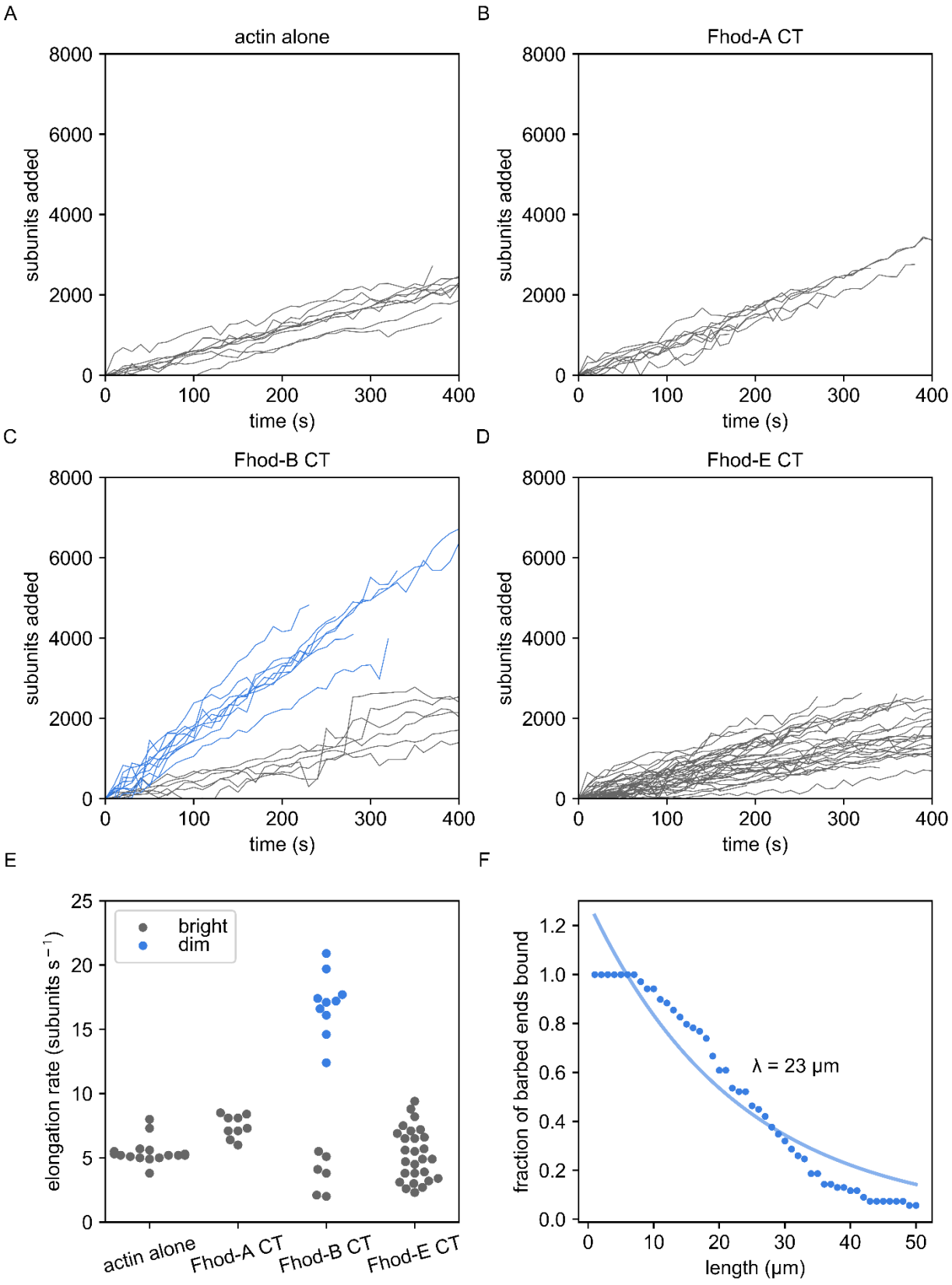
A
actin alone
B
Fhod-A CT
C
Fhod-B CT
D
Fhod-E CT
subunits added
time (s)
E
bright
dim
elongation rate (subunits s^{-1})
actin alone
Fhod-A CT
Fhod-B CT
Fhod-E CT
F
fraction of barbed ends bound
λ = 23 μm
length (μm)

Figure 3.4: Elongation rates and processivity of Fhod isoforms
Analysis of processive elongation from Figure 3.3. A-D, quantification of barbed end elongation with actin alone or in the presence of Fhod CT. Filament lengths are expressed as the number of actin subunits added from the start of analysis. Data from bright-appearing filaments (free barbed ends) are shown in gray. Data from dim-appearing filaments (formin-bound barbed ends) are shown in blue. E, quantification of elongation rates from A-D. Each point represents the elongation rate of one filament, determined by linear regression. Gray points were obtained from bright-appearing filaments and blue points were obtained from dim-appearing filaments. F, quantification of processive run length by Fhod-B CT. The run length for each Fhod-barbed end binding event was determined based on fluorescence intensity and used to calculate the fraction of barbed ends that remain bound to Fhod at each length. Data were fit to the exponential decay curve, $y = e^{-x/\lambda} * a$, where λ is the characteristic run length and a is a constant. Run lengths greater than 50 µm were excluded from analysis because these filaments tend to overlap or extend beyond the field of view.

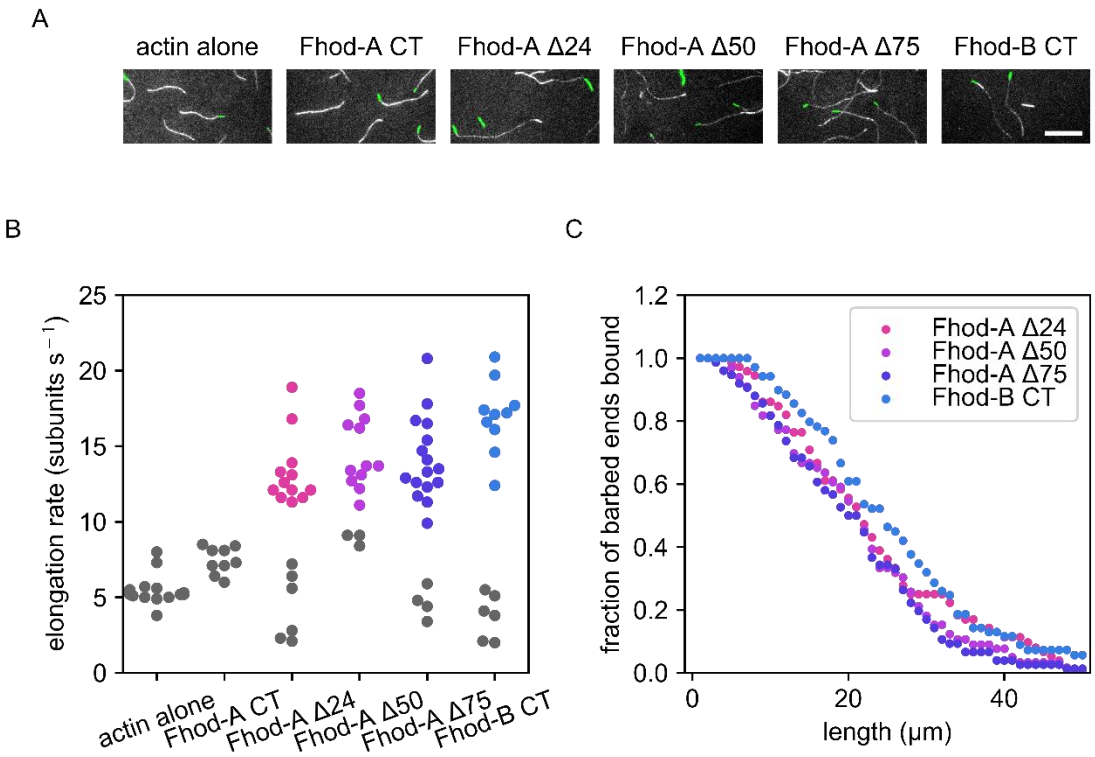

Figure 3.5: Truncation of the last 24 residues from Fhod-A CT restores processivity
A, TIRF microscopy images of actin filaments elongating alone or in the presence of the indicated Fhod construct. Final conditions were 0.5 μM F-actin seeds (1% biotinylated, decorated with equimolar AlexaFluor 647-phalloidin, shown in green), 1 μM G-actin (20% Oregon Green-labeled, shown in grayscale), 5 μM Chic, 0.5 nM Fhod. Images were 10 minutes after the start of acquisition. Scale bar is 10 μm. B, quantification of elongation rates from A. Each point represents the elongation rate of one filament, determined by linear regression. Gray points were obtained from bright-appearing filaments and colored points were obtained from dim-appearing filaments. Data for actin alone, Fhod-A CT, and Fhod-B CT are reproduced from Figure 3.4. C, quantification of processive run length by Fhod based on fluorescence intensity. Data were fit to the exponential decay curve, $y = e^{-x/\lambda} * a + b$, where λ is the characteristic run length and a and b are constants. Best-fit curves gave characteristic run lengths of 45 μm for Fhod-A Δ24, 40 μm for Fhod-A Δ 50, 37 μm for Fhod-A Δ 75, and 94 μm for Fhod-B CT. Data for Fhod-B CT are reproduced from Figure 3.4.

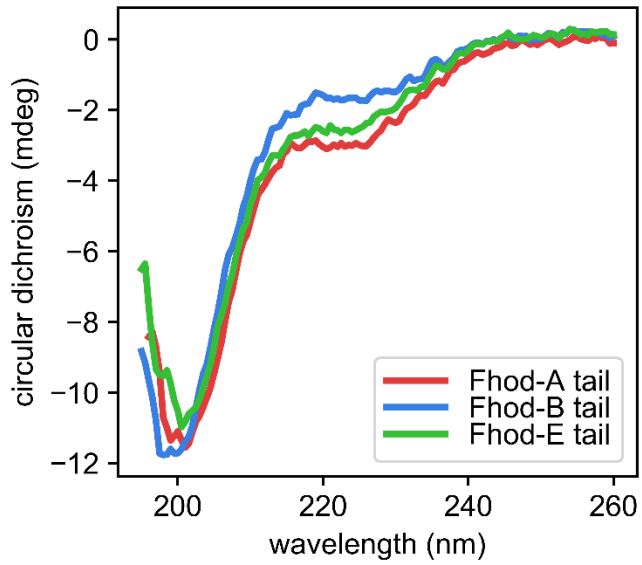

Figure 3.6: Fhod tails lack secondary structure
The tails of each Fhod isoform were analyzed by circular dichroism spectroscopy. Spectra for all three isoforms are consistent with random coil.

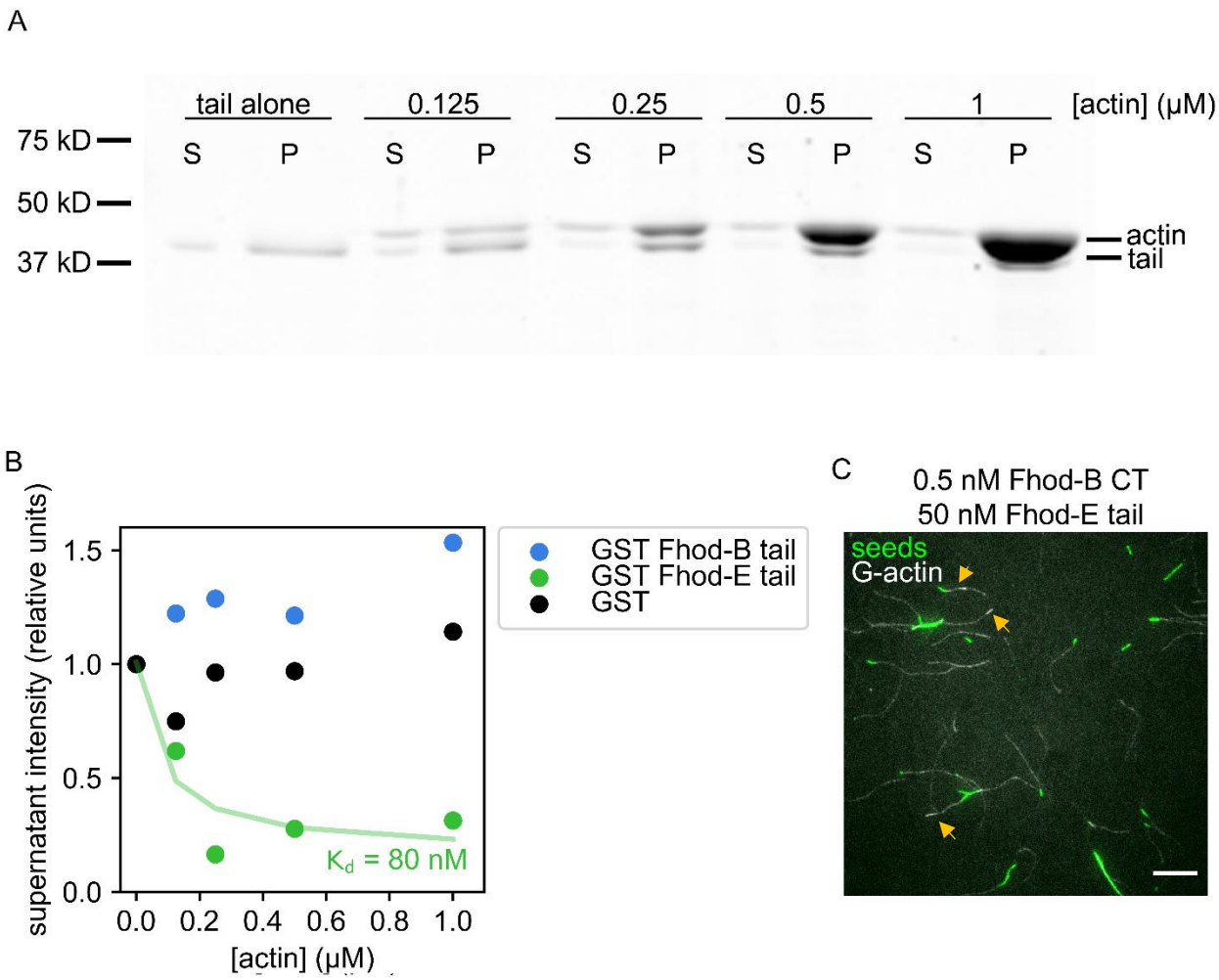

Figure 3.7: The Fhod-E tail binds tightly to filament sides but not the FH2 domain
A, high speed cosedimentation assay to measure binding of GST Fhod-E tail to sides of actin filaments. F-actin at the indicated concentration was mixed with 0.3 μM GST Fhod-E tail, then centrifuged at high speed to pellet actin filaments. The amount of Fhod tail remaining in the supernatant was analyzed by SDS-PAGE with SyproRed staining. B, quantification of supernatant intensity from high speed cosedimentation assays, as shown in A. The tail of isoform E, but not B, was depleted from the supernatant with increasing concentrations of F-actin, indicating binding. Data were fit to the simplified binding equation, $y = x/(x+K_d) * a + b$ to determine the K_d. C, TIRF microscopy image of actin filaments after 10 minutes of growth in the presence of Fhod-B CT and Fhod-E tail. Final conditions were 0.5 μM F-actin seeds (1% biotinylated, decorated with equimolar AlexaFluor 647-phalloidin, shown in green), 1 μM G-actin (20% Oregon Green-labeled, shown in grayscale), 5 μM Chic, 0.5 nM Fhod-B CT, 50 nM Fhod-E tail. Most filaments appear dim, with bright filaments (orange arrows) indicating Fhod-B dissociation events. Fhod-B CT processively elongates filaments in the presence of the Fhod-E tail. Scale bar is 10 μm.

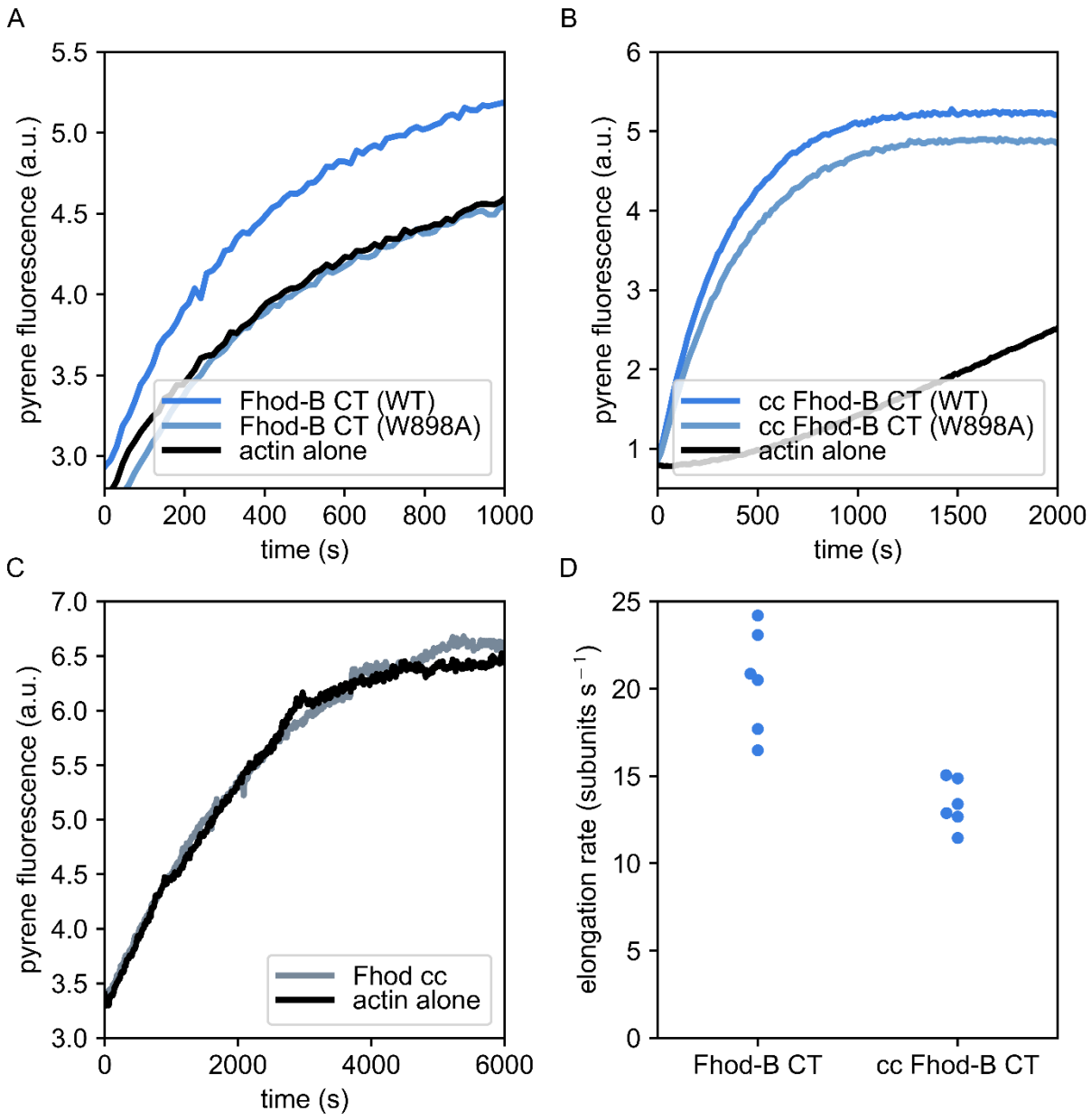

Figure 3.8: The dimeric Fhod N-terminus slows processive elongation
A, pyrene actin assembly assay with 4 µM actin (5% pyrene-labeled), 4 nM wild-type or W898A Fhod-B CT. The W898A mutation abolishes actin nucleation, suggesting that it disrupts dimerization of the FH2 domain. B, pyrene actin assembly assay with 2 µM actin (5% pyrene labeled), 4 nM wild-type or W898A cc Fhod-B CT. When the putative coiled coil is included, the W898A mutation no longer affects nucleation, suggesting that the coiled coil maintains dimerization of the FH2 domain. C, pyrene actin assembly assay with 2 µM actin (5% pyrene labeled), 0.6 µM Fhod coiled coil. The coiled coil does not affect actin assembly. D, quantification of barbed end elongation by TIRF microscopy. Each point represents the elongation rate of a dim-appearing actin filament. cc Fhod-B CT elongates barbed ends at a slower rate than Fhod-B CT.

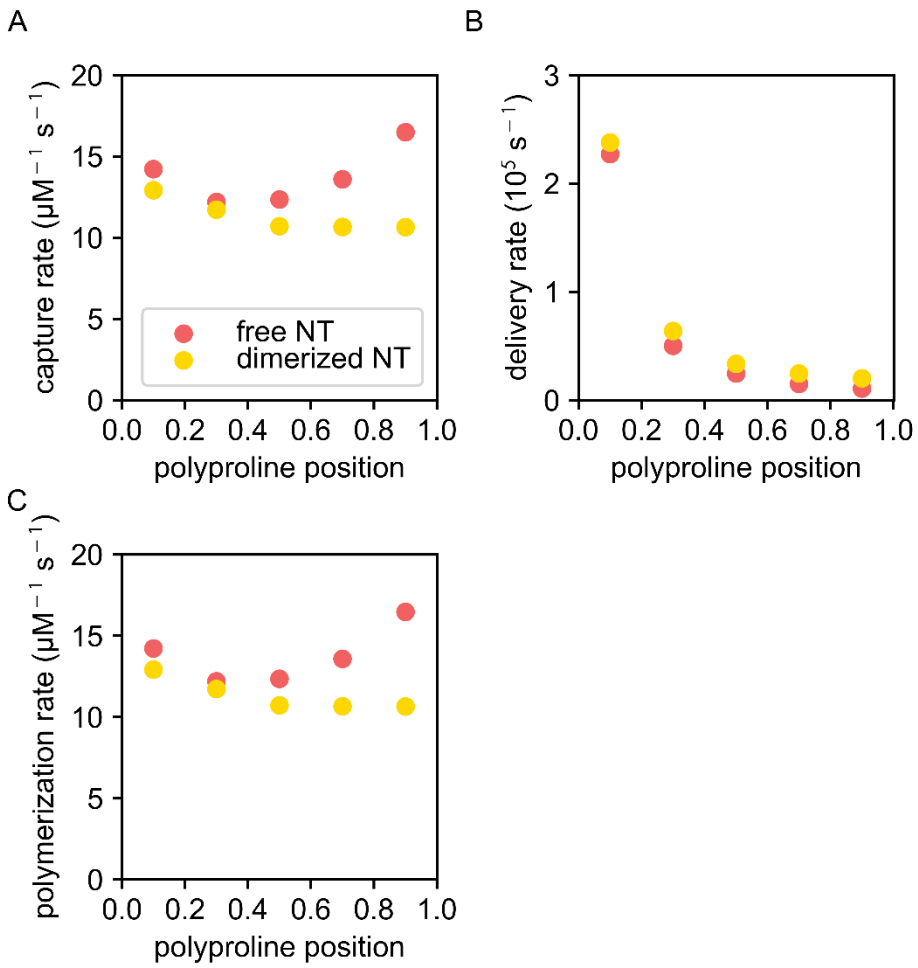

Figure 3.9: N-terminal dimerization slows elongation *in silico*
A, mathematical simulation of capture rates for polyproline tracks in an FH1 domain with a free or dimerized N-terminus. Polyproline positions are expressed as fractions of the FH1 length, with 0 at the FH2 domain and 1 at the N-terminus. N-terminal dimerization slows the capture rate at all positions, with the strongest effect at positions nearest the dimerization domain. B, mathematical simulation of delivery rates. N-terminal dimerization slightly accelerates the delivery rate at all polyproline positions. C, mathematical simulation of overall actin polymerization rate. As with capture rates, N-terminal dimerization slows elongation with the strongest effect at positions nearest the dimerization domain.

References

Bombardier, J.P., Eskin, J.A., Jaiswal, R., Correa, I.R., Jr., Xu, M.Q., et al. 2015. Single-molecule visualization of a formin-capping protein 'decision complex' at the actin filament barbed end. *Nat Commun*. 6:8707.

Bor, B., Vizcarra, C.L., Phillips, M.L., and Quinlan, M.E. 2012. Autoinhibition of the formin Cappuccino in the absence of canonical autoinhibitory domains. *Mol Biol Cell*. 23:3801-3813.

Bryant, D., Clemens, L., and Allard, J. 2017. Computational simulation of formin-mediated actin polymerization predicts homologue-dependent mechanosensitivity. *Cytoskeleton (Hoboken)*. 74:29-39.

Courtemanche, N. 2018. Mechanisms of formin-mediated actin assembly and dynamics. *Biophys Rev*. 10:1553-1569.

Drozdetskiy, A., Cole, C., Procter, J., and Barton, G.J. 2015. JPred4: a protein secondary structure prediction server. *Nucleic Acids Res*. 43:W389-394.

Fenix, A.M., Neininger, A.C., Taneja, N., Hyde, K., Visetsouk, M.R., et al. 2018. Muscle-specific stress fibers give rise to sarcomeres in cardiomyocytes. *Elife*. 7.

Goode, B.L., and Eck, M.J. 2007. Mechanism and function of formins in the control of actin assembly. *Annu Rev Biochem*. 76:593-627.

Gould, C.J., Maiti, S., Michelot, A., Graziano, B.R., Blanchoin, L., et al. 2011. The formin DAD domain plays dual roles in autoinhibition and actin nucleation. *Curr Biol*. 21:384-390.

Kan-o, M., Takeya, R., Taniguchi, K., Tanoue, Y., Tominaga, R., et al. 2012. Expression and subcellular localization of mammalian formin Fhod3 in the embryonic and adult heart. *PLoS One*. 7:e34765.

Kovar, D.R., Harris, E.S., Mahaffy, R., Higgs, H.N., and Pollard, T.D. 2006. Control of the assembly of ATP- and ADP-actin by formins and profilin. *Cell*. 124:423-435.

Lammel, U., Bechtold, M., Risse, B., Berh, D., Fleige, A., et al. 2014. The Drosophila FHOD1-like formin Knittrig acts through Rok to promote stress fiber formation and directed macrophage migration during the cellular immune response. *Development*. 141:1366-1380.

Li, F., and Higgs, H.N. 2003. The Mouse Formin mDia1 Is a Potent Actin Nucleation Factor Regulated by Autoinhibition. *Current Biology*. 13:1335-1340.

Littlefield, R., and Fowler, V.M. 1998. Defining actin filament length in striated muscle: rulers and caps or dynamic stability? *Annu Rev Cell Dev Biol*. 14:487-525.

Mi-Mi, L., Votra, S., Kemphues, K., Bretscher, A., and Pruyne, D. 2012. Z-line formins promote contractile lattice growth and maintenance in striated muscles of C. elegans. *J Cell Biol*. 198:87-102.

Otomo, T., Tomchick, D.R., Otomo, C., Panchal, S.C., Machius, M., et al. 2005. Structural basis of actin filament nucleation and processive capping by a formin homology 2 domain. *Nature*. 433:488-494.

Ramabhadran, V., Gurel, P.S., and Higgs, H.N. 2012. Mutations to the formin homology 2 domain of INF2 protein have unexpected effects on actin polymerization and severing. *J Biol Chem*. 287:34234-34245.

Schonichen, A., Mannherz, H.G., Behrmann, E., Mazur, A.J., Kuhn, S., et al. 2013. FHOD1 is a combined actin filament capping and bundling factor that selectively associates with actin arcs and stress fibers. *J Cell Sci*. 126:1891-1901.

Schulze, N., Graessl, M., Blancke Soares, A., Geyer, M., Dehmelt, L., et al. 2014. FHOD1 regulates stress fiber organization by controlling the dynamics of transverse arcs and dorsal fibers. *J Cell Sci*. 127:1379-1393.

Shwartz, A., Dhanyasi, N., Schejter, E.D., and Shilo, B.Z. 2016. The Drosophila formin Fhos is a primary mediator of sarcomeric thin-filament array assembly. *Elife*. 5.

Smith, M.B., Li, H., Shen, T., Huang, X., Yusuf, E., et al. 2010. Segmentation and tracking of cytoskeletal filaments using open active contours. *Cytoskeleton (Hoboken)*. 67:693-705.

Vavylonis, D., Kovar, D.R., O'Shaughnessy, B., and Pollard, T.D. 2006. Model of formin-associated actin filament elongation. *Mol Cell*. 21:455-466.

Vinson, V.K., De La Cruz, E.M., Higgs, H.N., and Pollard, T.D. 1998. Interactions of Acanthamoeba profilin with actin and nucleotides bound to actin. *Biochemistry*. 37:10871-10880.

Vizcarra, C.L., Bor, B., and Quinlan, M.E. 2014. The role of formin tails in actin nucleation, processive elongation, and filament bundling. *J Biol Chem*. 289:30602-30613.

Xu, Y., Moseley, J.B., Sagot, I., Poy, F., Pellman, D., et al. 2004. Crystal structures of a Formin Homology-2 domain reveal a tethered dimer architecture. *Cell*. 116:711-723.

Zuchero, J.B. 2007. In vitro actin assembly assays and purification from Acanthamoeba. *Methods Mol Biol*. 370:213-226.

Chapter 4: Actin assembly by Fhod1 and Fhod3 in human cardiomyocytes

Introduction

Sarcomeres, the fundamental contractile units of muscle cells, consist of interdigitating actin and myosin filaments. To generate a unified contraction across the muscle cell, these filaments must be assembled, organized, and maintained with remarkable precision. How muscle cells polymerize actin and organize actin filaments into sarcomeres has remained a longstanding question. In the predominant model, termed the premyofibril model, sarcomeres arise from precursor structures termed premyofibrils (Sanger et al., 2005). Premyofibrils are stress fiber-like structures containing actin filaments, non-muscle myosin II, and muscle-specific isoforms of several actin-binding proteins, including α-actinin, troponin, and tropomyosin. As premyofibrils progress to mature sarcomeres, they flow toward the center of the cell, align with each other, grow in width, and replace non-muscle myosin with muscle-specific myosin isoforms. This model is well supported by live imaging of cultured cardiomyocytes, where premyofibrils can clearly be observed flowing and rearranging to form sarcomeres (Dabiri et al., 1997; Fenix et al., 2018; Sanger et al., 2005).

The formin Fhod3 is required for premyofibril assembly and maturation to sarcomeres in cellular and animal models of cardiac development (Fenix et al., 2018; Iskratsch et al., 2010; Taniguchi et al., 2009). In adult mice, Fhod3 is no longer required for sarcomeres to maintain their morphology, but Fhod3 depletion eventually leads to cardiac hypertrophy and decreased contractility (Ushijima et al., 2018). In humans, polymorphisms and mutations to Fhod3 alter the risk of hypertrophic and dilated cardiomyopathies; most notably, numerous mutations to Fhod3 cause hypertrophic cardiomyopathy (Arimura et al., 2013; Esslinger et al., 2017; Ochoa et al.,

2018; Wooten et al., 2013). Fhod3 thus plays important roles in normal cardiac development and the pathophysiology of cardiomyopathies.

Fhod3 belongs to the formin class of actin nucleators, known for their ability to both nucleate and processively elongate actin filaments through their formin homology (FH) 1 and 2 domains (Goode and Eck, 2007). Neither nucleation nor elongation activity has been observed for Fhod3 *in vitro* (Taniguchi et al., 2009), raising the question of how Fhod3 contributes to sarcomere assembly *in vivo* and how mutations to Fhod3 cause hypertrophic cardiomyopathy. Here, we combine biochemical and cellular approaches to measure actin assembly by Fhod3. We find that Fhod3 nucleates and slowly elongates actin filaments *in vitro*, similar to other Fhod family members. We then show initial steps we have taken to study how Fhod3 and its paralog Fhod1 function in human embryonic stem cell-derived cardiomyocytes (hESC-CMs).

Results

Human Fhod3 nucleates actin filaments

We expressed the C-terminal half of human Fhod3 in *E. coli*, including both the muscle-specific splice isoform Fhod3L and the non-specific splice isoform Fhod3S (Iskratsch et al., 2010). In the C-terminal half of the protein, these isoforms differ only by the inclusion of 8 amino acids found in the C-terminal tail of Fhod3L but not Fhod3S; additional differences exist in the regulatory N-terminus. We partially purified both isoforms but were unable to remove a major truncation product from Fhod3L. Because Fhod3L appears as a doublet even in post-induction gel samples prior to lysis, we expect that the truncated form of Fhod3L is a product of incomplete translation rather than proteolytic cleavage. Based on MALDI mass spectrometry, we estimate that this product is missing the last ~138 amino acids of the C-terminal tail.

We used pyrene actin assembly assays to measure the effect of Fhod3 on actin dynamics. We found that both splice variants of Fhod3 accelerate the assembly of

Acanthamoeba actin in a dose-dependent manner (Figure 4.1). Although Fhod3L appeared much less potent than Fhod3S, this difference might be explained by the lower purity.

Because we previously found that human Fhod1 and, to a lesser extent, *Drosophila* Fhod nucleate muscle and non-muscle actin isoforms with different rates, we also measured the nucleation activity of Fhod3 isoforms with two mammalian sources of actin: rabbit skeletal muscle (predominantly α-skeletal actin) and human platelet (85% β-cytoplasmic actin, 15% γ-cytoplasmic actin). Both Fhod3L and Fhod3S nucleated actin from either mammalian source (Figure 4.2 A-D). We observed slightly faster nucleation rates with *Acanthamoeba* actin than mammalian actin, but no substantial differences in nucleation rates between the mammalian actins (Figure 4.2 E-F).

Human Fhod3 binds barbed ends but does not accelerate elongation

Formins can promote actin assembly by both nucleating actin filaments and processively elongating barbed ends; most formins inhibit barbed end growth in the absence of profilin, while accelerating elongation in the presence of profilin (Courtemanche, 2018; Goode and Eck, 2007). We tested the effect of Fhod3S on barbed end elongation using pyrene seeded elongation assays. In these experiments, a low concentration of actin monomers (0.5 µM) is used to prevent spontaneous nucleation and pointed-end elongation, so that increases in pyrene fluorescence can be attributed solely to incorporation of pyrene-actin at the barbed ends of preformed actin seeds. In the absence of profilin, Fhod3S caused a dose-dependent decrease in actin elongation rate, with a K_d of 0.5 nM (Figure 4.3 A,C). When we included profilin in the assay, Fhod3S had no observable effect on the elongation rate (Figure 4.3 B-C). These results, like our previous observations with *Drosophila* Fhod and human Fhod1 (Chapter 2), suggest that Fhod3S binds barbed ends and allows, but does not accelerate, elongation. Because *Drosophila* Fhod dissociates rapidly from growing barbed ends, with a characteristic run length of only ~2 µm (see chapters 2-3), we suspect that Fhod3S also fails to accelerate elongation

due to poor processivity. However, we cannot exclude the possibility that Fhod3S remains processively associated with the barbed end, while recruiting profilin-actin at a rate indistinguishable from the elongation rate of actin alone.

Fhod3 is required for sarcomere assembly in human embryonic stem cell-derived cardiomyocytes.

Our observation that Fhod3 can modulate both nucleation and elongation led us to ask which of these activities is required for sarcomere assembly and organization. To address this question, we required a genetically tractable system for structure-function experiments. We established human cardiomyocytes derived from embryonic stem cells (hESC-CMs) as a powerful model system, amenable to genetic manipulation and imaging. Human stem cells can be efficiently differentiated to cardiomyocytes that assemble sarcomeres and beat spontaneously in culture (Minami et al., 2012; Nakano et al., 2017).

We used siRNA oligonucleotides to deplete Fhod1 and Fhod3 in cardiomyocytes, observing over 80% knockdown efficiency with the three Fhod1 oligonucleotides and two Fhod3 oligonucleotides that we tested by qPCR (Figure 4.4 A, C). We also validated that Fhod3 depletion did not cause a non-specific depletion or compensatory increase of Fhod1 (Figure 4.4 B). In the majority of hESC-CMs treated with any of the four Fhod3 oligonucleotides, sarcomeres were severely disorganized or completely absent, with α-actinin instead localized to puncta (Figure 4.5). This same phenotype has been previously observed with Fhod3 depletion in human iPSC-derived cardiomyocytes (Fenix et al., 2018), primary cardiomyocytes *ex vivo* (Iskratsch et al., 2010; Taniguchi et al., 2009), and embryonic cardiomyocytes *in vivo* (Kan-o et al., 2012a).

We attempted to rescue this phenotype by transiently transfecting cells with an siRNA-resistant Fhod3 plasmid. However, we observed very low transfection efficiency with a plasmid carrying GFP alone; almost all GFP-positive cells were negative for α-actinin, suggesting that

only the undifferentiated cells could be transfected (Figure 4.6). Therefore, we expect that rescue experiments will require a more efficient transfection method, such as viral transduction, or transfection of stem cells prior to differentiation.

Fhod1 is not required for sarcomere or junction assembly in hESC-CMs

Finally, we asked what role Fhod1 plays in hESC-CMs. Transfection with any of the four Fhod1-targeting oligonucleotides had no obvious effect on sarcomere morphology (Figure 4.7). Because two groups observed Fhod1 localized to intercalated discs, the specialized junctions that mechanically and electrically couple neighboring cardiomyocytes (Al Haj et al., 2015; Dwyer et al., 2014), we asked whether Fhod1-depleted hESC-CMs could still form intercalated discs. We transfected hESC-CMs with two of the four Fhod1-targeting oligonucleotides, then stained for β-catenin, a component of adherens junctions. β-catenin localized to intercellular junctions, often with the broad, jagged appearance characteristic of intercalated discs (Figure 4.8). We observed no obvious change in β-catenin levels or morphology with Fhod1 siRNA. These results are consistent with newly published work in Fhod1 knockout mice, which survive to adulthood with no defects in sarcomere or intercalated disc morphology (Sanematsu et al., 2019).

Discussion

Here, we established that Fhod3 shares the capacity of other formins to nucleate actin filaments and bind barbed ends. In our preliminary biochemical data, human Fhod3 behaves similarly to *Drosophila* Fhod as a relatively potent actin nucleator but poor barbed end elongator. We suspect that the poor elongation ability of Fhod3 is due to low processivity, as we observed for *Drosophila* Fhod (Chapters 2-3). We have only measured barbed end elongation with Fhod3S, the splice variant that does not localize to sarcomeres. Since the tail significantly alters the processivity of *Drosophila* Fhod (Chapter 3), the 8 additional residues in the Fhod3L

tail might also modify its processivity. However, we note that Fhod isoforms across a range of systems, including muscle and non-muscle cells from *C. elegans*, *Drosophila*, and mammals, preferentially localize to the sides of filaments rather than barbed ends (Fenix et al., 2018; Kan-o et al., 2012b; Mi-Mi et al., 2012; Schonichen et al., 2013; Schulze et al., 2014; Shwartz et al., 2016). Therefore, we suspect that the poor processivity we observed for *Drosophila* Fhod is a conserved feature of Fhod3 and other Fhod family members.

We asked whether the biochemical properties we observed for Fhod3 are required for correct sarcomere assembly and organization. Previous work suggests, but does not prove, that nucleation activity by Fhod3 is required for sarcomere assembly. Classic point mutations I1127A and K1273D in the FH2 domain eliminate the ability of Fhod3 to assemble sarcomeres in primary cardiomyocytes (Taniguchi et al., 2009). We found that the corresponding lysine mutation in *Drosophila* Fhod impairs its ability to nucleate without affecting its affinity for barbed ends or sides of filaments (Chapter 2). Assuming our observation with *Drosophila* Fhod holds true for mammalian Fhod3, the inability of Fhod3 K1273D to rescue sarcomere assembly strongly supports the requirement of nucleation. However, the variable effects of FH2 point mutations across formins (Ramabhadran et al., 2012; Scott et al., 2011; Xu et al., 2004) makes it unsafe to assume that the lysine mutation will have the same effect on *Drosophila* and mammalian Fhods.

In addition, live imaging of cardiomyocytes treated with the pan-formin inhibitor smiFH2 (Rizvi et al., 2009) revealed that the retrograde flow and maturation of premyofibrils completely halted within three minutes of exposure to smiFH2 (Fenix et al., 2018). Because other formins are not required for sarcomere assembly (Fenix et al., 2018), this finding suggests that function of the Fhod3 FH2 domain plays a direct, active role in sarcomere assembly.

We sought to more directly test the importance of nucleation, elongation, and side-binding for sarcomere assembly in structure-function experiments. To carry out these experiments, we need mutants that separate each function, and a system to test the ability of

each mutant to rescue sarcomere assembly. Based on our previous work in *Drosophila* Fhod, we suspect that classic mutations in the FH2 domain might abolish nucleation while retaining actin binding and barbed end elongation. Since the mechanism by which polyproline tracks in the FH1 domain deliver profilin-actin to the barbed end is well described (Courtemanche and Pollard, 2012; Paul and Pollard, 2008), we can manipulate the elongation rate by adding, removing, or repositioning polyproline tracks. Formins vary in how they interact with sides of filaments (Harris et al., 2006), and Fhod family members have a stronger affinity for filaments than most other formins (Chapter 2). Therefore, there is not a straightforward way to selectively perturb side-binding of Fhod3.

Once we establish mutations that separate Fhod3 activities, we would need a system to add back Fhod3 mutants in cells depleted of endogenous wild-type Fhod3. Although we observe a clear loss of sarcomeres with Fhod3 depletion in hESC-CMs, we have not yet been able to rescue this phenotype due to the low transfection efficiency of these cells. However, transfection of hESCs and viral transduction of hESC-CMs are well-established (Eiges, 2016; Ribeiro et al., 2015). In the future, the system we establish can also be used to investigate how cardiomyopathy-associated Fhod3 mutations alter actin assembly *in vitro* and in cardiomyocytes.

Materials and Methods

Protein expression and purification

Human Fhod3S and Fhod3L cDNA was provided by Thomas Iskratsch (Iskratsch et al., 2010). The C-terminal half of each isoform (residues 787-1438 for Fhod3S and 963-1622 for Fhod3L) were cloned into pGEX-6P-2. Rosetta 2 cells were transformed with plasmids, grown to an OD of 0.6 in terrific broth, then induced with 0.25 mM IPTG at 18 °C overnight. Cell pellets were washed in PBS and flash frozen in liquid nitrogen.

Cell pellets expressing Fhod3S were resuspended in 20 mM HEPES pH 7.5, 150 mM NaCl, 1 mM DTT, 1 mM PMSF, and 2 µg/mL DNaseI. Cells were lysed by microfluidizing, centrifuged at 20,000 x g for 20 minutes, and applied to a HitrapSP-FF cation exchange column (GE Life Sciences). Protein was eluted with a step to 20 mM HEPES pH 7.5, 0.6 M NaCl, 1 mM DTT. Pooled fractions were cleaved with Prescission Protease and dialyzed overnight into 20 mM HEPES pH 7.5, 150 mM NaCl, 1 mM DTT. After dialyzing, protein was centrifuged at 20,000 x g for 20 minutes, then applied to a MonoS cation exchange column (GE Life Sciences) with a gradient of 150 – 950 mM NaCl over 40 column volumes to remove GST and uncleaved protein. Peak fractions were dialyzed into 10 mM Tris pH 8, 150 mM NaCl, 1 mM DTT. Fhod3L was purified on HitrapSP and MonoS columns as above, except using a gradient over 60 column volumes on the MonoS. Peak fractions were dialyzed into 10 mM Tris pH 8, 50 mM NaCl, 1 mM DTT, and applied to a MonoQ anion exchange column (GE Life Sciences) with a gradient of 50 – 850 mM NaCl over 80 column volumes. Peak fractions were dialyzed into 10 mM Tris pH 8, 150 mM NaCl, 1 mM DTT, 20% glycerol. Purified Fhod3S and Fhod3L were aliquoted, flash frozen in liquid nitrogen, and stored at -80 °C.

Actin was purified from *Acanthamoeba* and rabbit skeletal muscle and labeled with pyrene iodoacetamide as described (Spudich and Watt, 1971; Zuchero, 2007). Human platelet actin was purchased from Cytoskeleton. *S. pombe* profilin was purified according to the previously published protocol for *Drosophila* profilin (Bor et al., 2012), and its concentration was determined using the extinction coefficient of 1.63 OD/mg/mL (Lu and Pollard, 2001). Pyrene assays were performed and analzyed as described (Chapter 2).

Cell culture and transfection

H9 human embryonic stem cells were maintained and differentiated into cardiomyocytes using chemically defined media as described (Minami et al., 2012; Nakano et al., 2017). Two days after plating, cells were transfected with siRNA oligonucleotides (Qiagen) as follows: 1.5

µL Lipofectamine RNAiMAX (Invitrogen) and 1 pmol siRNA were mixed in 50 µL Opti-MEM reduced serum media (Gibco) and incubated for five minutes at room temperature. The mixture was then diluted ten-fold in prewarmed media and added to cells. Transfections were repeated the following day.

To validate knockdown efficiency, RNA extraction, reverse transcription, and quantitative PCR were performed as described (Nakano et al., 2017). The following primers were used: Fhod1 forward: CCACCTGCAGCCTGGAC, Fhod1 reverse: GAGGGAGACACTTGCAGAGC, Fhod3 forward: GCAAGAAGCACAGCATCATC, Fhod3 reverse: GAGGGCCCTTCTCAAATCTC, GAPDH forward: TTGAGGTCAATGAAGGGGTC, GAPDH reverse: GAAGGTGAAGGTCGGAGTCA.

Immunofluorescence

Cells were fixed, permeabilized, and stained according to the following incubations:

(1) 4% paraformaldehyde in PBS for ten minutes at room temperature
(2) three washes in PBS at room temperature for at least five minutes each
(3) 5% BSA, 1% Triton X-100 in PBS for two hours at room temperature
(4) primary antibodies diluted in 1% BSA, 0.1% Tween-20 in PBS overnight at 4 °C: mouse anti-α-actinin (Sigma #A7811; clone EA-53) 1:500; mouse anti-β-catenin (Thermo Fisher #14-2567-80; clone 15B8) 1:50
(5) three washes in PBS with 0.1% Tween-20 at room temperature for at least five minutes each
(6) AlexaFluor 488 donkey anti-mouse (Invitrogen #A21202) diluted 1:2,000 (α-actinin staining) or 1:5,000 (β-catenin staining) in 1% BSA, 0.1% Tween-20 in PBS at room temperature for two hours
(7) three washes in PBS with 0.1% Tween-20 as above.

After staining, cells were mounted in ProLong Gold with DAPI (Invitrogen). Images were acquired on a Leica DMI6000 microscope (Torres laboratory).

Figures

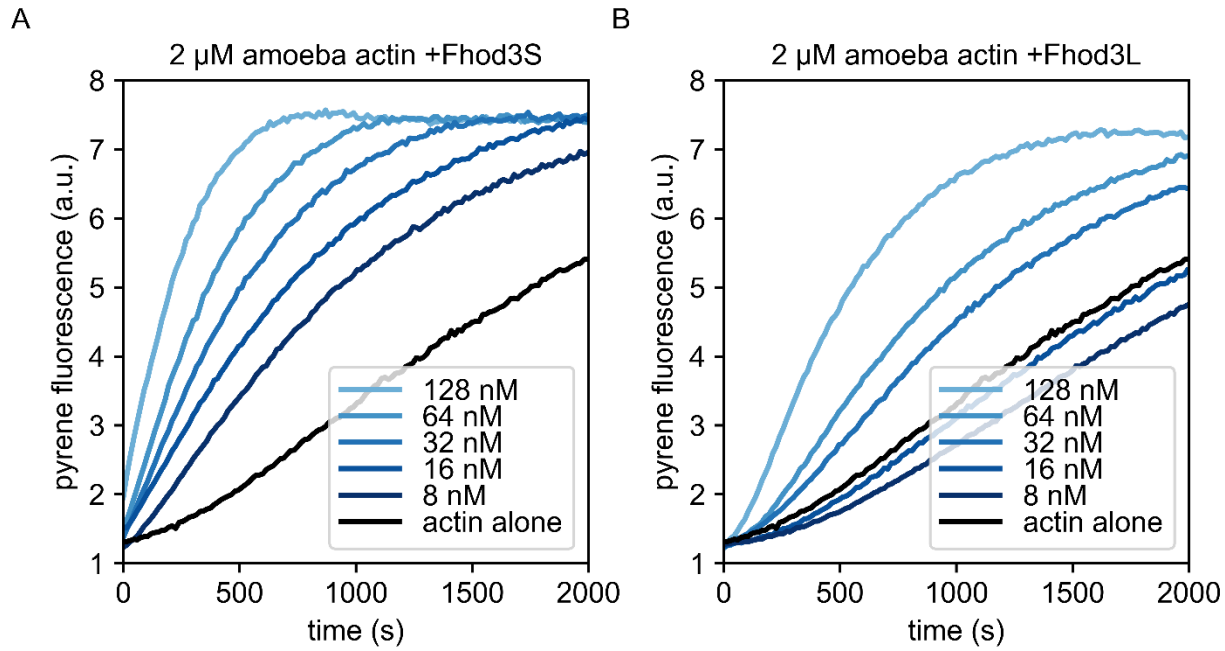

Figure 4.1: Fhod3 nucleates actin.
A, assembly of 2 μM *Acanthamoeba* actin (10% pyrene-labeled) in the presence of human Fhod3S. B, assembly of 2 μM *Acanthamoeba* actin (10% pyrene-labeled) in the presence of human Fhod3L.

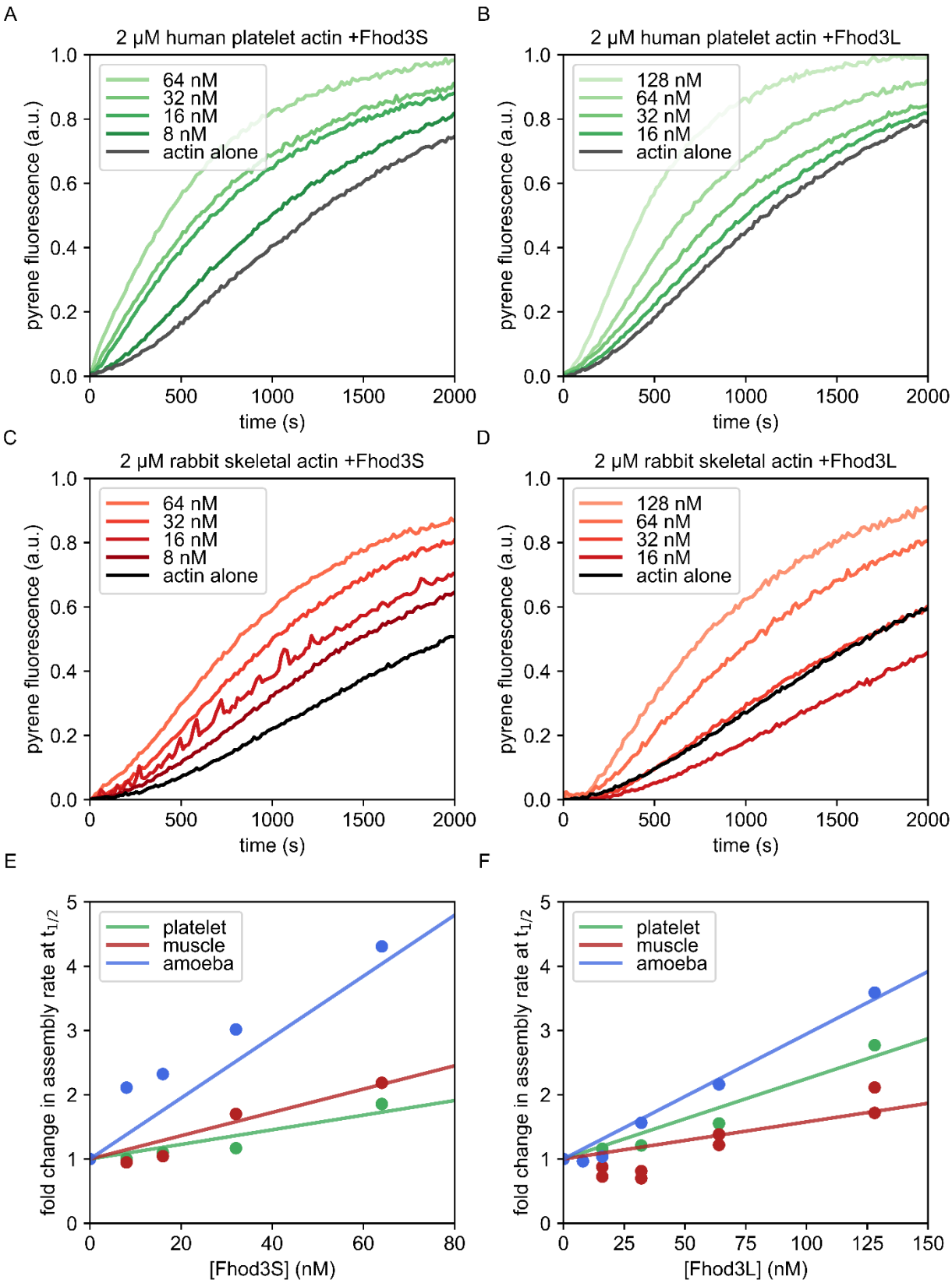
A
2 μM human platelet actin +Fhod3S
64 nM
32 nM
16 nM
8 nM
actin alone
pyrene fluorescence (a.u.)
time (s)
B
2 μM human platelet actin +Fhod3L
128 nM
64 nM
32 nM
16 nM
actin alone
pyrene fluorescence (a.u.)
time (s)
C
2 μM rabbit skeletal actin +Fhod3S
64 nM
32 nM
16 nM
8 nM
actin alone
pyrene fluorescence (a.u.)
time (s)
D
2 μM rabbit skeletal actin +Fhod3L
128 nM
64 nM
32 nM
16 nM
actin alone
pyrene fluorescence (a.u.)
time (s)
E
platelet
muscle
amoeba
fold change in assembly rate at t1/2
[Fhod3S] (nM)
F
platelet
muscle
amoeba
fold change in assembly rate at t1/2
[Fhod3L] (nM)

Figure 4.2: Fhod3 nucleates both muscle and non-muscle actin isoforms.
A, assembly of 2 µM actin (95% human platelet actin, 5% pyrene-labeled *Acanthamoeba* actin) in the presence of human Fhod3S. B, assembly of 2 µM actin (95% human platelet actin, 5% pyrene-labeled *Acanthamoeba* actin) in the presence of human Fhod3S. C, assembly of 2 µM rabbit skeletal muscle actin (5% pyrene-labeled) in the presence of human Fhod3S. D, assembly of 2 µM rabbit skeletal muscle actin (5% pyrene-labeled) in the presence of human Fhod3L. E, quantification of actin assembly rates with Fhod3S from A and C. Each point represents the slope of the pyrene fluorescence versus time at the time to half-polymerization, relative to the slope of actin alone. F, quantification of actin assembly rates with Fhod3L from B and D.

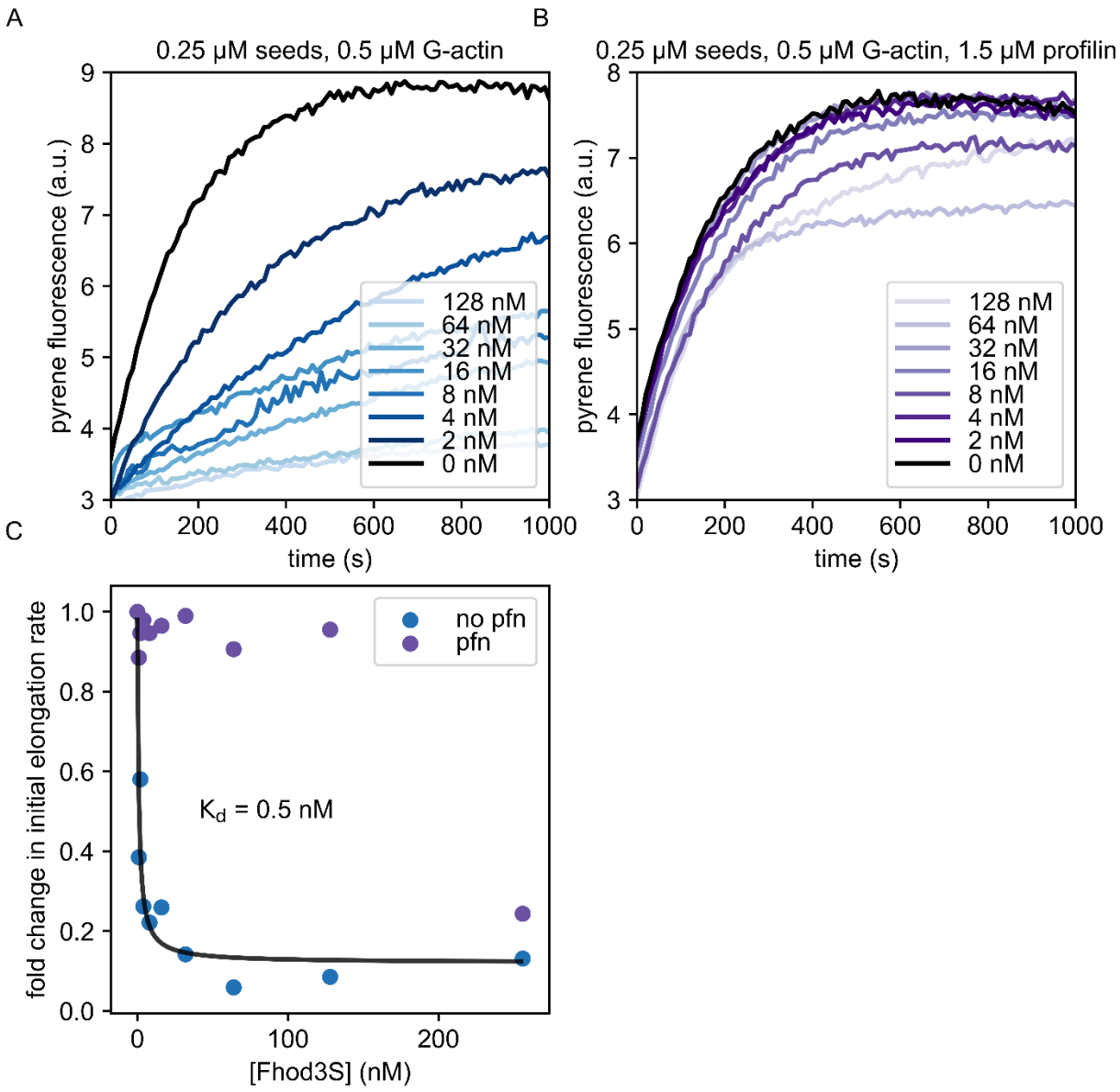

Figure 4.3: Fhod3 binds barbed ends but does not accelerate elongation.
A, pyrene seeded elongation assay with 0.25 μM sheared F-actin seeds, 0.5 μM *Acanthamoeba* actin (10% pyrene-labeled), and indicated concentrations of Fhod3S. B, pyrene seeded elongation assay as in A, with 1.5 μM *S. pombe* profilin. C, quantification of initial elongation rates from A and B over the first 100 seconds, relative to the elongation rate of actin alone. Elongation data in the absence of profilin were fit to the simplified binding equation, r = [Fhod3S] / ([Fhod3S] + K_d) * a + b, where r is the fold change in elongation rate.

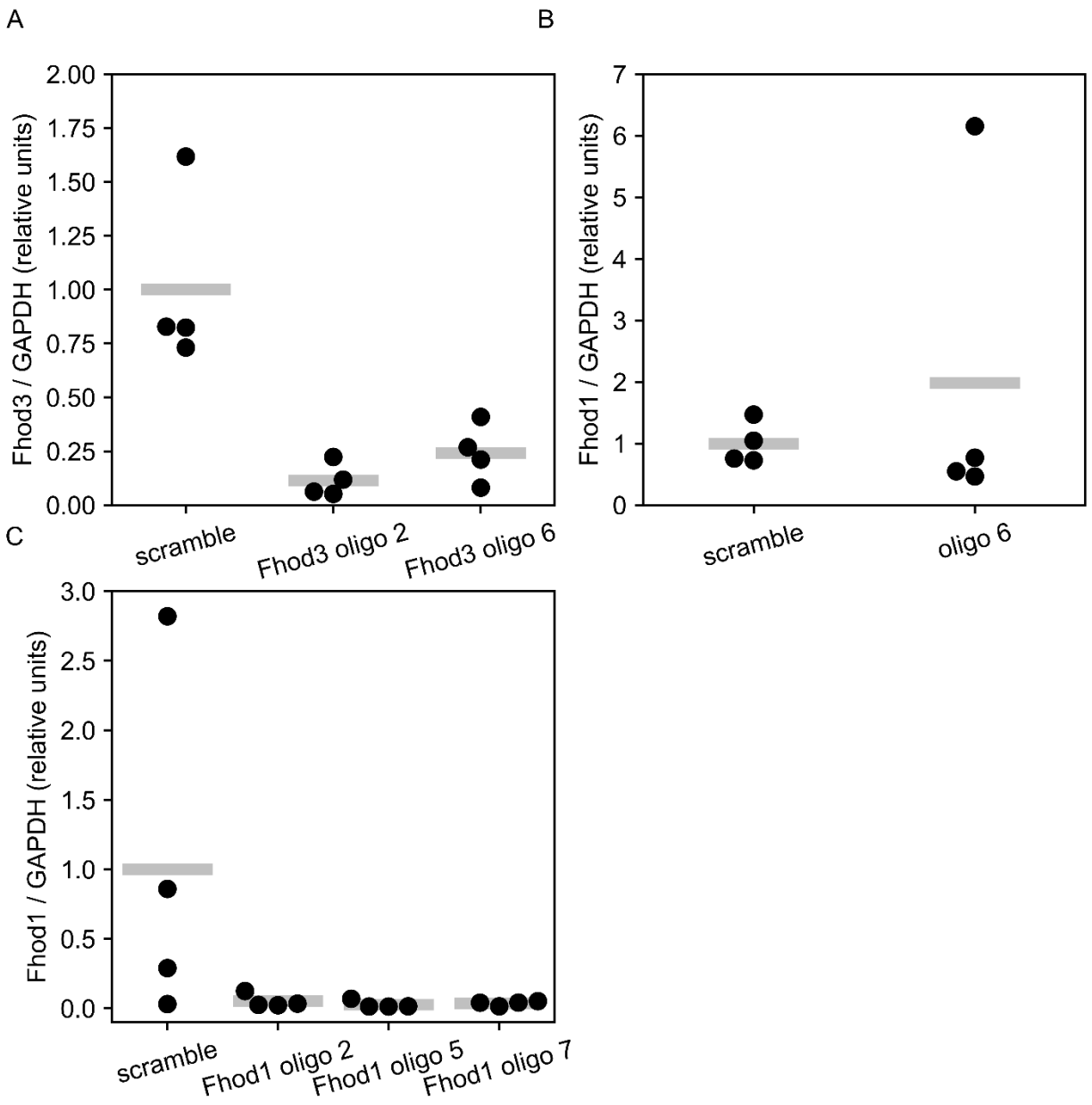

Figure 4.4: Depletion of Fhod1 and Fhod3 in hESC-CMs with siRNA oligonucleotides. qRT-PCR measurements of Fhod1 and Fhod3 expression after transfection with siRNA oligonucleotides. Ratios of Fhod/GAPDH RNA were normalized relative to scramble siRNA-transfected cells. Each point represents the average of three technical replicates. Bars indicate means. A, measurements of Fhod3 expression after transfection with Fhod3 siRNA oligonucleotides. B, measurements of Fhod1 expression after transfection with Fhod3 siRNA oligonucleotide 6. C, measurements of Fhod1 expression after transfection with Fhod1 siRNA oligonucleotides.

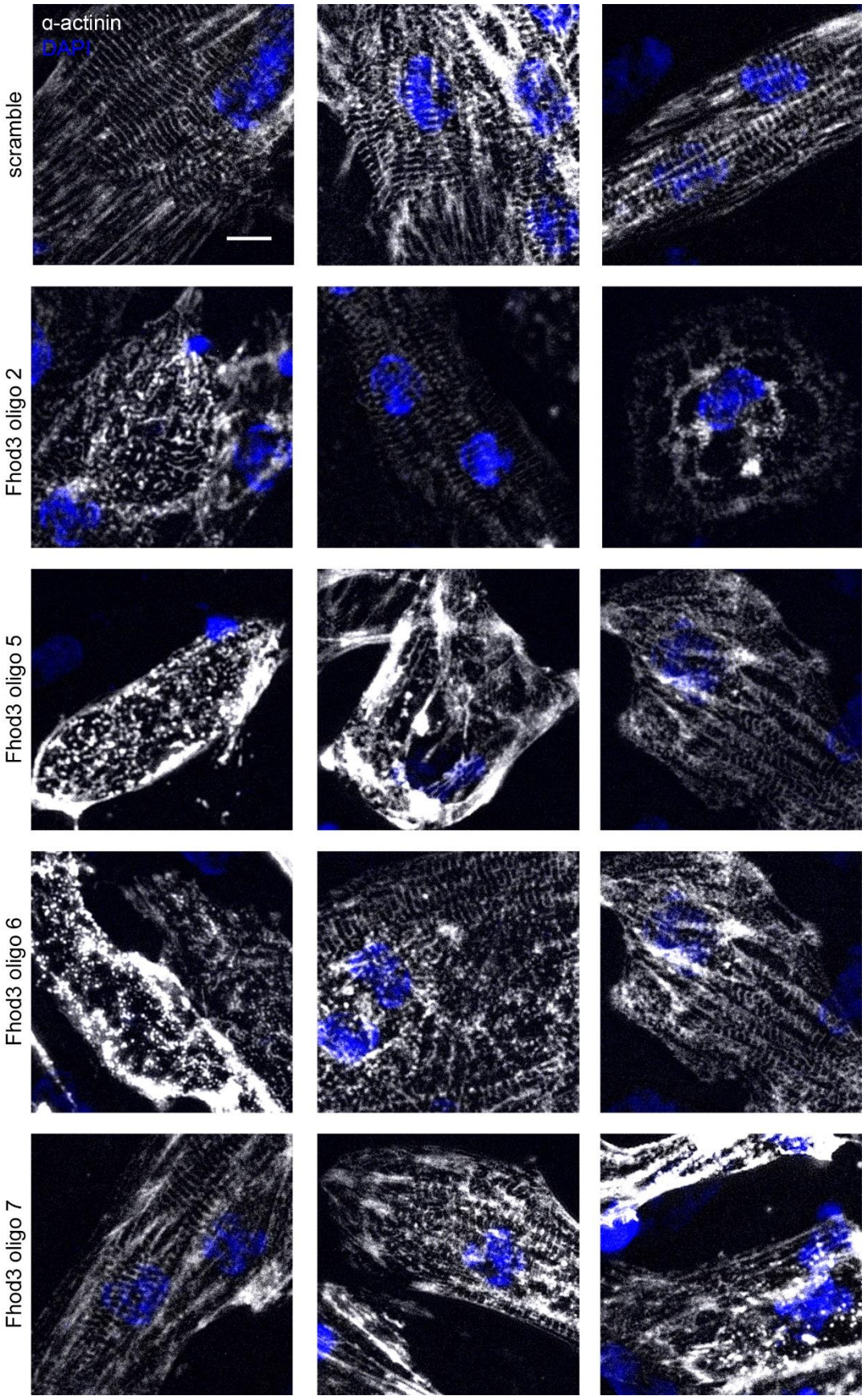
α-actinin
DAPI
scramble
Fhod3 oligo 2
Fhod3 oligo 5
Fhod3 oligo 6
Fhod3 oligo 7

Figure 4.5 Fhod3 depletion in hESC-CMs leads to defects in sarcomere organization. hESC-CMs were transfected with the indicated siRNA oligonucleotides, then stained for α-actinin (white) and nuclei (blue) and imaged on a widefield fluorescence microscope. Three representative images are shown for each condition. Scale bar is 10 μm.

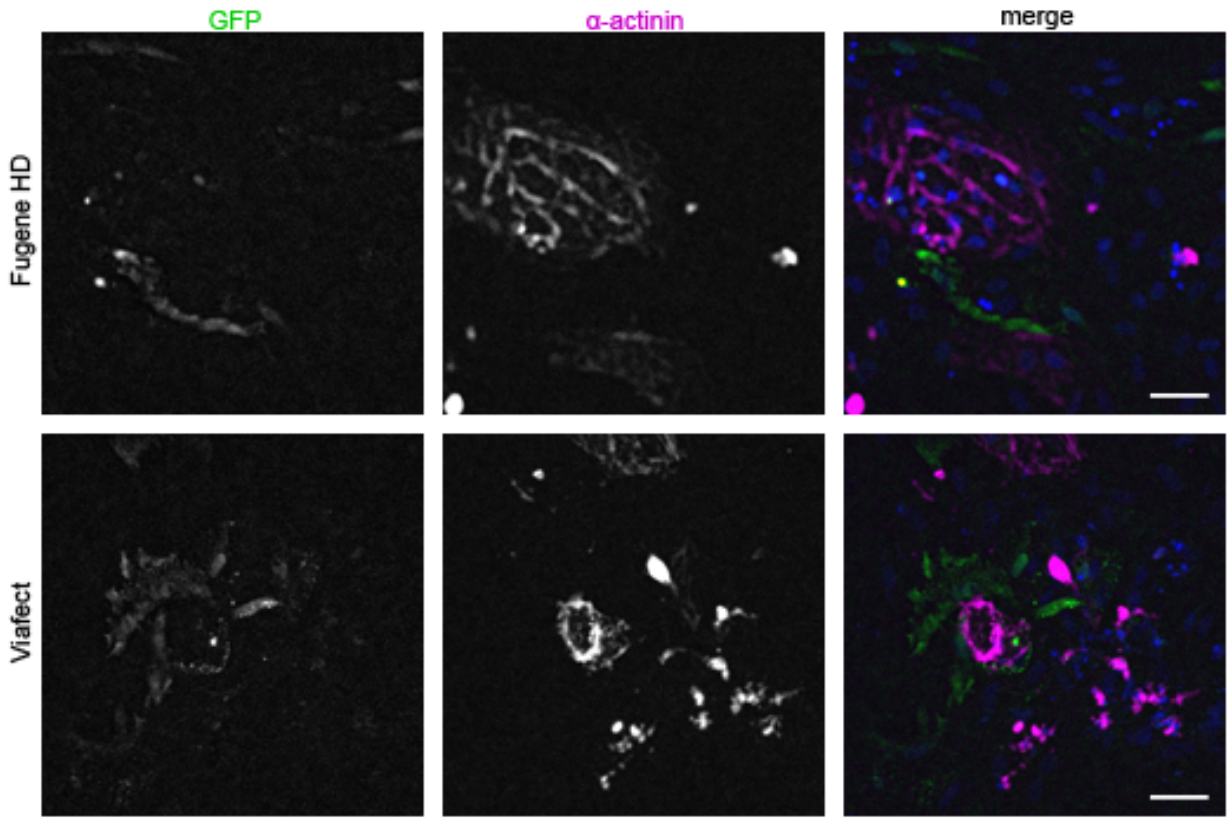

Figure 4.6: Plasmid transfection is inefficient in differentiated cardiomyocytes. hESC-CMs were transiently transfected with the pEGFP plasmid using the lipid-based transfection reagents Fugene HD or Viafect, then stained with antibodies against GFP and α-actinin. GFP-positive cells are sparse and rarely stain positively for α-actinin. Scale bars are 50 μm.

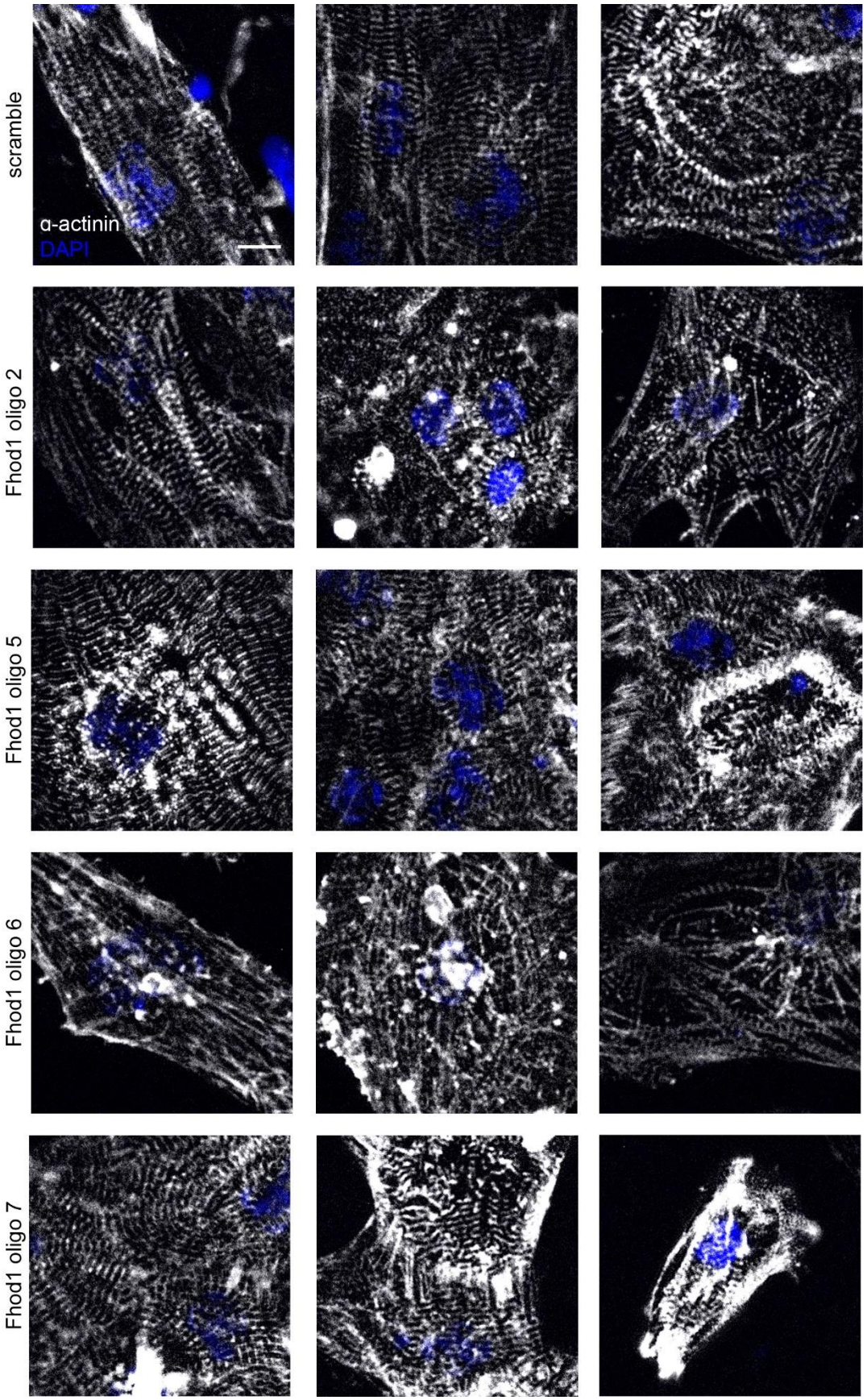
scramble
α-actinin
DAPI
Fhod1 oligo 2
Fhod1 oligo 5
Fhod1 oligo 6
Fhod1 oligo 7

Figure 4.7: Fhod1 is not required for sarcomere assembly.
hESC-CMs were transfected with the indicated siRNA oligonucleotides, then stained for α-actinin (white) and nuclei (blue) and imaged on a widefield fluorescence microscope. Three representative images are shown for each condition. Scale bar is 10 μm.

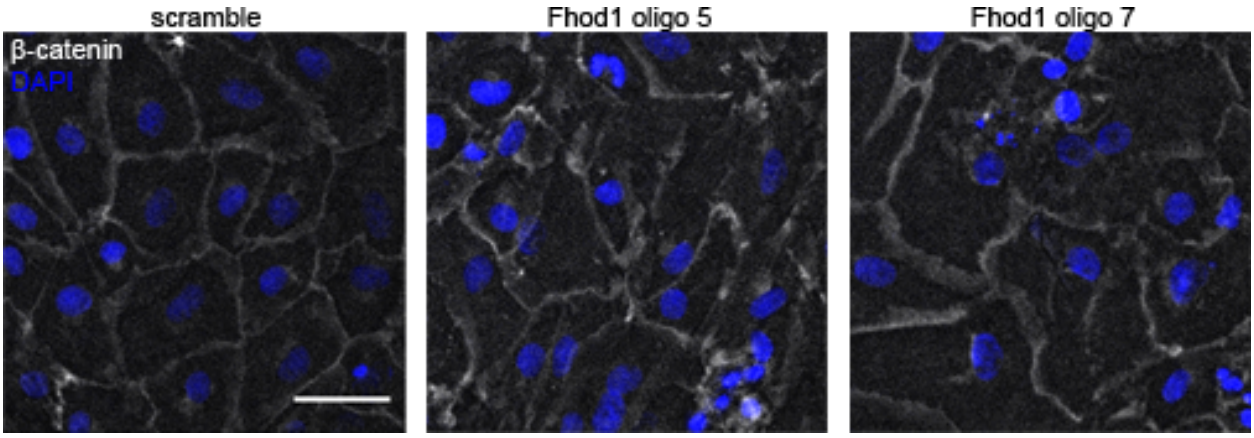

Figure 4.8: Fhod1 is not required for intercalated disc assembly.
hESC-CMs were transfected with scramble or Fhod1-targeting siRNA, then stained with a β-catenin antibody to visualize intercalated discs (white) and DAPI (blue). Scale bar is 50 μm.

References

Al Haj, A., Mazur, A.J., Radaszkiewicz, K., Radaszkiewicz, T., Makowiecka, A., et al. 2015. Distribution of formins in cardiac muscle: FHOD1 is a component of intercalated discs and costameres. *Eur J Cell Biol*. 94:101-113.

Arimura, T., Takeya, R., Ishikawa, T., Yamano, T., Matsuo, A., et al. 2013. Dilated Cardiomyopathy-Associated FHOD3 Variant Impairs the Ability to Induce Activation of Transcription Factor Serum Response Factor. *Circulation Journal*. 77:2990-2996.

Bor, B., Vizcarra, C.L., Phillips, M.L., and Quinlan, M.E. 2012. Autoinhibition of the formin Cappuccino in the absence of canonical autoinhibitory domains. *Mol Biol Cell*. 23:3801-3813.

Courtemanche, N. 2018. Mechanisms of formin-mediated actin assembly and dynamics. *Biophys Rev*. 10:1553-1569.

Courtemanche, N., and Pollard, T.D. 2012. Determinants of Formin Homology 1 (FH1) domain function in actin filament elongation by formins. *J Biol Chem*. 287:7812-7820.

Dabiri, G.A., Turnacioglu, K.K., Sanger, J.M., and Sanger, J.W. 1997. Myofibrillogenesis visualized in living embryonic cardiomyocytes. *Proc Natl Acad Sci U S A*. 94:9493-9498.

Dwyer, J., Pluess, M., Iskratsch, T., Dos Remedios, C.G., and Ehler, E. 2014. The formin FHOD1 in cardiomyocytes. *Anat Rec (Hoboken)*. 297:1560-1570.

Eiges, R. 2016. Genetic Manipulation of Human Embryonic Stem Cells. *Methods Mol Biol*. 1307:149-172.

Esslinger, U., Garnier, S., Korniat, A., Proust, C., Karakigas, G., et al. 2017. Exome-wide association study reveals novel susceptibility genes to sporadic dilated cardiomyopathy. *PLoS One*. 12:e0172995.

Fenix, A.M., Neininger, A.C., Taneja, N., Hyde, K., Visetsouk, M.R., et al. 2018. Muscle-specific stress fibers give rise to sarcomeres in cardiomyocytes. *Elife*. 7.

Goode, B.L., and Eck, M.J. 2007. Mechanism and function of formins in the control of actin assembly. *Annu Rev Biochem*. 76:593-627.

Iskratsch, T., Lange, S., Dwyer, J., Kho, A.L., dos Remedios, C., et al. 2010. Formin follows function: a muscle-specific isoform of FHOD3 is regulated by CK2 phosphorylation and promotes myofibril maintenance. *J Cell Biol*. 191:1159-1172.

Kan-o, M., Takeya, R., Abe, T., Kitajima, N., Nishida, M., et al. 2012a. Mammalian formin Fhod3 plays an essential role in cardiogenesis by organizing myofibrillogenesis. *Biol Open*. 1:889-896.

Kan-o, M., Takeya, R., Taniguchi, K., Tanoue, Y., Tominaga, R., et al. 2012b. Expression and subcellular localization of mammalian formin Fhod3 in the embryonic and adult heart. *PLoS One*. 7:e34765.

Lu, J., and Pollard, T.D. 2001. Profilin binding to poly-L-proline and actin monomers along with ability to catalyze actin nucleotide exchange is required for viability of fission yeast. *Mol Biol Cell*. 12:1161-1175.

Mi-Mi, L., Votra, S., Kemphues, K., Bretscher, A., and Pruyne, D. 2012. Z-line formins promote contractile lattice growth and maintenance in striated muscles of C. elegans. *J Cell Biol*. 198:87-102.

Minami, I., Yamada, K., Otsuji, T.G., Yamamoto, T., Shen, Y., et al. 2012. A small molecule that promotes cardiac differentiation of human pluripotent stem cells under defined, cytokine- and xeno-free conditions. *Cell Rep*. 2:1448-1460.

Nakano, H., Minami, I., Braas, D., Pappoe, H., Wu, X., et al. 2017. Glucose inhibits cardiac muscle maturation through nucleotide biosynthesis. *Elife*. 6.

Ochoa, J.P., Sabater-Molina, M., Garcia-Pinilla, J.M., Mogensen, J., Restrepo-Cordoba, A., et al. 2018. Formin Homology 2 Domain Containing 3 (FHOD3) Is a Genetic Basis for Hypertrophic Cardiomyopathy. *J Am Coll Cardiol*. 72:2457-2467.

Paul, A.S., and Pollard, T.D. 2008. The role of the FH1 domain and profilin in formin-mediated actin-filament elongation and nucleation. *Curr Biol*. 18:9-19.

Ramabhadran, V., Gurel, P.S., and Higgs, H.N. 2012. Mutations to the formin homology 2 domain of INF2 protein have unexpected effects on actin polymerization and severing. *J Biol Chem*. 287:34234-34245.

Ribeiro, A.J., Ang, Y.S., Fu, J.D., Rivas, R.N., Mohamed, T.M., et al. 2015. Contractility of single cardiomyocytes differentiated from pluripotent stem cells depends on physiological shape and substrate stiffness. *Proc Natl Acad Sci U S A*. 112:12705-12710.

Rizvi, S.A., Neidt, E.M., Cui, J., Feiger, Z., Skau, C.T., et al. 2009. Identification and characterization of a small molecule inhibitor of formin-mediated actin assembly. *Chem Biol*. 16:1158-1168.

Sanematsu, F., Kanai, A., Ushijima, T., Shiraishi, A., Abe, T., et al. 2019. Fhod1, an actin-organizing formin family protein, is dispensable for cardiac development and function in mice. *Cytoskeleton (Hoboken)*.

Sanger, J.W., Kang, S., Siebrands, C.C., Freeman, N., Du, A., et al. 2005. How to build a myofibril. *J Muscle Res Cell Motil*. 26:343-354.

Schonichen, A., Mannherz, H.G., Behrmann, E., Mazur, A.J., Kuhn, S., et al. 2013. FHOD1 is a combined actin filament capping and bundling factor that selectively associates with actin arcs and stress fibers. *J Cell Sci*. 126:1891-1901.

Schulze, N., Graessl, M., Blancke Soares, A., Geyer, M., Dehmelt, L., et al. 2014. FHOD1 regulates stress fiber organization by controlling the dynamics of transverse arcs and dorsal fibers. *J Cell Sci*. 127:1379-1393.

Scott, B.J., Neidt, E.M., and Kovar, D.R. 2011. The functionally distinct fission yeast formins have specific actin-assembly properties. *Mol Biol Cell*. 22:3826-3839.

Shwartz, A., Dhanyasi, N., Schejter, E.D., and Shilo, B.Z. 2016. The Drosophila formin Fhos is a primary mediator of sarcomeric thin-filament array assembly. *Elife*. 5.

Spudich, J.A., and Watt, S. 1971. The regulation of rabbit skeletal muscle contraction. I. Biochemical studies of the interaction of the tropomyosin-troponin complex with actin and the proteolytic fragments of myosin. *J Biol Chem*. 246:4866-4871.

Taniguchi, K., Takeya, R., Suetsugu, S., Kan, O.M., Narusawa, M., et al. 2009. Mammalian formin fhod3 regulates actin assembly and sarcomere organization in striated muscles. *J Biol Chem*. 284:29873-29881.

Ushijima, T., Fujimoto, N., Matsuyama, S., Kan, O.M., Kiyonari, H., et al. 2018. The actin-organizing formin protein Fhod3 is required for postnatal development and functional maintenance of the adult heart in mice. *J Biol Chem*. 293:148-162.

Wooten, E.C., Hebl, V.B., Wolf, M.J., Greytak, S.R., Orr, N.M., et al. 2013. Formin homology 2 domain containing 3 variants associated with hypertrophic cardiomyopathy. *Circ Cardiovasc Genet*. 6:10-18.

Xu, Y., Moseley, J.B., Sagot, I., Poy, F., Pellman, D., et al. 2004. Crystal structures of a Formin Homology-2 domain reveal a tethered dimer architecture. *Cell*. 116:711-723.

Zuchero, J.B. 2007. In vitro actin assembly assays and purification from Acanthamoeba. *Methods Mol Biol*. 370:213-226.

Chapter 5: Discussion

Fhod family members are essential for cell adhesion, motility, and contractility in a wide range of biological contexts. In many of these contexts, it was unclear how Fhods contribute to the assembly or function of the actin-based structure, particularly in the absence of *in vitro* data to support a role for Fhods in actin assembly. Here, we have established three major modes by which Fhod family members can interact with actin filaments: (1) They nucleate actin filaments, quite potently but sensitive to the actin isoform (Chapters 2 and 4). (2) They processively elongate actin filaments, but with a slower elongation rate and a much shorter dwell time than most other formins (Chapters 2 and 3). (3) They bind relatively tightly to sides of actin filaments to form actin bundles (Chapter 2). Having established these biochemical activities for Fhod family members, we now have a framework to understand how Fhods function and a wide range of new questions to ask.

Which biochemical activities of Fhod are required in cells?

We observed three distinct biochemical activities for Fhod family members, raising the question of which of these activities are required for function *in vivo*. This is a challenging problem for many formins: since the FH2 domain mediates all three activities, it can be challenging to perturb one activity without affecting the others. As a starting place, we introduced two classic mutations in a conserved isoleucine and lysine in the FH2 domain. These are often treated as complete loss-of-function mutations, based on their initial characterization in the yeast formin Bni1p (Xu et al., 2004). However, their effect on actin binding varies considerably across formins, and they do not always abolish actin binding (Ramabhadran et al., 2012; Scott et al., 2011).

We found that the isoleucine mutation in *Drosophila* Fhod and human Fhod1 abolished nucleation and barbed end binding while retaining the ability to bundle actin filaments (Chapter

2), although human Fhod1 with this mutation might still inhibit elongation of muscle actin (Appendix A). These biochemical measurements allow us to better interpret *in vivo* work with these mutants. In *Drosophila* indirect flight muscle, loss of Fhod leads to a severe defect in sarcomere assembly; flies expressing Fhod I966A can form sarcomeres, but they are sparse and poorly aligned (Shwartz et al., 2016). This work suggests that side-binding and bundling are sufficient to build some sarcomeres, but nucleation and/or barbed end elongation contribute substantially to sarcomere organization in indirect flight muscle. In mammalian fibroblasts, Fhod1 is required for nuclear movement, but Fhod1 I705A functions almost as well as wild-type Fhod1 (Kutscheidt et al., 2014). Therefore, there is at least one context where nucleation and barbed end binding appear completely dispensable, and Fhod1 functions instead by binding sides of actin filaments.

Unlike the isoleucine mutant, the lysine mutant of *Drosophila* Fhod (K1112A) impaired nucleation activity without affecting either barbed end or side binding (Chapter 2). This mutant has not been tested in flies, but the corresponding mutation in mammalian Fhod3 fails to assemble stress fibers in HeLa cells and sarcomeres in primary cardiomyocytes (Taniguchi et al., 2009), suggesting that actin nucleation activity is specifically required for Fhod3 function. In future work, this mutation will be a useful tool to separate the importance of nucleation versus elongation in *Drosophila* Fhod, and perhaps in mammalian homologs as well.

How are Fhod family members regulated?

Fhod family members are thought to be autoinhibited by interactions between their unconventional diaphanous inhibitory domain (DID) in the N-terminus and diaphanous autoregulatory domain (DAD) in the C-terminus. These domains interact *in vitro* with micromolar affinity (Schonichen et al., 2006), and Fhod overexpression in cells induces actin assembly only when the DID or DAD is mutated (Lammel et al., 2014; Schonichen et al., 2006; Schulze et al., 2014; Takeya et al., 2008). These observations strongly suggest an autoinhibitory interaction

between the DID and DAD. However, the interaction between the DID and DAD of INF2 is insufficient to inhibit actin assembly; a complex consisting of CAP and lysine-acetylated actin is also required to inhibit INF2 (A et al., 2019). Therefore, now that we can measure actin assembly by Fhod family members *in* vitro, it will be important to test whether the interaction between the DID and DAD results in autoinhibition of Fhod family members.

Canonically, autoinhibitory interactions between the DID and the DAD are relieved by binding of Rho GTPases to the DID. Although Rho GTPases interact with the DID of Fhod family members, it is unclear whether they relieve autoinhibition. *Drosophila* Fhod interacts with RhoA, Rac1, and Cdc42 in a GTP-independent manner (Lammel et al., 2014); human Fhod1 similarly interacts with both GTP- and GDP-bound Rac (Gasteier et al., 2003; Westendorf, 2001). Rho GTPases are thus unlikely to relieve autoinhibition of Fhod family members, because if they did relieve autoinhibition Fhod family members would be continually activated. However, Rac does control localization of Fhod1 in some contexts (Alvarez and Agaisse, 2013; Gasteier et al., 2003; Schulte et al., 2008). On the other hand, Fhod1 binds specifically to GTP-bound Ras GTPases (Schulte et al., 2008), although an effect of Ras GTPases on Fhod1 function has not been observed. Based on the above evidence, Rho GTPases are not thought to directly activate Fhod family members. Instead, autoinhibition is thought to be relieved by Rho-associated protein kinase (ROCK), which is activated downstream of the GTPase RhoA and phosphorylates a conserved set of three serines and threonines in the Fhod DAD (Iskratsch et al., 2013a; Lammel et al., 2014; Takeya et al., 2008).

We are now closer to being able to directly test how Rho GTPases and ROCK influence Fhod autoinhibition *in vitro*. Diaphanous formins are only partially activated by binding of Rho GTPases (Li and Higgs, 2003), requiring assistance of other binding partners such as anillin to achieve full activity (Chen et al., 2017). Therefore, it will be interesting to explore whether Fhod family members rely on additional factors besides ROCK to be activated. Several known Fhod binding partners might influence its activity: casein kinase 2 (CK2) phosphorylates a muscle-

specific exon in the C-terminal tail of Fhod3 (Iskratsch et al., 2013a), cardiac myosin-binding protein (cMYBP) interacts with the N-terminus of Fhod3 and directs its localization to sarcomeres (Matsuyama et al., 2018), and Src family kinases interact with the N-terminus and FH1 domain of Fhod1 in focal adhesions (Iskratsch et al., 2013b).

We explored alternative splicing as an additional mechanism to control Fhod activity. *Drosophila* Fhod undergoes extensive alternative splicing to produce four possible C-terminal tails. One of these tails (isoform B) lacks a DAD and is therefore predicted to be constitutively active. In addition, the truncation of this tail dramatically increased its processivity (Chapter 3). This work raises the possibility that alternative splicing can be used to regulate actin filament length. Mammalian Fhod1 and Fhod3 are also alternatively spliced in muscle versus non-muscle cells (Iskratsch et al., 2010; Tojo et al., 2003). Most of the differences between muscle and non-muscle variants are in the regulatory N-terminus. These differences most likely serve to control interactions with other binding partners such as cMyBP-C, which binds to a region of Fhod3 only found in muscle-specific splice variants. However, the N-terminus of Fhod family members was previously reported to interact with actin filaments (Schonichen et al., 2013), and the structure of this region can influence the ability of the FH1 domain to recruit profilin-actin during barbed end elongation (Chapter 3). Alternative splicing of Fhod3 also adds eight amino acids, including a CK2 phosphorylation site, to the C-terminal tail of the muscle-specific isoform (Iskratsch et al., 2010). This subtle change in the tail might also influence actin elongation, based on our observations with the *Drosophila* Fhod tail (Chapter 3).

How do mutations to Fhod3 cause cardiomyopathy?

A growing body of evidence implicates Fhod3 in hypertrophic cardiomyopathy (HCM) and dilated cardiomyopathy (DCM). Most strikingly, 13 mutations to Fhod3 were identified as likely pathogenic in families with hereditary hypertrophic cardiomyopathy (HCM), accounting for 1-2% of cases (Ochoa et al., 2018). An additional Fhod3 mutation (Y1249N) was identified in a

patient with hereditary DCM (Arimura et al., 2013). The Fhod3 polymorphism V1151I increases the risk of HCM (Wooten et al., 2013) while decreasing the risk of DCM (Esslinger et al., 2017). Fhod3 expression is also altered in HCM and DCM, with lower expression in DCM (Iskratsch et al., 2010) and higher expression in HCM (Wooten et al., 2013), although it remains unclear whether these expression changes contribute to or compensate for disease progression.

The Fhod3 mutations and polymorphism that cause or contribute to HCM follow autosomal dominant inheritance (Ochoa et al., 2018; Wooten et al., 2013). This inheritance pattern, combined with the observation that Fhod3 knockout is lethal during embryogenesis while having a milder hypertrophic phenotype in adulthood (Kan-o et al., 2012; Ushijima et al., 2018), suggests that these mutations are probably not simple loss-of-function alleles. Instead, they might disrupt localization or autoinhibition. Consistently, HCM-causing mutations are found throughout the Fhod3 gene but cluster in muscle-specific exons in the N-terminus (Ochoa et al., 2018), which are thought to control Fhod3 localization (Matsuyama et al., 2018). We hope that the systems we developed in Chapter 4 to measure Fhod3 function *in vitro* and in cells will allow us to determine how disease-causing Fhod3 mutants affect activity.

References

A, M., Fung, T.S., Kettenbach, A.N., Chakrabarti, R., and Higgs, H.N. 2019. A complex containing lysine-acetylated actin inhibits the formin INF2. *Nat Cell Biol*. 21:592-602.

Alvarez, D.E., and Agaisse, H. 2013. The formin FHOD1 and the small GTPase Rac1 promote vaccinia virus actin-based motility. *J Cell Biol*. 202:1075-1090.

Arimura, T., Takeya, R., Ishikawa, T., Yamano, T., Matsuo, A., et al. 2013. Dilated Cardiomyopathy-Associated FHOD3 Variant Impairs the Ability to Induce Activation of Transcription Factor Serum Response Factor. *Circulation Journal*. 77:2990-2996.

Chen, A., Arora, P.D., McCulloch, C.A., and Wilde, A. 2017. Cytokinesis requires localized beta-actin filament production by an actin isoform specific nucleator. *Nat Commun*. 8:1530.

Esslinger, U., Garnier, S., Korniat, A., Proust, C., Karakigas, G., et al. 2017. Exome-wide association study reveals novel susceptibility genes to sporadic dilated cardiomyopathy. *PLoS One*. 12:e0172995.

Gasteier, J.E., Madrid, R., Krautkramer, E., Schroder, S., Muranyi, W., et al. 2003. Activation of the Rac-binding partner FHOD1 induces actin stress fibers via a ROCK-dependent mechanism. *J Biol Chem*. 278:38902-38912.

Iskratsch, T., Lange, S., Dwyer, J., Kho, A.L., dos Remedios, C., et al. 2010. Formin follows function: a muscle-specific isoform of FHOD3 is regulated by CK2 phosphorylation and promotes myofibril maintenance. *J Cell Biol*. 191:1159-1172.

Iskratsch, T., Reijntjes, S., Dwyer, J., Toselli, P., Degano, I.R., et al. 2013a. Two distinct phosphorylation events govern the function of muscle FHOD3. *Cell Mol Life Sci*. 70:893-908.

Iskratsch, T., Yu, C.H., Mathur, A., Liu, S., Stevenin, V., et al. 2013b. FHOD1 is needed for directed forces and adhesion maturation during cell spreading and migration. *Dev Cell*. 27:545-559.

Kan-o, M., Takeya, R., Abe, T., Kitajima, N., Nishida, M., et al. 2012. Mammalian formin Fhod3 plays an essential role in cardiogenesis by organizing myofibrillogenesis. *Biol Open*. 1:889-896.

Kutscheidt, S., Zhu, R., Antoku, S., Luxton, G.W., Stagljar, I., et al. 2014. FHOD1 interaction with nesprin-2G mediates TAN line formation and nuclear movement. *Nat Cell Biol*. 16:708-715.

Lammel, U., Bechtold, M., Risse, B., Berh, D., Fleige, A., et al. 2014. The Drosophila FHOD1-like formin Knittrig acts through Rok to promote stress fiber formation and directed macrophage migration during the cellular immune response. *Development*. 141:1366-1380.

Li, F., and Higgs, H.N. 2003. The Mouse Formin mDia1 Is a Potent Actin Nucleation Factor Regulated by Autoinhibition. *Current Biology*. 13:1335-1340.

Matsuyama, S., Kage, Y., Fujimoto, N., Ushijima, T., Tsuruda, T., et al. 2018. Interaction between cardiac myosin-binding protein C and formin Fhod3. *Proc Natl Acad Sci U S A*. 115:E4386-E4395.

Ochoa, J.P., Sabater-Molina, M., Garcia-Pinilla, J.M., Mogensen, J., Restrepo-Cordoba, A., et al. 2018. Formin Homology 2 Domain Containing 3 (FHOD3) Is a Genetic Basis for Hypertrophic Cardiomyopathy. *J Am Coll Cardiol*. 72:2457-2467.

Ramabhadran, V., Gurel, P.S., and Higgs, H.N. 2012. Mutations to the formin homology 2 domain of INF2 protein have unexpected effects on actin polymerization and severing. *J Biol Chem*. 287:34234-34245.

Schonichen, A., Alexander, M., Gasteier, J.E., Cuesta, F.E., Fackler, O.T., et al. 2006. Biochemical characterization of the diaphanous autoregulatory interaction in the formin homology protein FHOD1. *J Biol Chem*. 281:5084-5093.

Schonichen, A., Mannherz, H.G., Behrmann, E., Mazur, A.J., Kuhn, S., et al. 2013. FHOD1 is a combined actin filament capping and bundling factor that selectively associates with actin arcs and stress fibers. *J Cell Sci*. 126:1891-1901.

Schulte, A., Stolp, B., Schonichen, A., Pylypenko, O., Rak, A., et al. 2008. The human formin FHOD1 contains a bipartite structure of FH3 and GTPase-binding domains required for activation. *Structure*. 16:1313-1323.

Schulze, N., Graessl, M., Blancke Soares, A., Geyer, M., Dehmelt, L., et al. 2014. FHOD1 regulates stress fiber organization by controlling the dynamics of transverse arcs and dorsal fibers. *J Cell Sci*. 127:1379-1393.

Scott, B.J., Neidt, E.M., and Kovar, D.R. 2011. The functionally distinct fission yeast formins have specific actin-assembly properties. *Mol Biol Cell*. 22:3826-3839.

Shwartz, A., Dhanyasi, N., Schejter, E.D., and Shilo, B.Z. 2016. The Drosophila formin Fhos is a primary mediator of sarcomeric thin-filament array assembly. *Elife*. 5.

Takeya, R., Taniguchi, K., Narumiya, S., and Sumimoto, H. 2008. The mammalian formin FHOD1 is activated through phosphorylation by ROCK and mediates thrombin-induced stress fibre formation in endothelial cells. *EMBO J*. 27:618-628.

Taniguchi, K., Takeya, R., Suetsugu, S., Kan, O.M., Narusawa, M., et al. 2009. Mammalian formin fhod3 regulates actin assembly and sarcomere organization in striated muscles. *J Biol Chem*. 284:29873-29881.

Tojo, H., Kaieda, I., Hattori, H., Katayama, N., Yoshimura, K., et al. 2003. The Formin family protein, formin homolog overexpressed in spleen, interacts with the insulin-responsive aminopeptidase and profilin IIa. *Mol Endocrinol*. 17:1216-1229.

Ushijima, T., Fujimoto, N., Matsuyama, S., Kan, O.M., Kiyonari, H., et al. 2018. The actin-organizing formin protein Fhod3 is required for postnatal development and functional maintenance of the adult heart in mice. *J Biol Chem*. 293:148-162.

Westendorf, J.J. 2001. The formin/diaphanous-related protein, FHOS, interacts with Rac1 and activates transcription from the serum response element. *J Biol Chem*. 276:46453-46459.

Wooten, E.C., Hebl, V.B., Wolf, M.J., Greytak, S.R., Orr, N.M., et al. 2013. Formin homology 2 domain containing 3 variants associated with hypertrophic cardiomyopathy. *Circ Cardiovasc Genet*. 6:10-18.

Xu, Y., Moseley, J.B., Sagot, I., Poy, F., Pellman, D., et al. 2004. Crystal structures of a Formin Homology-2 domain reveal a tethered dimer architecture. *Cell*. 116:711-723.

Appendix A: Preliminary data on isoform-specific nucleation by human Fhod1

Introduction

Mammals express six highly conserved actin isoforms: α-skeletal actin, α-cardiac actin, α-smooth actin, β-cytoplasmic actin, γ-cytoplasmic actin, and γ-smooth actin. Each pair of actin isoforms shares over 90% sequence identity, and yet they localize to distinct structures and cannot compensate for each other (Perrin and Ervasti, 2010). Several models exist to explain how each actin isoform can have a different function. First, there might be intrinsic differences between actin isoforms that alter their assembly and disassembly dynamics; so far, only subtle differences have been observed between β and γ cytoplasmic actin (Bergeron et al., 2010). Second, actin isoforms might vary in their interactions with actin-binding proteins. For example, the formins Delphilin (Silkworth et al., 2018), Fhod1 (Chapter 2), and mDia2 (Chen et al., 2017) nucleate actin in an isoform-specific manner. The actin severing protein cofilin (De La Cruz, 2005) has more cooperative binding to cytoplasmic actin filaments than to $\alpha_{skeletal}$ actin filaments. Tropomodulin (Tmod) 3 caps filaments composed of any actin isoform, but only sequesters monomers of cytoplasmic actin isoforms (Yamashiro et al., 2014). Finally, differences in function between actin genes might be explained by non-coding variations in nucleotide sequence. Whereas complete loss of the β-actin gene is embryonic lethal, editing the endogenous β-actin gene to encode γ-actin does not affect viability, with the only identified phenotype of progressive hearing loss (Patrinostro et al., 2018; Vedula et al., 2017). Therefore, most of the functional differences between β- and γ-actins are not explained by differences in their amino acid sequences.

Our observation that Fhod1 preferentially nucleates non-muscle actin isoforms is consistent with the reported localization of Fhod1 to intercalated discs (Al Haj et al., 2015;

Dwyer et al., 2014), which are thought to contain non-muscle actin isoforms (Bennett et al., 2006). Therefore, we hypothesized that the ability of Fhod1 to selectively nucleate non-muscle actin isoforms might account for the exclusion of α-actin from the intercalated disc.

In our initial experiments, we found that Fhod1 accelerated assembly of *Acanthamoeba* actin, but inhibited assembly of rabbit skeletal actin in pyrene actin assembly assays (Chapter 2). This result agreed with previously published work (Schonichen et al., 2013), as well as unpublished observations from other groups (Antoku and Gundersen, 2017). However, in subsequent experiments we now observe Fhod1 accelerating assembly of rabbit skeletal actin. This appendix describes our efforts to address this discrepancy in whether Fhod1 nucleates muscle actin.

Results

We measured the ability of Fhod1 to assemble three actin isoforms: *Acanthamoeba* actin, α-skeletal actin purified from rabbit skeletal muscle, and human β-cytoplasmic actin purified recombinantly from *Pichia pastoris* (Hatano et al., 2018). In contrast to our previous work (Chapter 2), we now observed Fhod1 nucleating both muscle and non-muscle actin (Figure A.1). We still find that Fhod1 preferentially nucleates non-muscle actin isoforms, but with only a ~2-fold difference in nucleation rate versus the completely opposing effects we previously reported.

We considered the following variables that might account for this discrepancy: the preparation of Fhod1, the preparation of actin, and the pH of the buffer. We found that both the old preparation of Fhod1-FFC, which was used in our previously published work, and a new preparation of Fhod1-FF nucleated rabbit skeletal actin (Figure A.2A). Fhod1 was able to nucleate rabbit skeletal actin from multiple preparations, although in our previous work we also observed inhibited assembly of rabbit skeletal actin from multiple actin preparations. Whereas previous work used actin labeled with pyrene-maleimide, we more recently labeled actin with

pyrene-iodoacetamide. However, when we retested actin labeled with pyrene-maleimide, we still observed Fhod1 nucleating actin (Figure A.2B), suggesting that the discrepancy in results was not simply an artifact of labeling chemistry. Because older preparations of muscle actin tend to aggregate, which can create the false appearance of faster actin assembly, we centrifuged rabbit skeletal actin at high speeds to separate monomeric actin from oligomers. Fhod1 nucleated actin from the top third of the supernatant and actin from the bottom third at identical rates (Figure A.2C). Finally, because actin is stored in Tris buffer, which has a temperature-sensitive pH, we tested the ability of Fhod1 to nucleate rabbit skeletal actin in buffer that was set to pH 8 either at room temperature (as done for previous experiments in Chapter 2) or at 4 °C (as done for other experiments shown here). This subtle change in pH did not affect the ability of Fhod1 to nucleate actin (Figure A.2D).

We found that Fhod1 inhibited actin assembly when introduced to pyrene assays directly from ion exchange columns, without a buffer exchange step (data not shown). Because Fhod1 elutes from cation exchange columns at high salt concentrations, we tested whether ionic strength modulates the effect of Fhod1 on actin assembly. To do this, we diluted Fhod1 in buffers with varying NaCl concentrations and incubated for 10 minutes before adding Fhod1 to the other reaction components. Fhod1 inhibited rabbit skeletal actin when incubated in 550 µM NaCl (Figure A.3A) but was still able to nucleate amoeba actin regardless of NaCl concentration (Figure A.3B). This result suggests that the ability of Fhod1 to inhibit rabbit skeletal actin assembly is salt-sensitive. However, in our previous work Fhod1 was stored in 150 mM NaCl, much lower than the NaCl concentrations we needed to observe inhibited actin assembly here.

To confirm that the ability of Fhod1 to nucleate rabbit skeletal actin depends on the FH2 domain, we tested nucleation activity with Fhod1 I705A, which we previously found to abolish the interaction between Fhod1 and *Acanthamoeba* actin (Chapter 2). This mutant no longer nucleated rabbit skeletal actin, and instead inhibited the assembly of rabbit skeletal actin, producing the unusually shaped curve we previously observed with wild-type Fhod1 and rabbit

skeletal actin (Figure A.4A). To ask whether Fhod1 I705A inhibits nucleation or elongation of rabbit skeletal actin, we allowed actin to polymerize for 20 minutes (Figure A.4B), then stabilized actin filaments with rhodamine-phalloidin and imaged by TIRF microscopy (Figure A.4C). Profilin and capping protein served as positive controls that inhibit nucleation and elongation, respectively. Fhod1 decreased the length of each filament without affecting the number of filaments per field of view (Figure A.4D-E), suggesting that it inhibits assembly of rabbit skeletal actin by capping barbed ends, not by suppressing nucleation.

Materials and Methods

Purification of Fhod1 CT, amoeba and rabbit skeletal actin, *S. pombe* profilin, and capping protein are described in Chapter 2. Fhod1 FF (residues 568-1016) was purified according to the same protocol as Fhod1 CT, except that it was dialyzed into 300 mM NaCl rather than 200 mM NaCl after elution off Talon resin and stored in 20% glycerol. Human β-cytoplasmic actin was expressed recombinantly in *Pichia pastoris* and purified as described (Hatano et al., 2018). Pyrene assays and TIRF microscopy experiments were performed as described in Chapter 2.

Figures

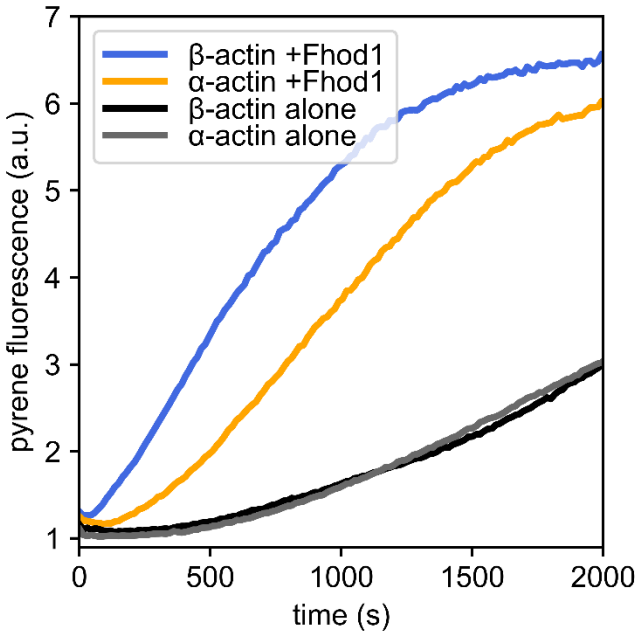

Figure A.1: Fhod1 nucleates both muscle and non-muscle actin
Pyrene actin assembly assays with 2 µM $\alpha_{skeletal}$ actin from rabbit muscle or recombinant $\beta_{cytoplasmic}$ actin expressed recombinantly in *Pichia* (10% pyrene-labeled) and 50 nM Fhod1 CT. Fhod1 accelerates assembly of both muscle and non-muscle actin.

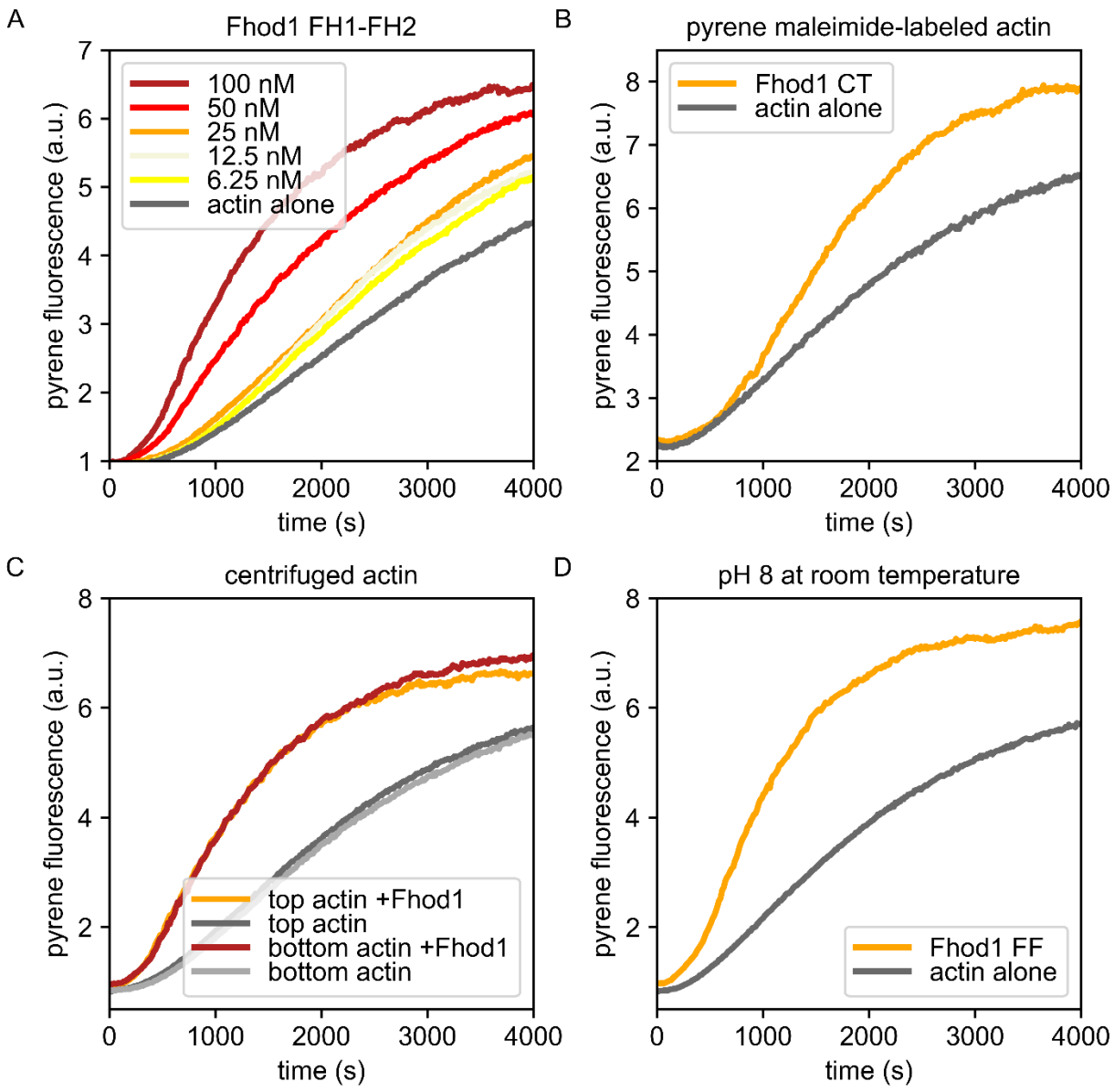

Figure A.2: Troubleshooting discrepancies in Fhod1 nucleating muscle actin
A, pyrene actin assembly assay with 2 µM rabbit skeletal actin (10% pyrene-labeled) and the indicated concentrations of recently purified Fhod1 FF (the FH1 and FH2 domains, excluding the C-terminal tail). Freshly prepared Fhod1 still nucleates muscle actin. B, pyrene actin assembly assay with 2 µM rabbit skeletal actin (10% labeled with pyrene-maleimide rather than pyrene-iodoacetamide) and 90 nM Fhod1 CT. C, pyrene actin assembly assay with 2 µM rabbit skeletal actin (10% pyrene-labeled) after centrifugation at 90k rpm for 1 hour to separate monomers from filaments. Fhod1 (75 nM) nucleates actin from both the upper and lower fractions. D, pyrene actin assembly with 2 µM rabbit skeletal actin (10% pyrene-labeled) and 75 nM Fhod1 FF. Buffers were set to pH 8 at room temperature, rather than at 4 °C. This slight difference in pH did not affect nucleation activity.

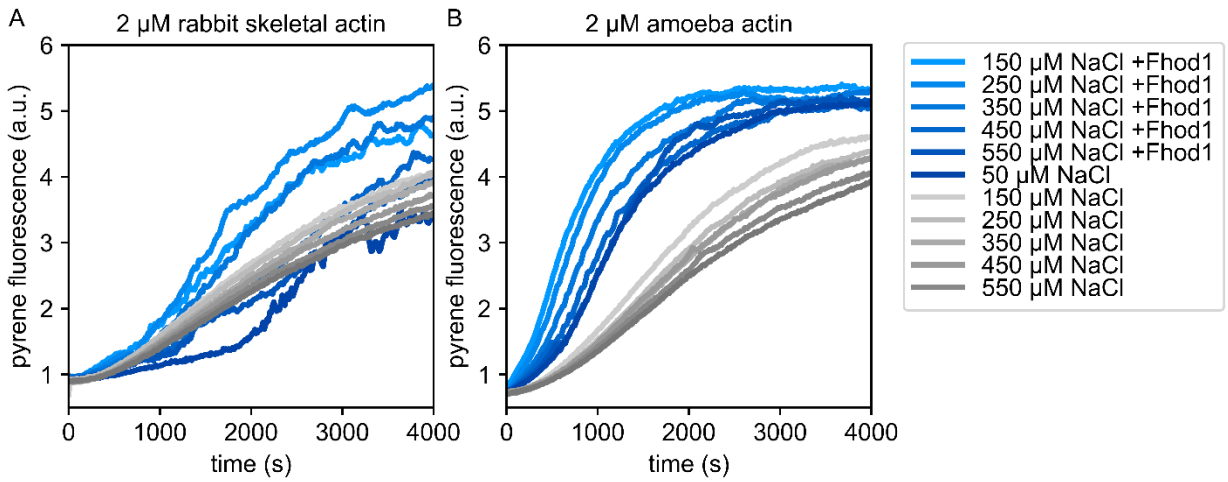

Figure A.3: Fhod1 inhibits assembly of rabbit skeletal actin under high ionic strength
A, pyrene actin assembly assay with 2 μM rabbit skeletal actin (10% pyrene-labeled) and 63 nM Fhod1 FF. Fhod1 (shades of blue) or Fhod1 storage buffer (grayscale) was diluted to 0.5 μM Fhod1 and the indicated concentration of NaCl and incubated for 10 minutes before addition to the pyrene assay. Final NaCl concentrations ranged from 3.3 to 36.7 μM. Fhod1 inhibits assembly of rabbit skeletal actin at the highest NaCl concentrations. B, pyrene actin assembly assay as in A, but with actin from *Acanthamoeba* rather than rabbit skeletal muscle. High ionic strength conditions slow assembly of amoeba actin, but do not cause Fhod1 to inhibit overall actin assembly.

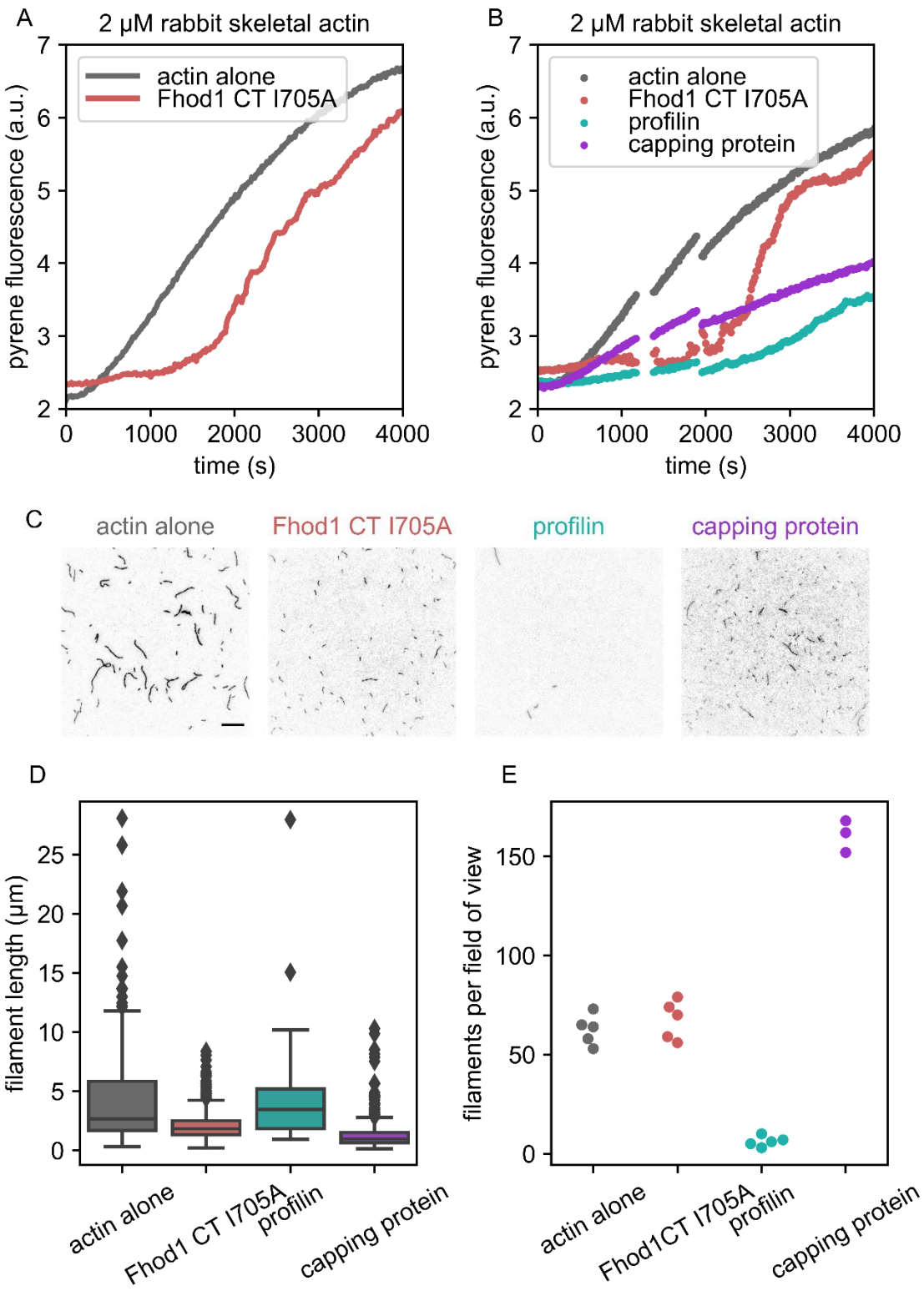
A
2 μM rabbit skeletal actin
actin alone
Fhod1 CT I705A
pyrene fluorescence (a.u.)
time (s)
B
2 μM rabbit skeletal actin
actin alone
Fhod1 CT I705A
profilin
capping protein
pyrene fluorescence (a.u.)
time (s)
C
actin alone
Fhod1 CT I705A
profilin
capping protein
D
filament length (μm)
actin alone
Fhod1 CT I705A
profilin
capping protein
E
filaments per field of view
actin alone
Fhod1CT I705A
profilin
capping protein

Figure A.4: Fhod1 CT I705A caps barbed ends of rabbit skeletal actin.
A, pyrene actin assembly assay with 2 µM rabbit skeletal actin (10% pyrene-labeled) and 40 nM Fhod1 CT I705A. Fhod1 CT I705A inhibits assembly of rabbit skeletal actin. B, pyrene actin assembly assay, as in A, with 40 nM Fhod1 CT I705A, 4 µM *S. pombe* profilin, or 2 nM mouse capping protein. Interruptions in data occur 20 and 30 minutes after the start of polymerization when actin was taken out of the reaction to image. C, TIRF microscopy images of actin filaments taken from the pyrene assay in B after 20 minutes of polymerization. Scale bar is 10 µm. D, quantification of filament lengths from C. Filament lengths are decreased with Fhod1 CT I705A and capping protein, but unchanged with profilin. D, quantification of the number of filaments in each field of view from C. Fhod1 CT does not affect filament density, whereas profilin decreases filament density and capping protein increases filament density.

References

Al Haj, A., Mazur, A.J., Radaszkiewicz, K., Radaszkiewicz, T., Makowiecka, A., et al. 2015. Distribution of formins in cardiac muscle: FHOD1 is a component of intercalated discs and costameres. *Eur J Cell Biol*. 94:101-113.

Antoku, S., and Gundersen, G.G. 2017. The interaction of FHOD1 with nesprin-2G activates a cryptic actin binding site and stimulates potent actin bundling activity: implications for nuclear movement. *In* 2017 ASCB Annual Meeting Abstracts. Vol. 27. Mol Biol Cell. 3727.

Bennett, P.M., Maggs, A.M., Baines, A.J., and Pinder, J.C. 2006. The transitional junction: a new functional subcellular domain at the intercalated disc. *Mol Biol Cell*. 17:2091-2100.

Bergeron, S.E., Zhu, M., Thiem, S.M., Friderici, K.H., and Rubenstein, P.A. 2010. Ion-dependent polymerization differences between mammalian beta- and gamma-nonmuscle actin isoforms. *J Biol Chem*. 285:16087-16095.

Chen, A., Arora, P.D., McCulloch, C.A., and Wilde, A. 2017. Cytokinesis requires localized beta-actin filament production by an actin isoform specific nucleator. *Nat Commun*. 8:1530.

De La Cruz, E.M. 2005. Cofilin binding to muscle and non-muscle actin filaments: isoform-dependent cooperative interactions. *J Mol Biol*. 346:557-564.

Dwyer, J., Pluess, M., Iskratsch, T., Dos Remedios, C.G., and Ehler, E. 2014. The formin FHOD1 in cardiomyocytes. *Anat Rec (Hoboken)*. 297:1560-1570.

Hatano, T., Alioto, S., Roscioli, E., Palani, S., Clarke, S.T., et al. 2018. Rapid production of pure recombinant actin isoforms in Pichia pastoris. *J Cell Sci*. 131.

Patrinostro, X., Roy, P., Lindsay, A., Chamberlain, C.M., Sundby, L.J., et al. 2018. Essential nucleotide- and protein-dependent functions of Actb/beta-actin. *Proc Natl Acad Sci U S A*. 115:7973-7978.

Perrin, B.J., and Ervasti, J.M. 2010. The actin gene family: function follows isoform. *Cytoskeleton (Hoboken)*. 67:630-634.

Schonichen, A., Mannherz, H.G., Behrmann, E., Mazur, A.J., Kuhn, S., et al. 2013. FHOD1 is a combined actin filament capping and bundling factor that selectively associates with actin arcs and stress fibers. *J Cell Sci*. 126:1891-1901.

Silkworth, W.T., Kunes, K.L., Nickel, G.C., Phillips, M.L., Quinlan, M.E., et al. 2018. The neuron-specific formin Delphilin nucleates nonmuscle actin but does not enhance elongation. *Mol Biol Cell*. 29:610-621.

Vedula, P., Kurosaka, S., Leu, N.A., Wolf, Y.I., Shabalina, S.A., et al. 2017. Diverse functions of homologous actin isoforms are defined by their nucleotide, rather than their amino acid sequence. *Elife*. 6.

Yamashiro, S., Gokhin, D.S., Sui, Z., Bergeron, S.E., Rubenstein, P.A., et al. 2014. Differential actin-regulatory activities of Tropomodulin1 and Tropomodulin3 with diverse tropomyosin and actin isoforms. *J Biol Chem*. 289:11616-11629.